

NOV 03 1989

NUREG/CR-5364
BNL-NUREG-52197

Summary of Advanced LMR Evaluations – PRISM and SAFR

Prepared by G. J. Van Tuyle, G. C. Slovik, B. C. Chan,
R. J. Kennett, H. S. Cheng, P. G. Kroeger

Brookhaven National Laboratory

Prepared for
U.S. Nuclear Regulatory Commission

MASTER

DISTRIBUTION OF THIS DOCUMENT IS UNLIMITED

DISCLAIMER

This report was prepared as an account of work sponsored by an agency of the United States Government. Neither the United States Government nor any agency Thereof, nor any of their employees, makes any warranty, express or implied, or assumes any legal liability or responsibility for the accuracy, completeness, or usefulness of any information, apparatus, product, or process disclosed, or represents that its use would not infringe privately owned rights. Reference herein to any specific commercial product, process, or service by trade name, trademark, manufacturer, or otherwise does not necessarily constitute or imply its endorsement, recommendation, or favoring by the United States Government or any agency thereof. The views and opinions of authors expressed herein do not necessarily state or reflect those of the United States Government or any agency thereof.

DISCLAIMER

Portions of this document may be illegible in electronic image products. Images are produced from the best available original document.

AVAILABILITY NOTICE

Availability of Reference Materials Cited in NRC Publications

Most documents cited in NRC publications will be available from one of the following sources:

1. The NRC Public Document Room, 2120 L Street, NW, Lower Level, Washington, DC 20555
2. The Superintendent of Documents, U.S. Government Printing Office, P.O. Box 37082, Washington, DC 20013-7082
3. The National Technical Information Service, Springfield, VA 22161

Although the listing that follows represents the majority of documents cited in NRC publications, it is not intended to be exhaustive.

Referenced documents available for inspection and copying for a fee from the NRC Public Document Room include NRC correspondence and internal NRC memoranda; NRC Office of Inspection and Enforcement bulletins, circulars, information notices, inspection and investigation notices; Licensee Event Reports; vendor reports and correspondence; Commission papers; and applicant and licensee documents and correspondence.

The following documents in the NUREG series are available for purchase from the GPO Sales Program: formal NRC staff and contractor reports, NRC-sponsored conference proceedings, and NRC booklets and brochures. Also available are Regulatory Guides, NRC regulations in the *Code of Federal Regulations*, and *Nuclear Regulatory Commission Issuances*.

Documents available from the National Technical Information Service include NUREG series reports and technical reports prepared by other federal agencies and reports prepared by the Atomic Energy Commission, forerunner agency to the Nuclear Regulatory Commission.

Documents available from public and special technical libraries include all open literature items, such as books, journal and periodical articles, and transactions. *Federal Register* notices, federal and state legislation, and congressional reports can usually be obtained from these libraries.

Documents such as theses, dissertations, foreign reports and translations, and non-NRC conference proceedings are available for purchase from the organization sponsoring the publication cited.

Single copies of NRC draft reports are available free, to the extent of supply, upon written request to the Office of Information Resources Management, Distribution Section, U.S. Nuclear Regulatory Commission, Washington, DC 20555.

Copies of industry codes and standards used in a substantive manner in the NRC regulatory process are maintained at the NRC Library, 7920 Norfolk Avenue, Bethesda, Maryland, and are available there for reference use by the public. Codes and standards are usually copyrighted and may be purchased from the originating organization or, if they are American National Standards, from the American National Standards Institute, 1430 Broadway, New York, NY 10018.

DISCLAIMER NOTICE

This report was prepared as an account of work sponsored by an agency of the United States Government. Neither the United States Government nor any agency thereof, or any of their employees, makes any warranty, expressed or implied, or assumes any legal liability of responsibility for any third party's use, or the results of such use, of any information, apparatus, product or process disclosed in this report, or represents that its use by such third party would not infringe privately owned rights.

NUREG/CR-5364
BNL-NUREG-52197
R1, R7, R8, 9L

NUREG/CR--5364

TI90 001756

Summary of Advanced LMR Evaluations – PRISM and SAFR

Manuscript Completed: February 1989
Date Published: October 1989

Prepared by
G. J. Van Tuyle, G. C. Slovik, B. C. Chan,
R. J. Kennett, H. S. Cheng, P. G. Kroeger

Brookhaven National Laboratory
Upton, NY 11973

Prepared for
Division of Regulatory Applications
Office of Nuclear Regulatory Research
U.S. Nuclear Regulatory Commission
Washington, DC 20555
NRC FIN A3827

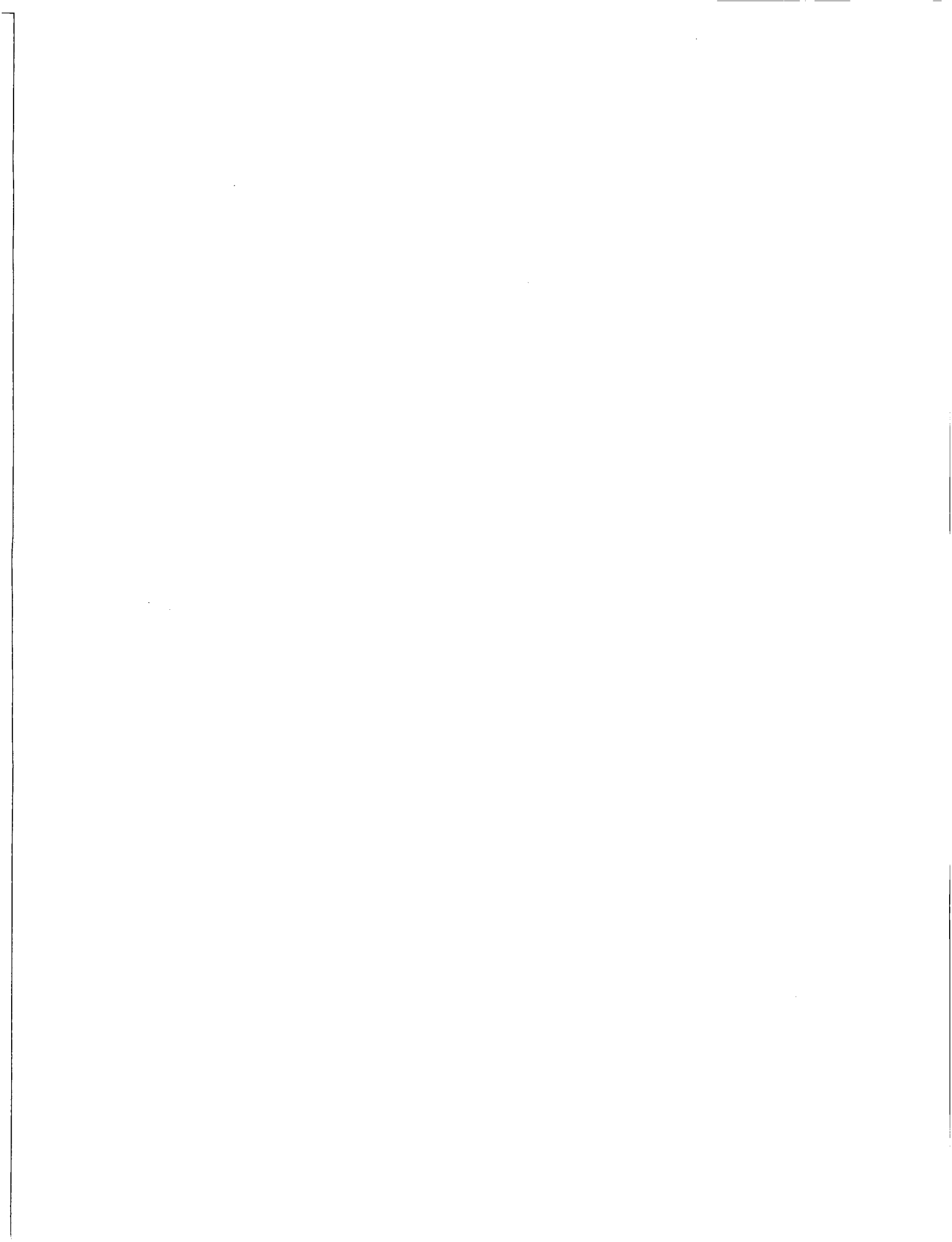
DISCLAIMER

This report was prepared as an account of work sponsored by an agency of the United States Government. Neither the United States Government nor any agency thereof, nor any of their employees, makes any warranty, express or implied, or assumes any legal liability or responsibility for the accuracy, completeness, or usefulness of any information, apparatus, product, or process disclosed, or represents that its use would not infringe privately owned rights. Reference herein to any specific commercial product, process, or service by trade name, trademark, manufacturer, or otherwise does not necessarily constitute or imply its endorsement, recommendation, or favoring by the United States Government or any agency thereof. The views and opinions of authors expressed herein do not necessarily state or reflect those of the United States Government or any agency thereof.

III

MASTER

DISTRIBUTION OF THIS DOCUMENT IS UNLIMITED



ABSTRACT

Independent Safety Analyses of the DOE sponsored Advanced Liquid Metal Reactor (LMR) Concepts: PRISM and SAFR, performed at BNL between 1986 and 1988, are reported. In most cases, BNL calculational results were very similar to those provided by General Electric (GE) for PRISM and the Rockwell International (RI)/Argonne National Laboratory (ANL) team for SAFR. Two key features of these designs are the inherent reactor "shutdown" (transition to low power in response to high temperatures) and passive shutdown heat removal (natural draft air cooling of the reactor vessel).

There are two key factors in the inherent shutdown, the reactivity feedback parameters and the projected reactor response during postulated unscrammed transients. Reactivity feedback parameters provided by the GE and RI/ANL teams were utilized in the BNL calculations, after some comparative studies and simplified calculations confirmed that the supplied parameters were at least approximately correct. Independent computer analyses of the unscrammed response to various challenges yielded results that were very similar to those submitted for both designs, and indicated that the inherent shutdown should work for many postulated events. However, for the loss-of-flow (LOF) events, there are some very low probability events where the safety margins are minimal, given that the positive sodium void worth makes sodium boiling highly undesirable.

The passive shutdown heat removal was also considered in two components. Performance of the air cooled vessel system, designated RVACS for PRISM and RACS for SAFR, indicated that these systems should perform at least as well as the vendors are projecting, and that these systems are highly fault tolerant - particularly with respect to partial blockages of the air flow pathways. Analyses of the long term heat-up events, with and without operation of RACS or RVACS, indicated that the large heat capacities of these systems assures long, slow heat-up events that would allow time to partially unblock the air flow pathways if necessary.



EXECUTIVE SUMMARY

In support of the U. S. Nuclear Regulatory Commission (NRC), Brookhaven National Laboratory (BNL) has performed independent analyses of two advanced Liquid Metal Reactor (LMR) concepts. The designs, sponsored by the U. S. Department of Energy (DOE), the Power Reactor Inherently Safe Module (PRISM) [Berglund, 1987] and the Sodium Advanced Fast Reactor (SAFR) [Baumeister, 1987], were developed primarily by General Electric (GE) and Rockwell International (RI), respectively. Technical support was provided to DOE, RI, and GE, by the Argonne National Laboratory (ANL), particularly with respect to the characteristics of the metal fuels.

There are several examples in both PRISM and SAFR where inherent or passive systems provide for a safe response to off-normal conditions. This is in contrast to the engineered safety systems utilized on current U. S. Light Water Reactor (LWR) designs.

One important design inherency in the LMRs is the "inherent shutdown", which refers to the tendency of the reactor to transition to a much lower power level whenever temperatures rise significantly. This type of behavior was demonstrated in a series of unscrammed tests at EBR-II [N.E.D., 1986]. The second key design feature is the passive air cooling of the vessel to remove decay heat. These systems, designated RVACS in PRISM and RACS in SAFR, always operate, and are believed to be able to prevent core damage in the event that no other means of heat removal is available.

Our effort was focused mainly to confirm the inherent reactor shutdown and the passive shutdown heat removal for two major reasons. First, these are the new design features that set these designs apart from more conventional liquid metal cooled reactors, such as Phenix, SNR-300, CRBR, MONJU, and the Soviet breeder reactors. Second, if both the inherent shutdown and the passive shutdown heat removal were absolutely reliable, and therefore infallible, then one would have to conclude that a core melt would be nearly impossible.

For this initial evaluation of these preliminary designs, using computer codes that were not ideally suited for the PRISM and SAFR reactors and coolant systems, we attempted to resolve the key technical issues. These efforts are briefly summarized below.

Reactivity Feedbacks

Using several detailed neutronics codes, ANL (both designs) and GE (for PRISM only) were able to evaluate key reactivity feedbacks for PRISM and SAFR. We compared the feedback parameters against those for similar designs, and we also made two simple calculations to estimate some of these feedbacks. Our comparison with other reactor designs indicated that ANL's (and GE's) estimates were in line with the feedbacks for other reactors. However, we also noted the EBR-II is the more unusual core, as it has a very small Doppler feedback and a strongly negative sodium void worth. Thus, extrapolation from the tiny EBR-II core is not a trivial process. Regarding our estimates of the reactivity feedback parameters for the radial expansion feedback, we found our

estimate using "Fermi-Age Theory" to be very close to that provided for PRISM and SAFR.

We have thus concluded that estimates of the reactivity feedback parameters for PRISM and SAFR are probably reasonably accurate. However, we are cautious about the uncertainties in these feedbacks and believe that the margins for the inherent shutdown must be large at this time in order to compensate for these uncertainties.

Transient Models

The LMR licensing codes developed at BNL for the NRC were developed during the development of the CRBRP. As SAFR and PRISM have features that were not envisioned at that time, our principal computer code, SSC, needed considerable modifications. Circumstances permitted only the most crucial programming changes to be completed for this review, and further changes will be needed for safety and licensing evaluation of the revised PRISM design.

The SSC reactor model was adjusted to model the metal fuel reactivity feedbacks and provided a reasonably good capability to model the inherent shutdown. However, we could not represent some features of the primary "loop", particularly the RACS/RVACS overflow. Thus, we limited the SSC calculations to the first few minutes of the unscrammed transients.

In order to model the complexities of the primary system flow network, we used one of our more versatile codes, MINET. However, the MINET reactor model is not sophisticated enough to analyze the inherent shutdown. Further, parts of the RACS/RVACS system performance required the use of another code, PASCOL.

As a result of these circumstances, confirmation of the transient performance of the PRISM and SAFR systems required some degree of ingenuity. However, our calculations, taken altogether, confirm most of the analyses provided by the design teams.

PRISM Unscrammed Events

Our SSC calculations for the three major unscrammed events, including loss-of-heat sink (LOHS), loss of flow (LOF), and transient over power (TOP), were very similar to those submitted by GE. Safety margins appear to be significant for all three events, with the unscrammed LOF having the smallest margins. Three related unscrammed events were also analyzed, including a pipe break, a TOP/LOF combination, and an LOF missing one (of four) pump coast-down. The pipe break, which results in a flow short-circuit rather than a loss of sodium inventory, is slightly worse than an instantaneous stoppage of one of the pumps and results in a rapid power reduction (the inherent shutdown) and appears to be largely benign. The combined TOP/LOF is less likely than either a TOP or an LOF, and has smaller safety margins than either. The margin for the unscrammed LOF missing one pump coastdown is nearly zero. As the chance of losing one of the coastdowns, which are provided for the electromagnetic (EM) pumps by the synchronous machines, has to be significant, it would be prudent for GE to design to better accommodate this event, i.e., to ride out an unscrammed LOF on three pump coastdowns.

SAFR Unscrammed Events

For the three basic unscrammed events, i.e., the LOHS, LOF, and TOP events, our SSC calculational results were similar to those provided by ANL for RI/SAFR. The only problem here was that the ANL calculations show control rod drive line expansion that is very quick, and this helps their calculated safety margins. To get this quick expansion of the control rod drive lines, RI must design the structures above the core so as to direct hot core outlet sodium along the drive lines. For our calculations, we assumed that this is achievable, although we have some reservations. Note also that having the inherent shutdown rely partly on freely moving control rods leaves a potential common mode failure, i.e., stuck rods could prevent scram and reduce inherent "shutdown" effectiveness.

While the SSC results were similar to those submitted by ANL, as long as the enhanced control rod drive line expansion was utilized, these calculations consistently showed somewhat smaller safety margins for SAFR than for PRISM. This traces directly to RI's desire to run SAFR significantly hotter than PRISM in order to use a superheated steam cycle and achieve higher thermal efficiency (40% versus 32%). Should GE decide to convert PRISM to use a superheated steam cycle, we would expect their safety margins to shrink accordingly.

In addition to the three basic unscrammed events, we looked at two variations - a 20 cent TOP combined with an LOF and a pump seizure (one of two centrifugal pumps). The safety margins for the 20 TOP/LOF were not large for SAFR, and would be smaller for a 35 TOP/LOF (note: 20 is based on large seismic event, whereas 35 represents maximum control rod withdrawal worth). However, RI plans to design their control systems to prevent pump trip until scram has been achieved (rather than just a scram signal generated).

For the pump seizure event, it was determined that the rapid reduction in reactor flow rate could be accommodated inherently as long as the other pump continued to function. However, the other pump should see a surge in flow (25 to 30%), and cavitation may be anticipated. Eventually, the second pump would fail, and the delay becomes a very important parameter - the longer, the better. A related concern is that pump seizures are actually more likely during a coastdown, so RI may have had to design to survive the ULOF with only one coastdown (if DOE had continued funding SAFR development).

Evaluation of RACS/RVACS Performance

In order to assess the passive cooling system, we adapted the PASCOL code, which we developed to model the comparable system in the Modular High Temperature Gas Reactor (MHTGR), which is designated the RCCS. We specified the reactor vessel temperature and calculated the natural draft air flow, and the various heat transfer processes. Using conservative parameters, we were able to match the performance predictions made by both GE and RI/ANL. Parametric cases showed excellent fault tolerance, particularly with regard to partial blockages of the air flow passages. In short, performance of the PRISM RVACS and SAFR RACS should be at least as good as projected, and the problems associated with partial blockages appear to be minimal.

Protected LOHS Events - Simple Models

One advantage of pool type LMRs, particularly if metal fuel is used, is that the high heat capacity, high thermal conductivity system can survive a fairly lengthy heat up event, i.e., a total loss of heat removal. This can be demonstrated using simple hand calculations. These hand calculations gave results that were quite similar to those provided by GE and RI/ANL, for cases with and without functioning air-cooled vessel systems. If the air flow is totally blocked, many hours are available to unblock the air flow pathways, or conceivably to arrange for an ad-hoc evacuation.

MINET Calculations of Long LOHS Events

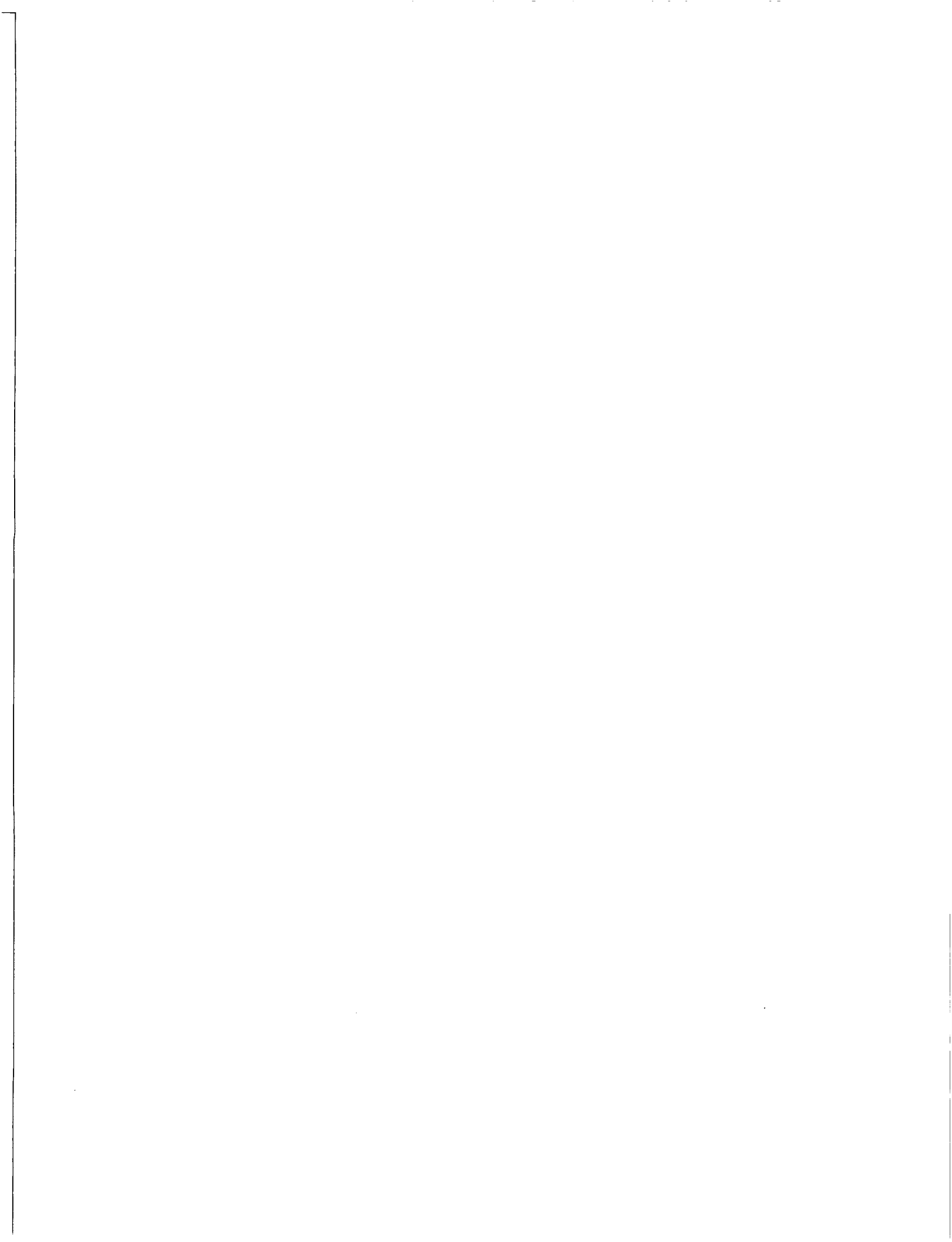
A computer code calculation of a postulated LOHS, with RVACS cooling only, was performed using MINET. Results were very similar to those provided by GE, particularly during the first day of transient time. Both code calculations indicated that the sodium spillover that increases RVACS performance occurs about 5 1/2 hours into the event.

Summary

Most of the key calculations submitted by the SAFR and PRISM design teams were independently verified and/or replicated. While the inherent "shutdown" appears to work for key postulated events, some variant cases were identified as posing significant safety concerns - in that the inherent shutdown safety margins would be too small. The passive means of shutdown cooling, using RACS or RVACS, appears to be an excellent approach, as the performance is projected to be good and the reliability should be very high.

TABLE OF CONTENTS

	<u>Page</u>
Abstract	iii
Executive Summary.	v
List of Figures	xi
List of Tables	xvii
Acknowledgements	xix
1. Introduction	1
2. Examination of the Reactivity Feedback Parameters	5
3. Transient Models	17
4. PRISM Unscrammed Events	25
5. SAFR Unscrammed Events	59
6. Evaluation of RACS/RVACS Performance	87
7. Protected LOHS Events - Simple Models.	93
8. MINET Simulation of PRISM LOHS-RVACS Event	111
9. Summary	115
References	119



LIST OF FIGURES

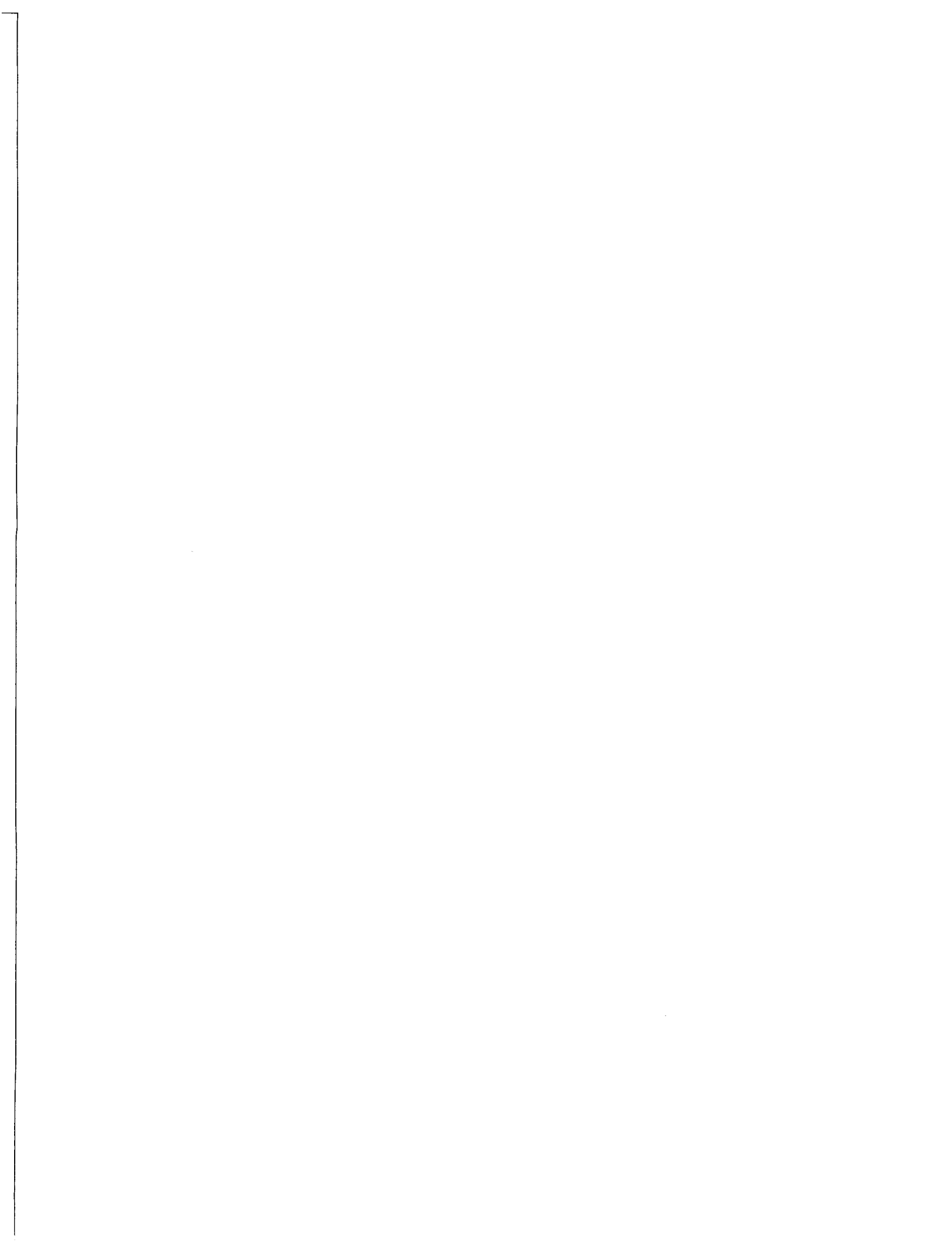
<u>Figure</u>		<u>Page</u>
1	PRISM Module Primary Sodium and RVACS Air Flow Circuits	2
2	SAFR Module Primary Sodium Flow Paths Under Normal Conditions, During DRACS Operation, and During RACS Operation. Also: DRACS and RACS	4
3	PRISM Core Layout	12
4	SAFR Core Layout	13
5	Radial Expansion Reactivity for PRISM and SAFR	15
6	SSC Schematic of SAFR (and PRISM)	18
7	Restraint System and Expected Shape from the Limited Free Bowling and Design	22
8	Schematic Representation of PRISM and SAFR Used in MINET Pipe Break Analysis	24
9	SSC Prediction for PRISM ULOHS for Power and Core Flow	26
10	Reactivity Feedbacks for ULOHS from SSC	27
11	Peak Average and Hot Driver Assembly Coolant Temperatures Compared to the Saturation Temperature	28
12	Fuel Temperature Distribution at Peak Location for ULOHS	29
13	SSC Prediction for a 35 Cent UTOP for Power and Core Flow	31
14	SSC Prediction of Reactivity Feedbacks for a 35 Cent UTOP	32
15	For 35 Cent UTOP: Peak Average and Hot Driver Assembly Coolant Temperature Compared to Saturation Temperature	33
16	Fuel Temperature Distribution at Peak Location for 35 Cent UTOP	34
17	SSC Prediction for PRISM ULOF/LOHS: Relative Power and Core Flow	35
18	SSC Prediction for PRISM ULOS/LOHS: Reactivity Feedbacks	36
19	SSC Prediction for PRISM ULOF/LOHS: Peak Average and Hot Driver Assembly Coolant Temperatures Compared to the Saturation Temperature	38

<u>Figure</u>		<u>Page</u>
20	SSC Prediction for PRISM ULOF/LOHS: Fuel Temperature Distribution at Peak Location	39
21	SSC Prediction for PRISM 35 Cent UTOP/LOF: Relative Power and Flow Rate	40
22	SSC Prediction for PRISM 35 Cent UTOP/LOF: Reactivity Feedbacks	41
23	SSC Prediction for PRISM 35 Cent UTOP/LOF: Peak Average and Hot Driver Assembly Temperatures Compared to the Saturation Temperature	42
24	SSC Prediction for PRISM 35 Cent UTOP/LOF: Fuel Temperature Distribution at Peak Location	43
25	SSC Prediction for PRISM 35 Cent UTOP/LOF: Core Exit Temperature	45
26	SSC Prediction for PRISM 35 Cent UTOP/LOF: IHX Inlet and Outlet Temperatures	46
27	PRISM-MINET Analysis - Core Inlet Flow Rate vs. Time	47
28	SSC Prediction for PRISM Pipe Break: Relative Power and Core Flow	48
29	SSC Prediction for PRISM Pipe Break: Reactivity Feedbacks	49
30	SSC Prediction for PRISM Pipe Break: Core Outlet Temperatures and Saturation Temperature	50
31	SSC Prediction for PRISM Pipe Break: Driver Temperatures	51
32	SSC Prediction for PRISM Pipe Break: Peak Temperatures	52
33	SSC Prediction for PRISM 3 Pump Coastdown: Relative Power and Core Flow	54
34	SSC Prediction for PRISM 3 Pump Coastdown: Reactivity Feedbacks	55
35	SSC Prediction for PRISM 3 Pump Coastdown: Outlet and Saturation Temperatures	56
36	SSC Prediction for PRISM 3 Pump Coastdown: Driver Temperatures	57

<u>Figure</u>		<u>Page</u>
37	SSC Prediction for PRISM 3 Pump Coastdown: Peak Temperatures	58
38	SSC Prediction for SAFR ULOHS: Relative Power and Core Flow .	60
39	SSC Prediction for SAFR ULOHS: Reactivity Feedbacks.	61
40	SSC Prediction for SAFR ULOHS: Peak Sodium and Saturation Temperatures	62
41	SSC Prediction for SAFR ULOHS: Fuel Temperatures	63
42	SSC Prediction for SAFR 20 Cent. UTOP: Relative Power and Core Flow	65
43	SSC Prediction for SAFR 20 Cent. UTOP: Reactivity Feedbacks . .	66
44	SSC Prediction for SAFR 20 Cent. UTOP: Sodium Saturation and Outlet Temperatures	67
45	SSC Prediction for SAFR 20 Cent. UTOP: Fuel Temperatures . . .	68
46	SSC Prediction for SAFR 36 Cent. UTOP: Relative Power and Core Flow	70
47	SSC Prediction for SAFR 36 Cent. UTOP: Reactivity Feedbacks . .	71
48	SSC Prediction for SAFR 36 Cent. UTOP: Sodium Saturation and Outlet Temperatures	72
49	SSC Prediction for SAFR 36 Cent. UTOP: Fuel Temperatures . . .	73
50	SSC Prediction for SAFR ULOF: Relative Power and Flow	75
51	SSC Prediction for SAFR ULOF: Reactivity Feedbacks	76
52	SSC Prediction for SAFR ULOF: Sodium Saturation and Outlet Temperatures	77
53	SSC Prediction for SAFR 20 Cent. UTOP/LOF: Relative Power and Flow	79
54	SSC Prediction for SAFR 20 Cent. UTOP/LOF: Reactivity Feedbacks	80
55	SSC Prediction for SAFR 20 Cent. UTOP/LOF: Sodium Saturation and Outlet Temperatures	81

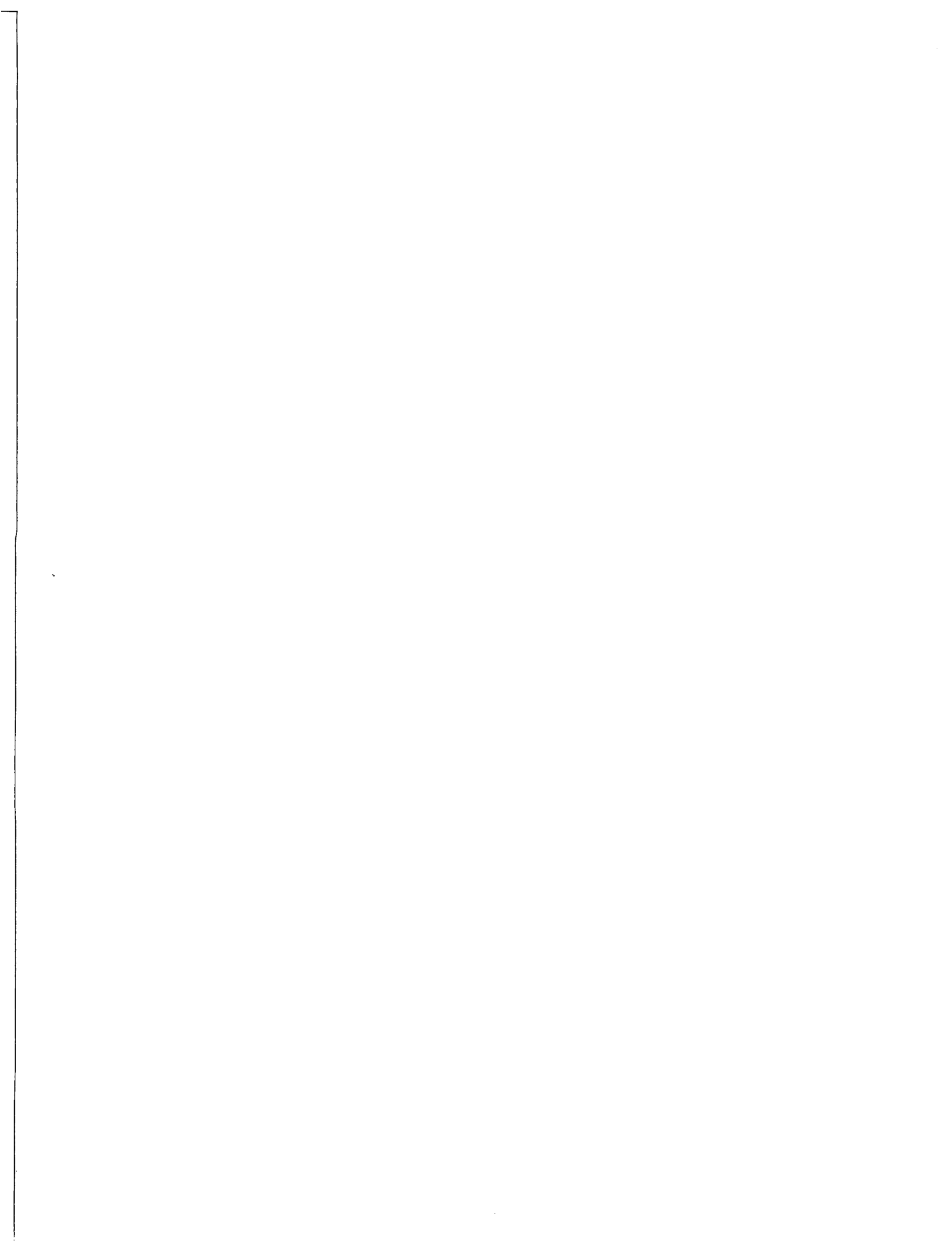
<u>Figure</u>		<u>Page</u>
56	MINET Prediction of SAFR Core Flow Rate for Various LOF Cases	83
57	SSC Prediction for SAFR Pump Seizure: Relative Power and Key Temperatures	84
58	SSC Prediction for SAFR Pump Seizure: Reactivity Feedbacks . .	85
59	Schematic of Passive Air Cooling System for Advanced LMRs . . .	88
60	Top View, Section of SAFR Vessels and RACS (Note Fins)	89
61	PRISM Passive Air Cooling System Performance During Decay Heat Removal as Function of Inlet and Outlet Ducting Flow Resistances	90
62	Integral Decay Heat vs. Time After Scram for PRISM and SAFR . .	95
63	PRISM Decay Heat and RVACS Heat Rejection During LOHS	96
64	Integral Heat Removal vs. Hours After Scram for PRISM and SAFR	97
65	SAFR LOHS Temperatures and Heat Loads and Losses, includes BNL's Calculated Temperatures	98
66	PRISM Core Outlet Temperature vs. Hours into LOHS, includes BNL's Calculated Temperatures, Neglecting Containment Vessel Mass	99
67	PRISM Core Outlet Temperatures vs. Hours into LOHS, includes BNL Calculated Temperatures including Containment Vessel Mass .	100
68	Projected SAFR Adiabatic Heatup Temperatures Using Reference Decay Heat	102
69	Projected SAFR Adiabatic Heatup Temperatures, 15% Extra Decay Heat	103
70	Projected SAFR Adiabatic Heatup Temperatures vs. RI/ANL Estimations	104
71	Projected PRISM Adiabatic Heatup Temperatures Using Reference Decay Heat	105
72	Projected PRISM Adiabatic Heatup Temperatures, 15% Extra Decay Heat	106

<u>Figure</u>		<u>Page</u>
73	Schematic Drawing of PRISM Below-Grade Components	107
74	Projected Vessel Temperatures from PRISM Earth Heatup Event . .	108
75	Projected PRISM Earth Heatup Temperatures Using 15% Extra Decay Heat	109
76	Projected PRISM Earth Heatup Temperatures Using Reference Decay Heat	110
77	Representation of PRISM Used for Long LOHS	112
78	Calculated Reactor Outlet Sodium Temperatures	113



LIST OF TABLES

<u>Table</u>		<u>Page</u>
1	Reactivity Feedbacks, $\Delta k / \Delta T(K)$, [$\times 10^{-6}$]	7
2	PRISM RVACS Performance During Decay Heat Removal Operation as Function of Steel Emmissivities	91
3	SAFR SHRS Thermal Performance with RACS Only as Function of Collector Heat Transfer Effectiveness	91



ACKNOWLEDGEMENTS

The effort to evaluate the PRISM and SAFR designs has been managed in the recent period within NRC Research by the Advanced Reactors and Generic Issues Branch (ARGIB) in the Division of Regulatory Applications. The current Branch Chief of ARGIB, Tom King, has been actively involved in reviewing these designs since the effort began under Nuclear Reactor Regulation three years ago and has made every effort to manage the best possible design review effort, even during periods when tight fiscal restraints severely hindered the program. Similarly, project managers Cardis Allen (now with SAIC) and Ralph Landry provided excellent guidance and showed considerable faith and patience while we worked to adapt our computer codes for applications considerably different than they were designed for. Other NRC staffers, including Section Leader Jerry Wilson, as well as John Flack and Monideep Dey, provided useful comments and input as well.

As PRISM and SAFR are relatively new concepts that continue to evolve, we required an enormous amount of information from the design teams. DOE managers Frank Gavigan and Ross Humphreys, as well as DOE licensing liaison George Sherwood, made every effort to assure the smooth transmission of information regarding these designs. At General Electric, Neil Brown, Geza Gyorey, and many others responded to our every request, as did their counterparts at Rockwell International, especially Bob Lancet and Dale Rogers. Both designs are supported by a large research and development at Argonne National Laboratory, as part of the Integral Fast Reactor (IFR) program - particularly with respect to the metal fuels. The principal liaison between ANL and the NRC/BNL review teams, Dean Pederson, was a major contributor to the entire review process and provided BNL with every possible assistance. Several others at ANL were more than helpful, particularly Dave Wade, Jim Cahalan, and Roald Wigland.

Any report of this size requires major efforts in the assembly/typing and editing processes. The editing job fell on the shoulders of Jim Guppy, Head of BNL's Reactor Analysis Division, and the improvements he made are much appreciated. The typing and processing of the report was ably performed by Mrs. Linda Hanlon.

1. INTRODUCTION

In support of the U.S. Nuclear Regulatory Commission (NRC), Brookhaven National Laboratory (BNL) has performed independent analyses of two advanced Liquid Metal Reactor (LMR) concepts. The designs, sponsored by the U.S. Department of Energy (DOE), the Power Reactor Inherently Safe Module (PRISM) [Berglund, 1987] and the Sodium Advanced Fast Reactor (SAFR) [Baumeister, 1987], were developed primarily by General Electric (GE) and Rockwell International (RI), respectively. Technical support was provided to DOE, RI, and GE, by the Argonne National Laboratory (ANL), particularly with respect to the characteristics of the metal fuels.

There are several examples in both PRISM and SAFR where inherent or passive systems provide for a safe response to off-normal conditions. This is in contrast to the engineered safety systems utilized on current U.S. Light Water Reactor (LWR) designs.

One important design inherency in the LMRs is the "inherent shutdown", which refers to the tendency of the reactor to transition to a much lower power level whenever temperatures rise significantly. This type of behavior was demonstrated in a series of unscrammed tests at EBR-II [N.E.D., 1986].

The second key design feature is the passive air cooling of the vessel to remove decay heat. These systems, designated RVACS in PRISM and RACS in SAFR, always operate and are believed to be able to prevent core damage in the event that no other means of heat removal is available.

PRISM

The advanced LMR design proposed by GE is a 1245 MWe PRISM plant. It is composed of nine reactor modules arranged in three identical 415 MWe power blocks. Each power block has three identical reactor modules that jointly supply steam to a single turbine generator. There is one steam generator for each reactor module. The steam generator is a recirculating type with a separate steam drum from which dry, saturated steam is piped to a common turbine header, from the three parallel steam generator blocks, and then to the power block turbine.

Figure 1 shows the reactor module internals, located below grade in a silo. The reactor module consists of the containment vessel, reactor vessel and its internals, reactor closure and rotatable plug, intermediate heat exchangers (IHX), electromagnetic (EM) pumps, control rod drives (CRD), in-vessel transfer machine (IVTM), and module support structures. The two IHXs and four EM pumps are suspended from the reactor closure, and six control rod drives (CRD), the UIS and an in-vessel fuel transfer machine (IVTM) are suspended from the rotatable plug.

Primary system sodium is circulated through the core and the shell side of the IHXs by the EM pumps. The heat generated in the core is transferred to the intermediate sodium that flows inside the IHX tubes.

The PRISM reactor utilizes the ternary Pu-U-Zr metal fuel, with HT9 clad-

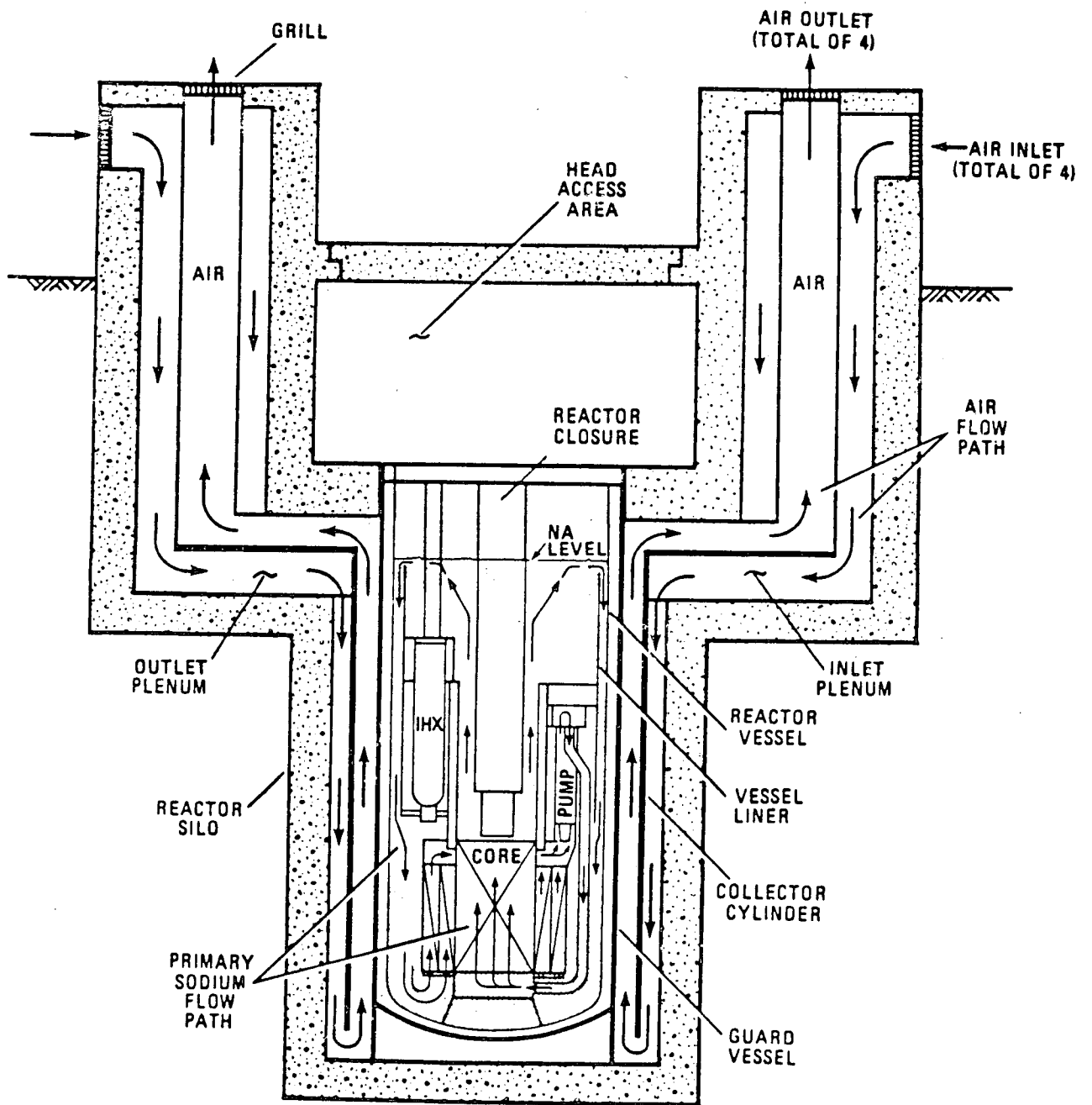


Figure 1 PRISM Module Primary Sodium and RVACS Air Flow Circuits

ding. The core restraint system is designed to alter the natural bowing feedback so the reactivity feedback contribution is generally small and negative. This is achieved by using the limited bowing restraint system.

SAFR

SAFR is a modular power system (see Figure 2) using a 900 MWt reactor to generate superheated steam which drives a 350 MWe turbine. Four modules (or Power Paks) combine to make a standard SAFR plant of 1400 Mwe. Each power pak uses four IHXs which are paired to transfer heat to two steam generators. The primary sodium is circulated through the core and tube side of the IHXs, by two centrifugal pumps. The intermediate sodium passes through the shell side of the IHX.

The SAFR reactor is similar to the PRISM unit, although the core is somewhat larger. In order to minimize the sodium density feedback (positive), the core is shorter and has a much larger diameter than PRISM. As a result, the "inherent shutdown" performs about the same for both PRISM and SAFR.

Sections to Follow

Reactivity feedbacks in the metal fuel cores of PRISM and SAFR provide the "inherent shutdown" characteristic, which is extrapolated from EBR-II. These feedbacks are discussed in Section 2.

Transient modeling involves modeling the reactor kinetics and accurately evaluating the reactivity feedbacks, as well as simulating the normal coolant system and shutdown heat removal systems. The modeling is described in Section 3.

Several postulated unscrammed events were analyzed for both designs. Analyses for PRISM are described in Section 4, and results for SAFR are discussed in Section 5.

The safety grade passive shutdown heat removal systems, designated RACS in SAFR and RVACS in PRISM, were evaluated with respect to nominal performance and degree of fault tolerance. This work is summarized in Section 6.

Two inherent characteristics of pool-type LMRs having metal fuel cores are high heat capacity and high thermal conductivity within the vessel. Thus, even with little, if any, heat removal these designs can survive lengthy periods before any fuel damage or radioactive releases would be anticipated. This can be demonstrated using simple "hand calculations", as described in Section 7.

In Section 8, computer calculations of the long LOHS events using the MINET Code are discussed. This work represents PRISM and SAFR systems in some detail, and shows how some of the flow patterns and local temperature distributions change as the RACS/RVACS systems operate under nominal conditions, i.e., with the sodium spilling down along the inside of the reactor vessel wall.

The effort is then summarized in Section 9.

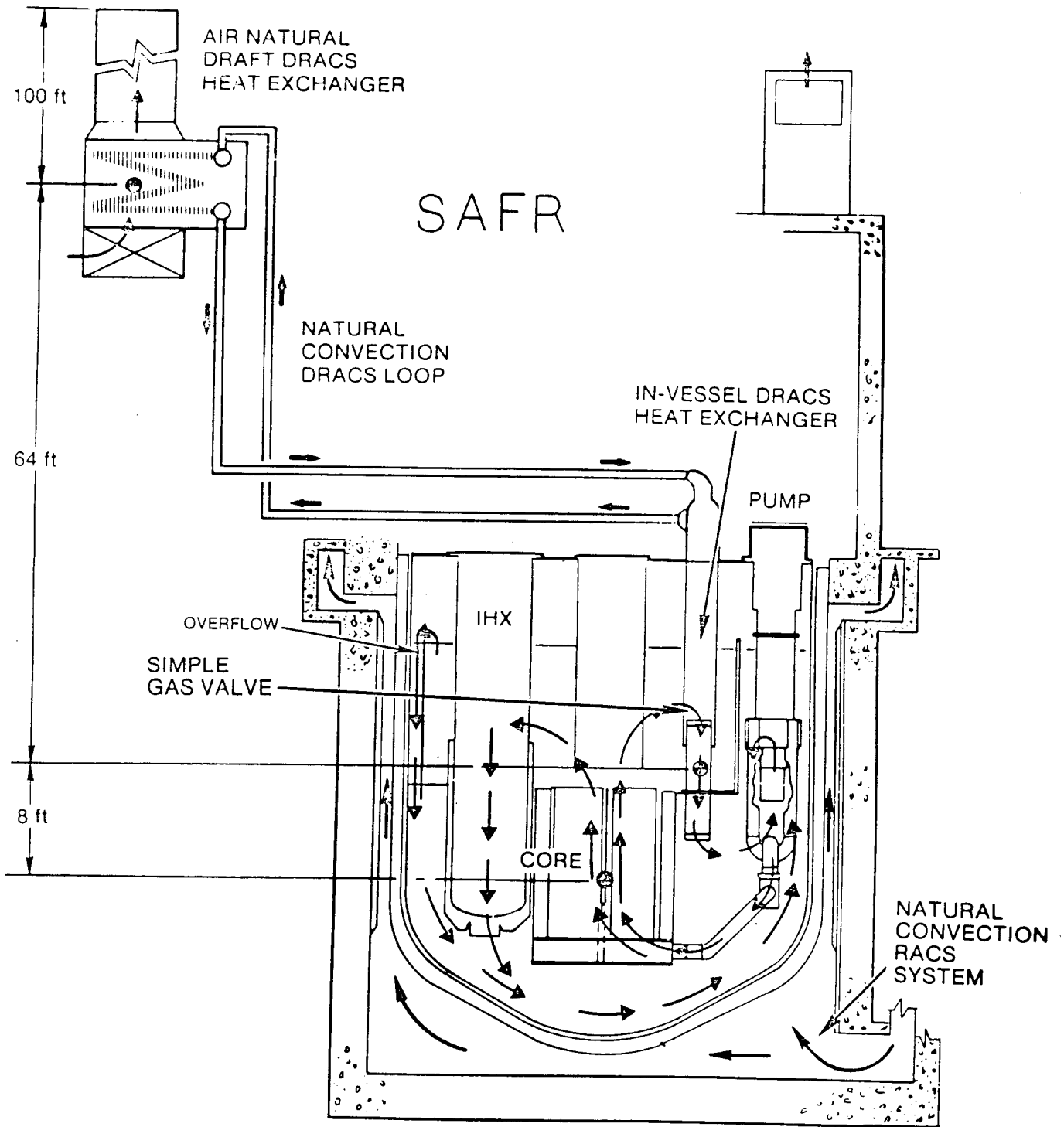


Figure 2 SAFR Module Primary Sodium Flow Paths Under Normal Conditions, During DRACS Operation, and During RACS Operation. Also: DRACS and RACS

2. EXAMINATION OF THE REACTIVITY FEEDBACK PARAMETERS

A major advantage of the use of metal fuel in the modular LMRs is that the reactor transitions to a lower power level when it overheats. This response is referred to as the "inherent shutdown", although the reactor remains critical - hopefully near decay heat levels. In a dramatic series of tests at EBR-II (see N.E.D., 101, April 1986), this capability was demonstrated in the small metallic core. However, the extrapolation from the EBR-II tests to the larger PRISM and SAFR reactors relies upon the use of sophisticated computer models. These models are focused in two areas - evaluating the reactivity feedbacks and analyzing the reactor response to postulated transients. To date, most of the BNL effort has been focused on the transients, but some work has been done to partially verify the reactivity feedbacks provided by RI/ANL and GE - and this material is covered below.

In general, RI uses ANL computational methods for calculating the SAFR reactivity feedbacks; while the PRISM calculations are based on GE methods, which have been validated against the ANL methods. The ANL methods involve the multigroup cross section generation using MC²-II, fuel assembly design and burnup calculations using NIFD/REBUS/DIF3D, reactor core calculations using DIF3D, perturbation calculations using VARI-3D, and core restraint and bowing evaluations using NUBOW-3D. These methods require time-consuming and expensive steady-state calculations. While this is necessary for the final design, the lengthy calculations tend to lose sight of the underlining physics.

2.1 Key Reactivity Feedbacks

Several reactivity feedbacks are important in the inherent shutdown response for the metal cores. Because of the smaller Doppler feedback in the metal core, reactivity feedbacks having little importance in oxide cores are important in the metal core. The main reactivity feedbacks are as follows:

Doppler Feedback:

As the fuel temperature increases, more neutrons are parasitically absorbed in the resonance energy range. For metal fuel, Doppler feedback is a smaller negative factor than it is for oxide fuel because of the harder energy spectrum. The Doppler still adds negative reactivity on a power increase, but its effect is reduced in metal fuel. This allows the temperature decrement to be small (~1.70) which means the reactor can be controlled by other natural feedbacks (i.e., Axial and Radial Expansion).

Sodium Density/Void Feedback:

For a small liquid metal cooled reactor, such as EBR-II, this is a negative feedback, and is helpful. For the larger PRISM reactor, this is a positive feedback. As long as the sodium is subcooled, this contribution is modest. If the sodium boils, this feedback could add around five dollars of reactivity to the reactor within a few seconds.

Axial Fuel Expansion:

Metal fuel expand significantly when it heats up. Axial expansion, with-

in the cladding, increases the core size and decreases the effective density of the core materials. This increases the probability that a neutron will escape the core, giving a significant negative reactivity feedback. The size of this feedback changes after about two percent burnup, when the fuel swells in contact with the cladding. Then the axial expansion is controlled by the expansion rate of the cladding, since metal fuel has little strength.

Radial Expansion:

The radial dimension of the core is determined largely by the assembly spacing. This spacing is determined by the grid plate below the core and by two sets of load pads above the core. When the structures heat up and expand, they spread the reactor and reduce the core density - increasing leakage and thereby reducing the net reactivity.

Bowing:

When a plate is heated more on one side than the other, the heated side will expand more than the other, and the center of the plate will bow into the hotter direction. This type of behavior occurs in the LMR assemblies, and it has some reactivity contribution, but it is difficult to accurately calculate. PRISM and SAFR use the limited free bow restraint system, which limits the importance of bowing, and makes the contribution negative under conditions of interest.

Control Rod Driveline Expansion:

The control rod drive lines, which are in the upper internal structure, expand when they are heated, inserting the control rods further into the reactor, adding negative reactivity.

Vessel Expansion:

Since the control rod drives attach to the top of the vessel, and the reactor attaches to a point much lower along the vessel wall, the expansion of the vessel wall as it heats up pulls the control rods out somewhat. This is a positive feedback, but it is not a major safety factor because it is quite slow to act.

2.2 Cross-Comparison of Feedbacks

The key reactivity feedback parameters estimated by GE for PRISM have been compared to the equivalent feedbacks for SAFR, Super Phenix [IAEA, 1985], EBR-II [Feldman, 1984], and FFTF [Padilla, 1988] (the latter two were measured, i.e., estimated from experimental data), as shown in the table below. While PRISM and SAFR have strong similarities, EBR-II is much smaller, and FFTF and Super Phenix use oxide fuel. According to Hummel and Okrent (Reactivity Coefficients in Large Fast Power Reactors, American Nuclear Society, 1978), the Doppler feedback for an oxide core should be about three times larger than that for a metal core. Sodium density worth depends largely on core geometry (leakage), which explains the negative feedback in the small EBR-II core and the near-zero feedback in FFTF. Regarding radial and axial expansion, there are again strong similarities between all five reactors.

Table 1
 Reactivity Feedbacks, $\Delta k/\Delta T(K)$, [$\times 10^{-6}$]
 [Referenced to Nominal Conditions]

	<u>PRISM</u>	<u>SAFR</u>	<u>EBR-II</u>	<u>FFTF</u>	<u>SuPhx</u>
Doppler	-6.1	-4.2	-0.4	-14.6	-12.0
Na Density	6.7	5.9	-8.7	- 0.7	6.0
Radial Exp.	-6.9	-9.7	-9.3	-22.0	-10.0
Axial Exp.	-2.7	-2.9	-4.8	- 1.8	- 2.0

Because of the consistency in the various feedback parameters, it appears likely that the values cited by GE are approximately correct. However, the fact that EBR-II is obviously quite different from the other cores decreases one's confidence in extrapolating from the EBR-II test series.

The fifth reactivity feedback mechanism mentioned in Section 2.1, bowing, is difficult to estimate and thus carries large uncertainties. Fortunately, the limited-free-bow core restraint system makes the non-linear component (bowing) of the radial expansion both relatively small and negative. To date, we have ignored this feedback (which is generally conservative) and hope to be able to continue this practice.

The sixth and seventh feedbacks trace directly to the control rod worth curves and are not difficult to confirm. The principal question here is with respect to timing, i.e., how quickly do the control rod drive lines and the reactor vessel expand?

2.3 Estimating Radial Expansion Feedback [Cheng, 1988]

The small core of LMRs makes it possible to describe accurately the radial expansion reactivity in terms of a point reactor model. The present model is based on a non-leakage probability representation of the effective neutron multiplication factor:

$$k_{\text{eff}} = k_{\infty} e^{-B^2 M^2} \quad (1)$$

where k_{∞} is the infinite medium neutron multiplication factor, M^2 is the neutron migration area, and B^2 is the geometric buckling.

Consider a point reactor with appropriate average properties. We shall use one-group model for neutron cross sections (properly averaged over the entire neutron spectrum in the reactor core). In the one group model, k_{∞} is given by:

$$k_{\infty} = \frac{\nu \sum_f}{\sum_a} = \frac{\nu N \sigma_f}{N \sigma_a} \quad (2)$$

where N is the average atom density in the core. The migration area M^2 is defined as [Duderstadt, 1976]:

$$M^2 = \frac{1}{3 \sum_{tr} \sum_a} = \frac{1}{3N^2 \sigma_{tr} \sigma_a} \quad (3)$$

with σ_{tr} being the microscopic transport cross section and σ_a the microscopic absorption cross section.

The geometric buckling B^2 is the key to the present model. For a cylindrical core of radius R and height H , the geometric buckling is given by [Lamarsh, 1966]:

$$B^2 = \left(\frac{\pi}{H}\right)^2 + \left(\frac{2.405}{R}\right)^2 \quad (4)$$

where \tilde{R} and \tilde{H} are the extrapolated radius and height of the core, respectively.

Consider a reference critical reactor at steady state. Using Eq.(1) for the reference state with the subscript o , we have:

$$k_o = k_\infty e^{-B_o^2 M_o^2} \quad (5)$$

The perturbed reactor after the radial expansion has a multiplication factor of:

$$k = k_\infty e^{-B^2 M^2} \quad (6)$$

Note that k_∞ remains unchanged due to the radial expansion because the radial expansion affects primarily the atom density N which appears in both the numerator and denominator of k_∞ as seen in Eq. (2). The effect of the radial expansion on k_∞ thus cancels out. It should be mentioned that the radial expansion also effects the neutron spectrum and hence the microscopic cross sections in Eq. (2). This is, however, a secondary effect and neglected in the present model.

$$\rho_{RX} = \frac{k - k_o}{k} = 1 - e^{(B^2 M^2 - B_o^2 M_o^2)} \quad (7)$$

One clear observation is that radial expansion reactivity is always negative since $B_o^2 M_o^2 < B^2 M^2$ if the core is expanded due to thermal expansion and assembly bowing.

The definition of the atom density is important to the present model. It is defined as:

$$N = N_A \left(\frac{M_a}{VA}\right) \quad (8)$$

where N_A is the Avogadro's number (6.023×10^{23}), A is the atomic weight of the material composition in the core, M_a is the total mass of the reactor core, and V is the volume of the core:

$$V = \pi \tilde{R}^2 \tilde{H} \quad (9)$$

Substituting Eq. (8) into Eq. (3) we obtain an expression for the migration area M^2 :

$$M^2 = \frac{1}{3 \sigma_{tr} \sigma_a} \left(\frac{A}{N_A M_a} \right)^2 v^2 \quad (10)$$

We now define α as the linear thermal expansion coefficient, ΔT_R as the temperature change in core material in the radial direction, and ΔT_z as that in the axial direction. Using these parameters, we can specify the core radius and height under the altered temperature conditions:

$$\tilde{R} = \tilde{R}_o (1 + \alpha \Delta T_R) \quad (11)$$

$$\tilde{H} = \tilde{H}_o (1 + \alpha \Delta T_z) \quad (12)$$

By substituting Eqs. (11) and (12) into Eq. (9) we obtain an expression for the altered core volume V :

$$V = \pi \tilde{R}_o^2 (1 + \alpha \Delta T_R)^2 \tilde{H}_o (1 + \alpha \Delta T_z), \quad (13)$$

which is then substituted into Eq. (10) to get:

$$M^2 = C \tilde{R}_o^4 \tilde{H}_o^2 (1 + \alpha \Delta T_R)^4 (1 + \alpha \Delta T_z)^2, \quad (14)$$

where

$$C = \frac{\pi^2}{3} \frac{A}{M_a^2} \frac{1}{N_A^2 \sigma_{tr} \sigma_a} \quad (15)$$

Here we have assumed that the core mass M_a remains constant. This is a good assumption because, as temperature increases, the density decreases and the volume increases so that the mass tends to stay constant.

The expressions in Eqs. (4) and (14) are multiplied to obtain an expression for $B^2 M^2$:

$$B^2 M^2 = C (1 + \alpha \Delta T_R)^4 (1 + \alpha \Delta T_z)^2 * \left\{ \pi^2 \tilde{R}_o^4 \left(\frac{\tilde{H}_o}{\tilde{H}} \right)^2 + 5.784 \tilde{R}_o^2 \tilde{H}_o^2 \left(\frac{\tilde{R}_o}{\tilde{R}} \right)^2 \right\} \quad (16)$$

From Eqs. (11) and (12):

$$\left(\frac{\tilde{R}}{R_0}\right)^2 = (1 + \alpha\Delta T_R)^2 \quad (17)$$

$$\left(\frac{\tilde{H}}{H_0}\right)^2 = (1 + \alpha\Delta T_z)^2 \quad (18)$$

Then Eqs. (17) and (18) are substituted into Eqs. (16) to obtain:

$$B^2M^2 = CR_0^2(1 + \alpha\Delta T_R)^2 \{ \pi^2\tilde{R}_0^2 (1 + \alpha\Delta T_R)^2 + 5.784 \tilde{H}_0^2 (1 + \alpha\Delta T_z)^2 \} \quad (19)$$

The expression for B^2M^2 provided in Eq. (19) is for expansion in both the radial and axial directions. To evaluate the contribution due to radial expansion, we set the axial expansion term, ΔT_z , to zero leaving:

$$B^2M^2 \approx CR_0^2(1 + \alpha\Delta T_R)^2 \{ \pi^2\tilde{R}_0^2(1 + \alpha\Delta T_R)^2 + 5.784\tilde{H}_0^2 \} \quad (20)$$

From Eq. (20), we can also identify $B_0^2M_0^2$ by setting ΔT_R to zero:

$$B_0^2M_0^2 = CR_0^2 \{ \pi^2\tilde{R}_0^2 + 5.784 \tilde{H}_0^2 \} \quad (21)$$

Thus, by subtracting Eq. (21) from Eq. (20) we find the exponent in Eq. (7):

$$B^2M^2 - B_0^2M_0^2 = CR_0^4\pi^2\{(1 + \alpha\Delta T_R)^4 - 1\} + CR_0^2 \cdot 5.784 \tilde{H}_0^2 \{(1 + \alpha\Delta T_R)^2 - 1\} \quad (22)$$

Substituting Eq. (22) into Eq. (7) yields an analytical expression for the radial expansion reactivity worth:

$$\rho_{RX} = 1 - e^{\{C_1[(1 + \alpha\Delta T_R)^4 - 1] + C_2[(1 + \alpha\Delta T_R)^2 - 1]\}} \quad (23)$$

where

$$C_1 = \pi^2\tilde{R}_0^4 C \quad (24)$$

$$C_2 = 5.784 \tilde{R}_0^2 \tilde{H}_0^2 C \quad (25)$$

and

$$C = (1/3) \left\{ \frac{\pi A}{M_a N_a} \right\}^2 \frac{1}{\sigma_{tr} \sigma_a} \quad (26)$$

In the present model, it is essential to obtain the core average param-

eters in Eq. (26). To this end, one must consider all the material compositions in the core. The PRISM core consists of the fuel (U-26 w/o Pu-10 w/o Zr), the structure (HT-9), the coolant (Na), the radial shields (HT-9) and the control assemblies (B₄C) as shown in Figure 3. The SAFR core is comprised of the fuel (U-26 w/o Pu-10% Zr), the structure (HT-9), the coolant (Na), the stainless steel radial shields, the B₄C radial shields, and the control assemblies (B₄C) as shown in Figure 4.

The core average atomic weight is obtained from the atomic weight of various materials via mass weighting:

$$A = \frac{\sum_n \rho_n V_n A_n}{\sum_n \rho_n V_n} \quad (27)$$

where ρ_n is the density of material n, V_n is the volume occupied by the material n, and A_n is the atomic weight of material n which is computed from the atomic weights of isotopes in material n.

The one-group microscopic cross sections, σ_{tr} and σ_a , of various isotopes are obtained from [Wirtz, 1978]. The core average σ_{tr} and σ_a are defined in terms of those of the material compositions in the core:

$$\sigma_j = \frac{\sum_n \phi_n V_n \sigma_{j,n}}{\sum_n \phi_n V_n} ; j = tr, a \quad (28)$$

where ϕ_n is the average neutron flux in the material n.

The core mass is computed from the volumes occupied by various materials in the core as follows:

$$M_a = \sum_n \rho_n V_n \quad (29)$$

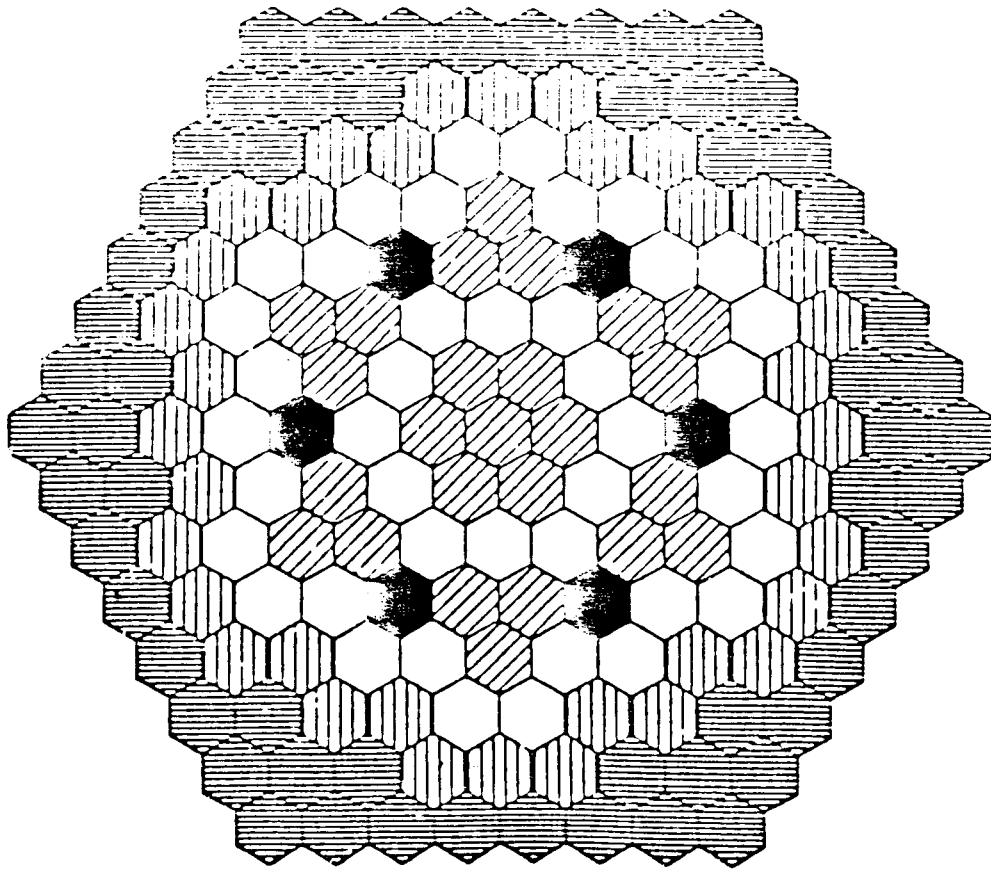
where the material volume V_n is given by:

$$V_n = \sum_i N_i VF_{i,n} V_{hex} \quad (30)$$

Here i is the assembly type (e.g. driver fuel, internal and radial blankets, and radial shields). N_i is the number of assembly type i , $VF_{i,n}$ is the volume fraction of material n in assembly i , and V_{hex} is the volume of a hexagonal assembly:

$$V_{hex} = 0.86602 b^2 H \quad (31)$$

with b being the flat-to-flat length of the hexagonal assembly.








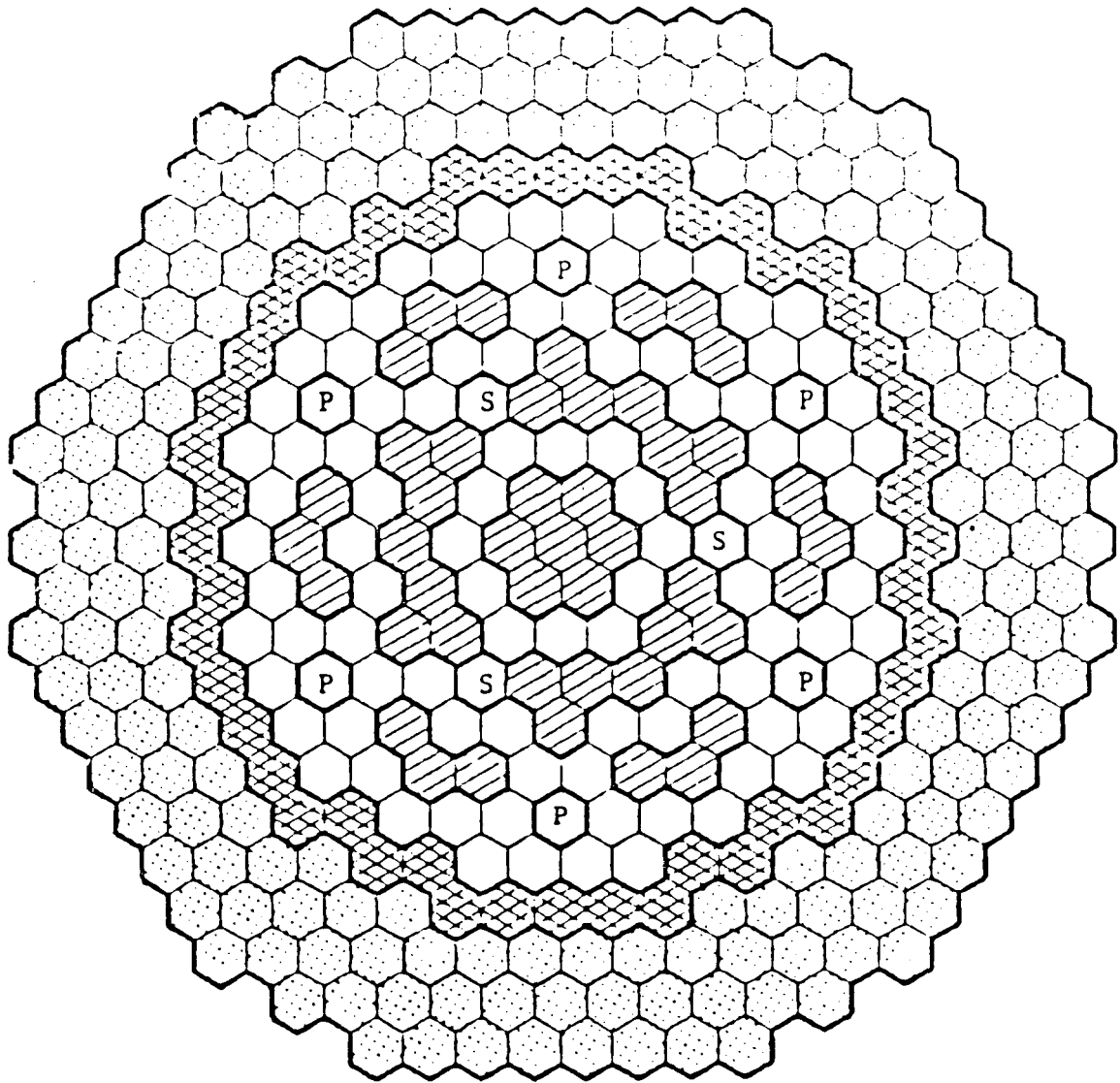
	FUEL	42
	INTERNAL BLANKET	25
	RADIAL BLANKET	36
	RADIAL SHIELD	60
	CONTROL/SHUTDOWN	6
		<hr/>
	TOTAL	169

Figure 3 PRISM Core Layout









- | | | | |
|---|-----------------------|---|---|
|  | Driver (96) |  | Steel Reflector (54)
B ₄ C Shield (126) |
|  | Internal Blanket (46) |  | Primary Control (6) |
|  | Radial Blanket (48) |  | Secondary Control (3) |

Figure 4 SAFR Core Layout

The material densities used are obtained from [Hofman, 1985]:

$$\rho_{\text{HT9}} = 7.76 * (1.00634834 - 1.285972 \times 10^{-5} T - 3.144763 \times 10^{-8} T^2 + 1.06236 \times 10^{-11} T^3) \quad (32)$$

$$\rho_{\text{fuel}} = 16.06509 - 8.12202 \times 10^{-4} T - 1.01005 \times 10^{-7} T^2 \quad (33)$$

$$\rho_{\text{Na}} = 1.0118 - 0.22054 \times 10^{-3} T - 1.9226 \times 10^{-8} T^2 + 5.637 \times 10^{-12} T^3 \quad (34)$$

where the density is in unit of g/cc and T in °K.

The thermal expansion in the core is considered to be due primarily to the structure material (HT-9). The linear expansion coefficient of HT-9 is given by [Hofman, 1985]:

$$\begin{aligned} \alpha &= 10^{-6} * (4.286596 + 0.0209651 T - 1.0624 \times 10^{-5} T^2) \\ &\quad \text{for } 293^\circ\text{K} \leq T \leq 650^\circ\text{K} \\ &= 14.587 \times 10^{-6} \quad \text{for } T \geq 650^\circ\text{K} \end{aligned} \quad (35)$$

where α is in K^{-1} and T in °K.

The simple analytical model described above was used to evaluate the radial expansion reactivity for both PRISM and SAFR. The cylindrical cores of PRISM and SAFR are comprised of hexagonal fuel assemblies as shown in Figure 3 for PRISM and Figure 4 for SAFR, respectively. The structural material used in both PRISM and SAFR is HT-9 alloy. The temperature dependence of the thermal expansion coefficient and density were taken into account as shown in Eqs. (32) through (35).

The results of calculations using the present analytical model are presented in Figure 5. It is seen that the radial expansion reactivity exhibits a fairly linear behavior. The data shown in Figure 5 were least-square fitted with a linear regression analysis. The slopes of these fitted curves are summarized below along with the values reported by vendors:

	<u>PRISM (\$/cm)</u>	<u>SAFR (\$/cm)</u>
This work	-2.368	-1.706
GE	-2.294	
RI		-1.630

The agreement is quite good (+3% for PRISM and +5% for SAFR).

-15-116

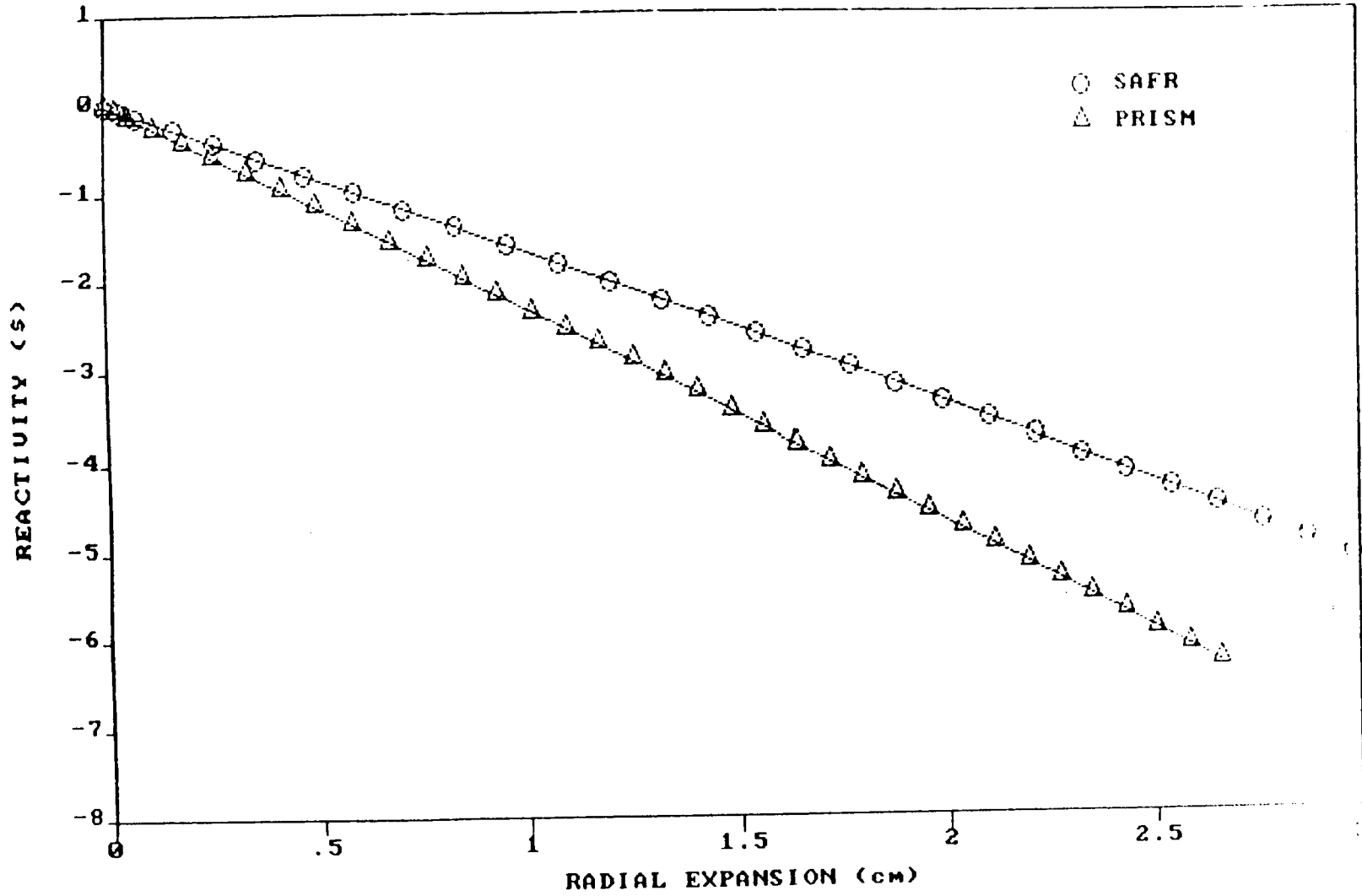
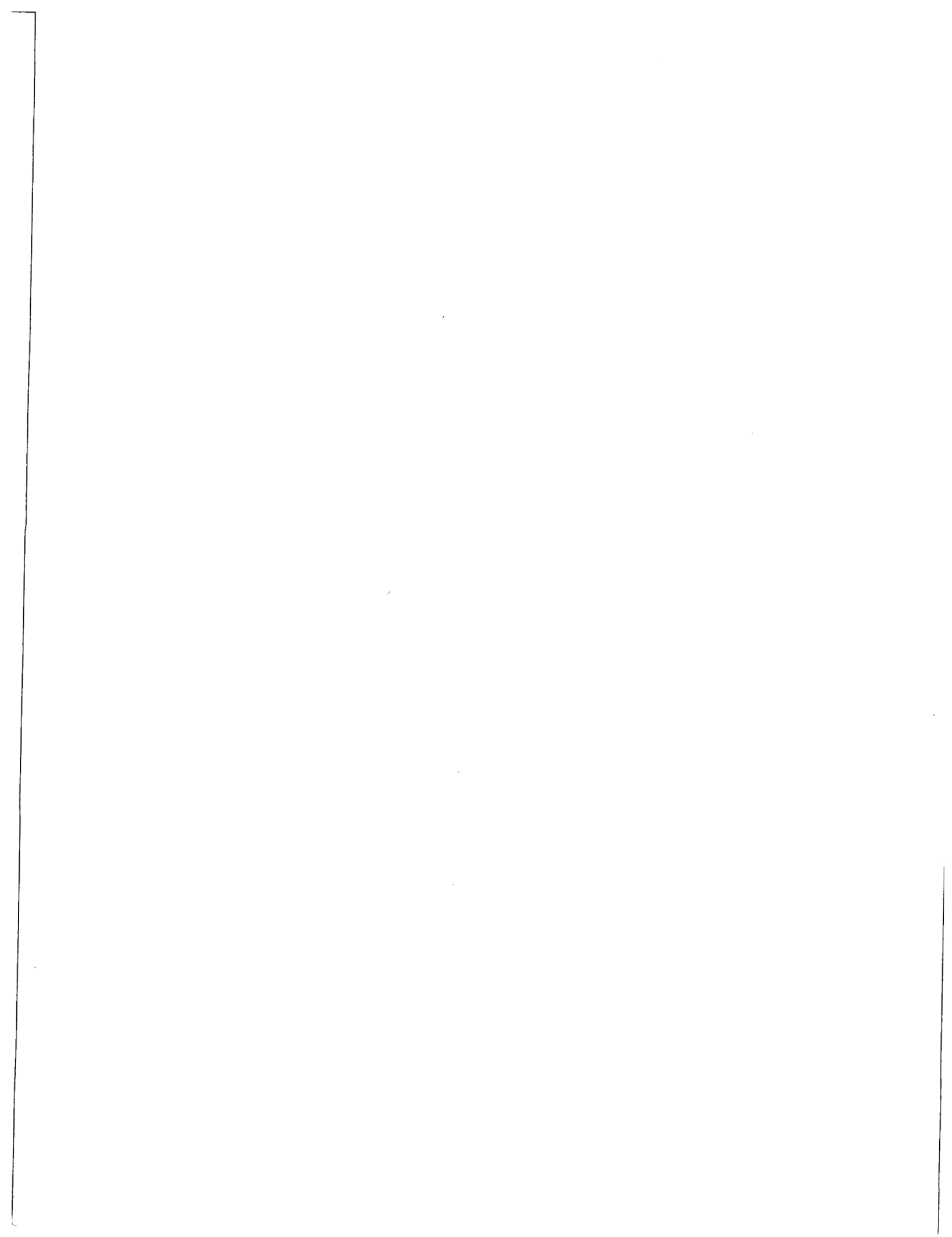


Figure 5 Radial Expansion Reactivity for PRISM and SAFR



3. TRANSIENT MODELS

Two different codes were used in this analysis for complimentary purposes. SSC [Guppy, 1983] was developed at BNL, for analyzing LMR transients. SSC models core regions in detail, as well as the primary system, the IHX, intermediate loop, steam generator, and the major components of the ternary loop. However, there are features of the primary flow circuit that can not be represented accurately by the current version of the SSC, so we use the MINET Code [Van Tuyle, 1984] for that part of the analysis.

3.1 SSC Modeling

The basic representation indicated in Figure 6 was used for both PRISM and SAFR. The head curves for both pump types are modeled in SSC using a table lookup. The core was represented using seven channels: fuel (or driver), internal blanket, radial blanket, control assembly, shield assemblies, hot driver, and hot internal blanket. Each channel has two axial nodes below the fuel, six axial nodes in the fuel region and four nodes to represent the upper gas plenum.

Reactivity Feedbacks

As the temperature increases during an event, the negative feedbacks from the radial expansion, grid plate expansion, axial expansion, Doppler, and control rod driveline expansion are activated, and these generate a net negative reactivity for the core. These feedbacks respond according to their associated time constants, to overcome the positive reactivity from the sodium density effect and any external source. Because of the small Doppler feedback in metal fuel, and the correspondingly small temperature defect, the drop in power can be quite large. With the smaller Doppler feedback, the metal fuel cores could be vulnerable to reactivity insertion events. However, inserted rod worth is minimized by a near zero reactivity swing, so the potential reactivity additions from rod withdrawal are quite small. Each of the important reactivity feedbacks are discussed below.

Doppler

Doppler feedback is generally the fastest acting feedback mechanism since it is almost instantly affected by core power level. Doppler removes reactivity from the system as the temperature rises and can thus help limit the extent of power increases. As the fuel temperature drops with a power reduction, Doppler adds reactivity and tends to limit the power decrease.

Each of the six axial levels in the SSC fuel representation was given equal weight and was referenced to the cold shutdown temperature. The Doppler coefficient is given in the form of:

$$\alpha = T \frac{dK}{dT}$$

which lead to the reactivity equation for the Doppler as:

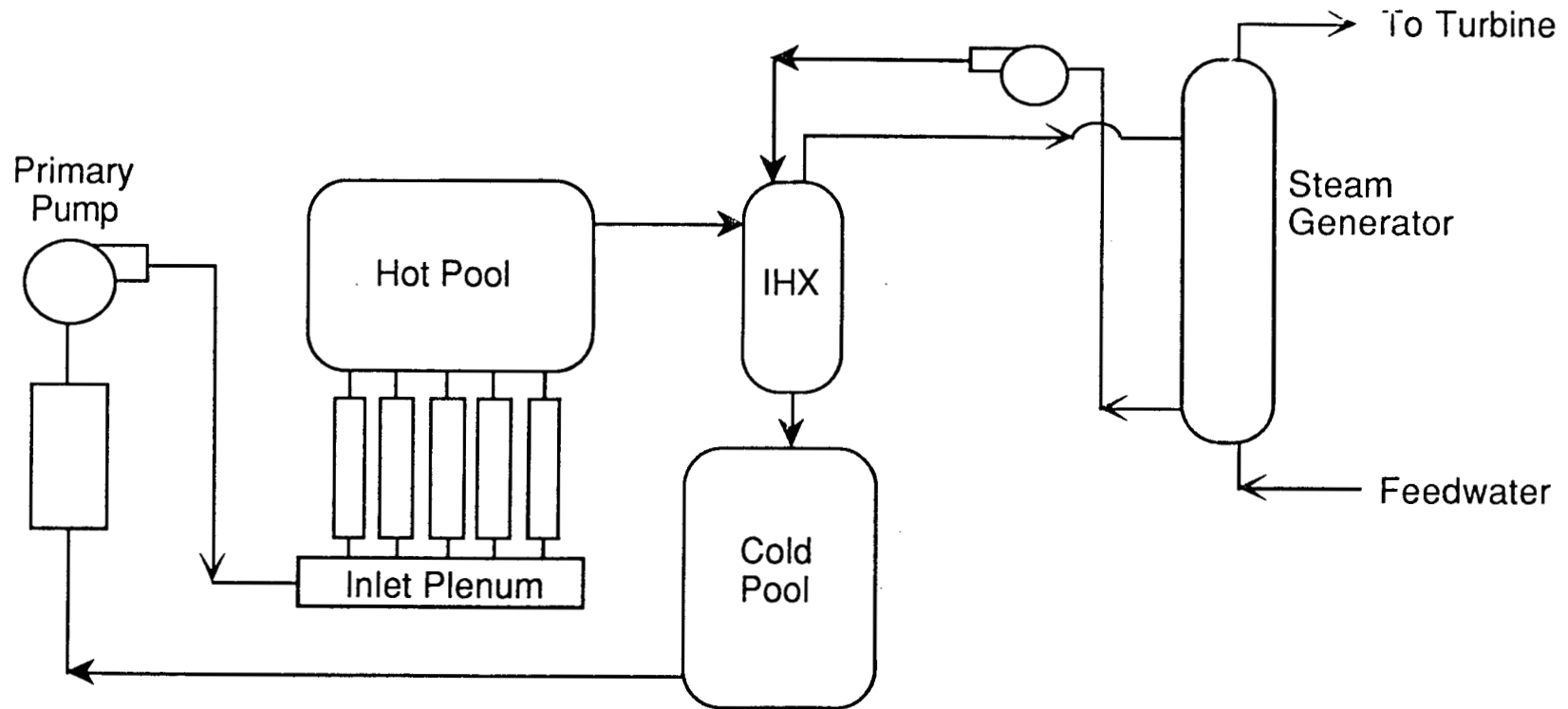


Figure 6 SSC Schematic of SAFR (and PRISM)

$$\rho_R(t) = \sum_{i=1}^3 \sum_{j=1}^6 \alpha_i \cdot \ln \left(\frac{T_{AVj}}{T_{Ref}} \right) - \rho_{Ro} \quad (36)$$

- K = Multiplication factor
 α_i = Node Weighted Doppler Coefficient
 T_{AV} = Average Node Fuel Temperature
 T_{Ref} = Reference Fuel Temperature
 j = 6 Axial Levels in the Fuel Channel
 i = 3 Different Fuel Channels (i.e., driver, internal blanket, and radial blanket)
 ρ_{Ro} = Steady-State Reference Value for Doppler Reactivity

where the standard definition of neutronic reactivity is defined as:

$$\rho = \frac{K - 1}{K}$$

By definition, the reactivities are referenced to zero at $t=0.0s$.

Fuel Thermal Expansion

The fuel thermal expansion is a relatively fast acting feedback mechanism. The radial fuel slug thermal expansion is accommodated within the pin and does not affect the core reactivity significantly. Axial fuel expansion increases the core height as temperatures rise, and changes the reactivity of the system by increasing the neutron leakage. The result is a rapid negative feedback contribution from an increase in fuel temperature, or a rapid positive feedback in response to a decrease in fuel temperature.

The ternary U-Pu-Zr fuel swells out to contact the cladding (HT9) material around 2-3% atom burnup. After the fuel-clad "lockup" occurs, the fuel thermally expands according to the thermal expansion of the clad material. This is because the strength of metal fuel is very limited, and thus its expansion is dominated by the clad expansion. Experiments have shown that a 4% axial elongation is possible in the 1.9 to 5.3 % burnup range. More experiments are scheduled to be run in the future.

All analyses performed using SSC assumed that the fuel is in contact with the HT9 clad. This is the most likely state for the equilibrium core since only 25% of the core will be reloaded at each refueling, and the fuel is in an unlocked state only briefly. The fuel elongations in SSC calculations were calculated by using an average strain, weighted with Young's modulus:

$$\epsilon = \frac{\epsilon_f Y_f A_f + \epsilon_c Y_c A_c}{Y_f A_f + Y_c A_c}$$

where

ϵ = strain ($\Delta l/l$)
 Y = Young's Modulus
 A = Nominal cross sectional area
subscript c = clad
 f = fuel

The PRISM evaluation was performed using Eq. (36), interpolating between its initial fuel length and its elongated length at any given time. Each region was power weighted. The SAFR feedback was evaluated by using the form:

$$\rho_A(t) = \sum_{i=1}^3 \alpha_i \sum_{j=1}^6 (L_{1j} - L_{0j}) - \rho_{A0} \quad (37)$$

ρ_A = axial expansion feedback
 L_{1i} = new elongated length
 L_{i0} = initial length at cold conditions
 ρ_{A0} = steady-state value of feedback

 α_i = fuel axial expansion reactivity coefficient for channel i
 i = reactivity contribution from driver, internal and radial blanket
 j = segments in the fuel

These two different methods to calculate the reactivity feedback, (i.e., Eq. (36) versus Eq. (37)) are needed to accommodate the differences in the way each designer supplied his reactivity coefficients.

Sodium Density Feedback

Thermal expansion of the sodium is the only significant positive reactivity feedback. The thermal expansion results in fewer sodium atoms within and surrounding the core. The reduced density surrounding the core results in fewer neutrons being scattered back into the core, and produces a small negative feedback effect by increasing the leakage around the periphery. However, the dominant effect is to reduce the collisions between neutrons and sodium atoms, which hardens the neutron energy spectrum and yields a net positive reactivity feedback effect.

The feedback formulation was of the same form as Eq. (36) for both PRISM and SAFR. The reference density was at the refueling temperature. Each node was given equal weighting.

Control Rod Drive Line and Vessel Thermal Expansion

Both of the advanced designs have taken advantage of the thermal expansion of the control rod drive line. The worth of this expansion is highly dependent upon the initial position of the primary control rods. The current PRISM design includes a stop for the primary control rods at the 10% insertion point. The SAFR design allows the control rods to be completely removed.

Both designs also have control rod drive lines made of SS316, since the corresponding thermal expansion coefficient is 30% greater than that of HT9. The SAFR design utilizes a flow collector below its Upper Internal Structure (UIS) to direct hot channel sodium flow across the drive lines. PRISM has the UIS designed such that the drive lines are positioned outside the structure where they are exposed to the mixed sodium temperature exiting the core.

The thermal expansion of the reactor vessel ultimately limits the amount of negative reactivity inserted by the control rod drive line. The reactor vessel is cantilevered from the top and expands down and slowly withdraws the control rods from the core. Fortunately the time constant for the reactor vessel is about 700s, while the control rod drive line expansion time constant is around 28s. Thus, the initial response to increased sodium outlet temperatures is a negative feedback, while the long term effect could end up being positive.

Control rod and vessel expansion are calculated in SSC using single node temperatures for the vessel and control rod drive line masses. The total elongated length is calculated by subtracting the vessel expansion from the control rod drive line expansion to determine the net control rod expansion into the core. No credit was taken for the fact that the fuel is also expanding axially into the control rods. Finally, it should be mentioned that, in SSC, the flow collector for the control rod drive line in SAFR was assumed to collect 86% of its flow from neighboring driver assemblies and only 14% from the control assembly. The worth of the expansion was determined by using a form of Eq. (37).

Radial Dilation

The radial expansion of the core is a result of thermal expansion, as well as the design of the core and restraint system. The core assemblies are restrained at three locations: the inlet nozzle, the above core load pad (ACLP), and the top of the core load pads (TLP). These locations are shown in Figure 7. The TLPs are restrained at the core edge by the core former ring. The ACLPs are not restrained at the core edge. The inlet nozzles are inserted into the inlet modules which are fixed by the inlet grid plate. This restraint system is called the "limited free bow" design.

The radial power profile across the core results in a decreasing temperature gradient from center to periphery. The side of the assembly duct facing the core center is hotter than the side away from the core center, so that the differential thermal expansion of the duct tends to cause the assembly to take a shape that is convex to the core center line, as shown in Figure 7. The interaction between adjacent assemblies and core restraint system forces the core to deflect outward and reduces the neutronic efficiency of the core. This is because the assembly tries to "flower" outward but is constrained by the top load pads and top former ring to maintain its radial position at the top of the assembly. Core compaction would then result in the region of the active core if it were not for the above core load pads, which stop the inward movement at their elevation. The movement caused by the rigid ACLP produces a reverse deflection on the assembly, which results in outward bowing in the active core region as the temperatures are increased and, therefore, a negative

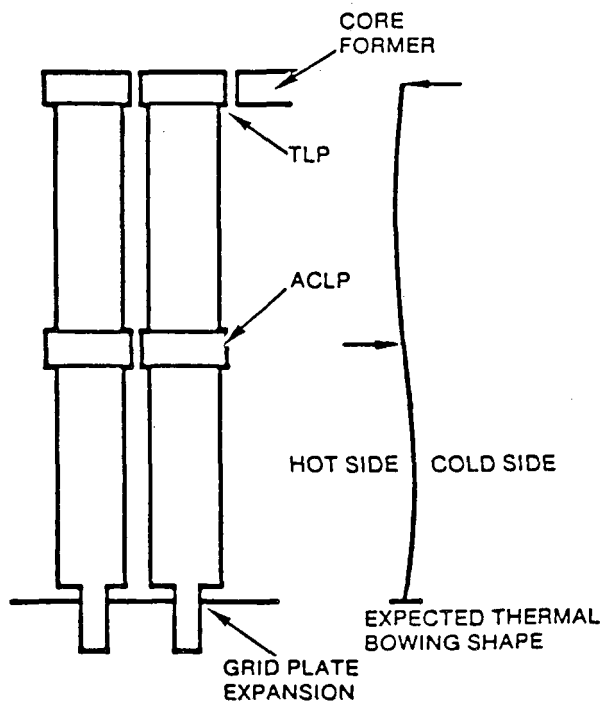


Figure 7 Restraint System and Expected Shape from the Limited Free Bowing and Design

bowing reactivity feedback. In addition there is an overall expansion at the ACLP plane due to the increased core temperatures. The duct region is thin and has a small heat capacity, causing the bowing feedback effect to respond within a few seconds. The effect of this growth in volume and outer surface area of the core is to increase the loss of neutrons from the core region through the surface area. This causes a reduction in core reactivity.

The reactivity of the system is also reduced by the thermal expansion of the core. An increase in temperature causes a reduction in reactivity because of the increase in neutron leakage (larger total mean free path) from the changes in core density and surface area. This results from changes in the coolant, fuel, and duct wall temperatures.

In the SSC calculation, no credit was given for the thermal bowing of the assemblies. It is noted that its effect may reduce the risk associated with several severe accident sequences. However, the total worth of the (limited-free) bowing carries significant uncertainties. Bowing should add negative reactivity to the system. At this time, it doesn't appear that bowing can insert any positive reactivity during any portion of the accident reviewed to date. Hence, neglecting it is a conservative assumption.

SSC tracks the radial expansion of the core from thermal expansion only. This is accomplished by tracking the structure temperatures at the above core load pads (just above the fueled area) and at the grid plate. Each assembly that passes through a slice in the core is monitored. At every time step a new radius at the above core load pads is calculated and compared to its steady-state value. Either Eq. (36) or Eq. (37) is used to find the reactivity feedback, consistent with the type of coefficient supplied.

The coefficients supplied for radial expansion were calculated using a uniform increase over the core radius. However, the above core load pad (ACLP) responds to the core exit sodium temperature while the grid plate responds to the core inlet temperature. This causes non-uniform expansions, and the worth of each component must be weighed. From geometrical considerations, the split for PRISM is 65% from ACLP and 35% from grid plate. In SAFR, the split is 70% ACLP and 30% grid plate.

3.2 MINET Modeling

The MINET code [Van Tuyle, 1984] was used to perform the thermal hydraulic evaluations that involve significant re-distribution in sodium flow within the core inlet network. The approximate configuration of the components within the reactor vessel can be inferred from Figure 8, which is a schematic drawing of the current MINET representation of both systems. Hot sodium flow exits the core and passes into the hot pool. Hot primary sodium transfers heat into the intermediate loop sodium while flowing down through the intermediate heat exchangers (IHXs) into the cold pool. The pumps draw sodium from the cold pool and drive it through two headers and eight pipes into the inlet plenum and into the core. There are no valves in the primary system and all valves shown in Figure 8 are solely for simulating postulated breaks and associated flow paths. (There are additional features in the MINET representation for simulating the emergency cooling system overflow, as well as leaks into and out of the containment vessel.)

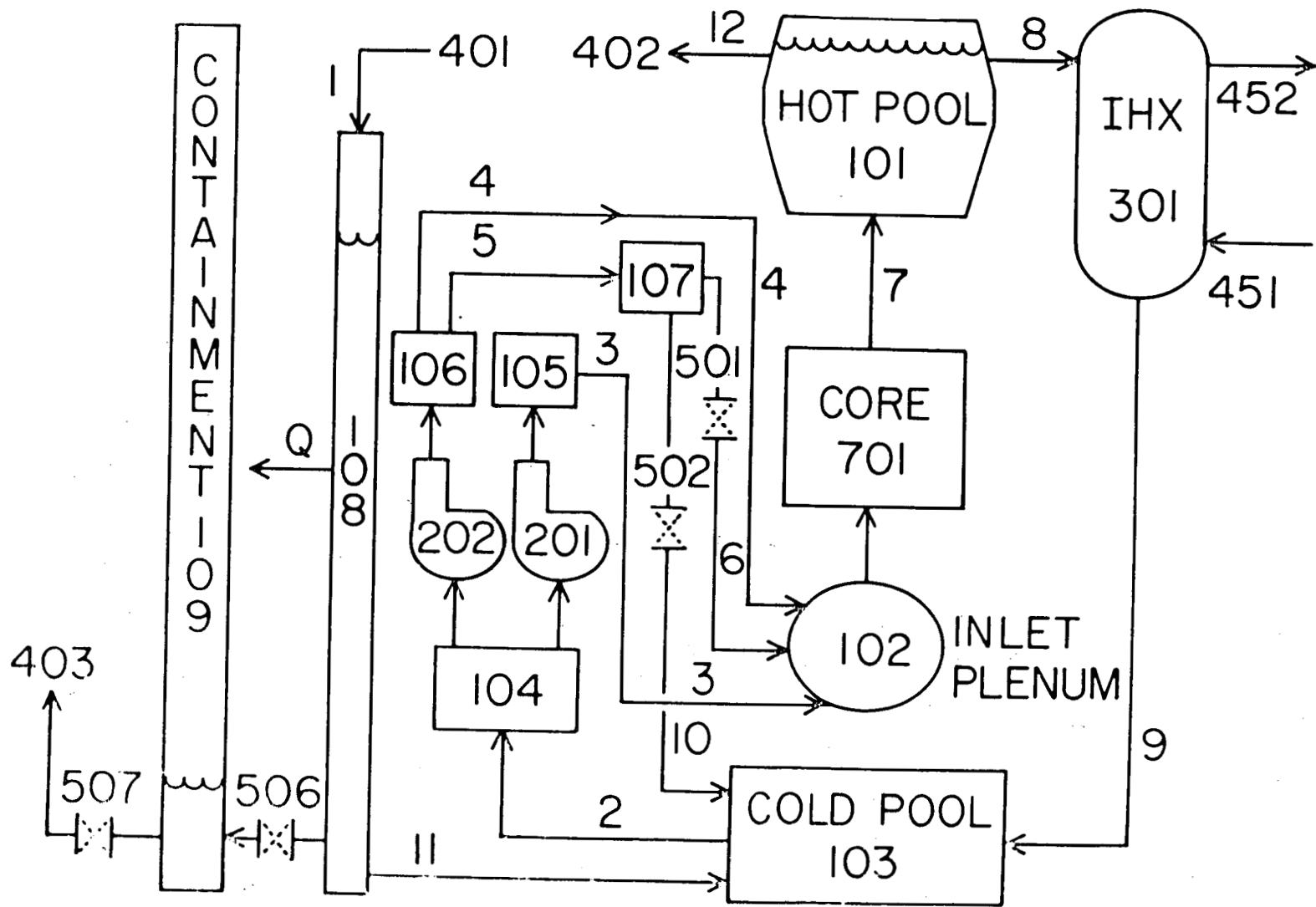


Figure 8 Schematic Representation of PRISM and SAFR Used in MINET Pipe Break Analysis

4. PRISM UNSCRAMMED EVENTS

The transient responses of the PRISM reactor system to various unscrammed events were evaluated using SSC and, to a lesser degree, MINET. In nearly every case, the BNL calculational results were very similar to those submitted by GE.

Six unscrammed events are covered in this section. The first three, i.e., the loss of heat sink (LOHS), the transient-over-power (TOP), and the loss of flow (LOF), are the more likely events and form the basic BDBE events (design basis events without scram). Three less likely events were also analyzed, including a combined TOP/LOF, an unscrammed pipe break (one of eight) event, and an unscrammed LOF missing one pump coastdown.

4.1 Loss of Heat Sink (LOHS) BDBE

This event is initiated by a sudden stoppage of the immediate loop flow. Physically this would be equivalent to the intermediate loop sodium being dumped into the IHTS dump tank during a sodium/water reaction event, with the reactor system failing to scram.

The power history, along with the core flow, as predicted by SSC is shown in Figure 9. The power remains level for about 30 s before the increased temperatures reach the core and trigger the feedbacks. The increase in temperature at the inlet plenum causes grid expansion (which has the highest negative worth) and sodium density reduction, as indicated in Figure 10. The figure shows that the negative feedbacks outpace the positive ones and decrease the power to 9% by 350 s. The total reactivity settles in at -15 cents, which forces the power down until it reaches decay heat levels. The radial expansion term includes both the ACLP and grid plate dilation and is the dominant mitigating feedback.

The GE results are similar, but predict a faster power drop since their total reactivity was more negative than that calculated using SSC. Some of the difference comes from the axial fuel expansion, where GE assumes the fuel is not bound to the cladding. The control rod drive line also showed a maximum value of -10 cents during the event before the vessel expansion began pulling the rods outward. The SSC results showed no control rod drive line negative feedback and a positive effect when the vessel elongates. However, the grid plate expansion inserts enough negative reactivity to override these lesser differences, and causes the two simulations to produce similar results.

The peak temperatures predicted during this event had large safety margins. In Figure 11 the maximum sodium temperature from the average driver and the hot driver are plotted against the sodium saturation temperature. The margin to boiling was found to be 470 K (846°F), which was close to the 484 K (872°F) found in the GE calculation. As seen in Figure 12, the peak fuel center line temperature in the hot driver was 1004 K (1348°F), which is close to the 1025 K (1385°F) determined by GE. The margin to fuel melting was 362 K (652°F). No clad damage is expected from the low temperatures estimated to occur during this event.

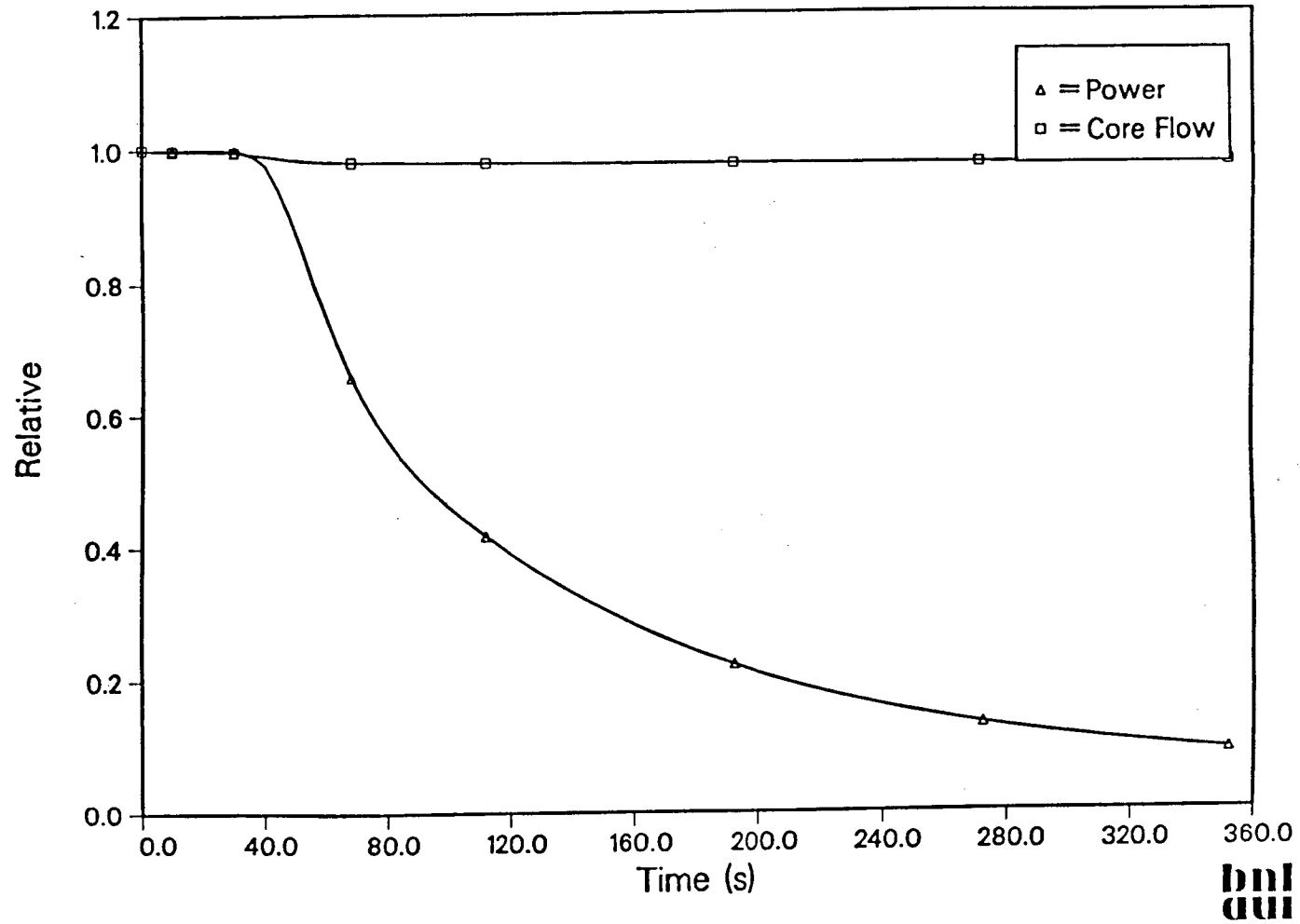


Figure 9 SSC Prediction for PRISM ULOHS for Power and Core Flow

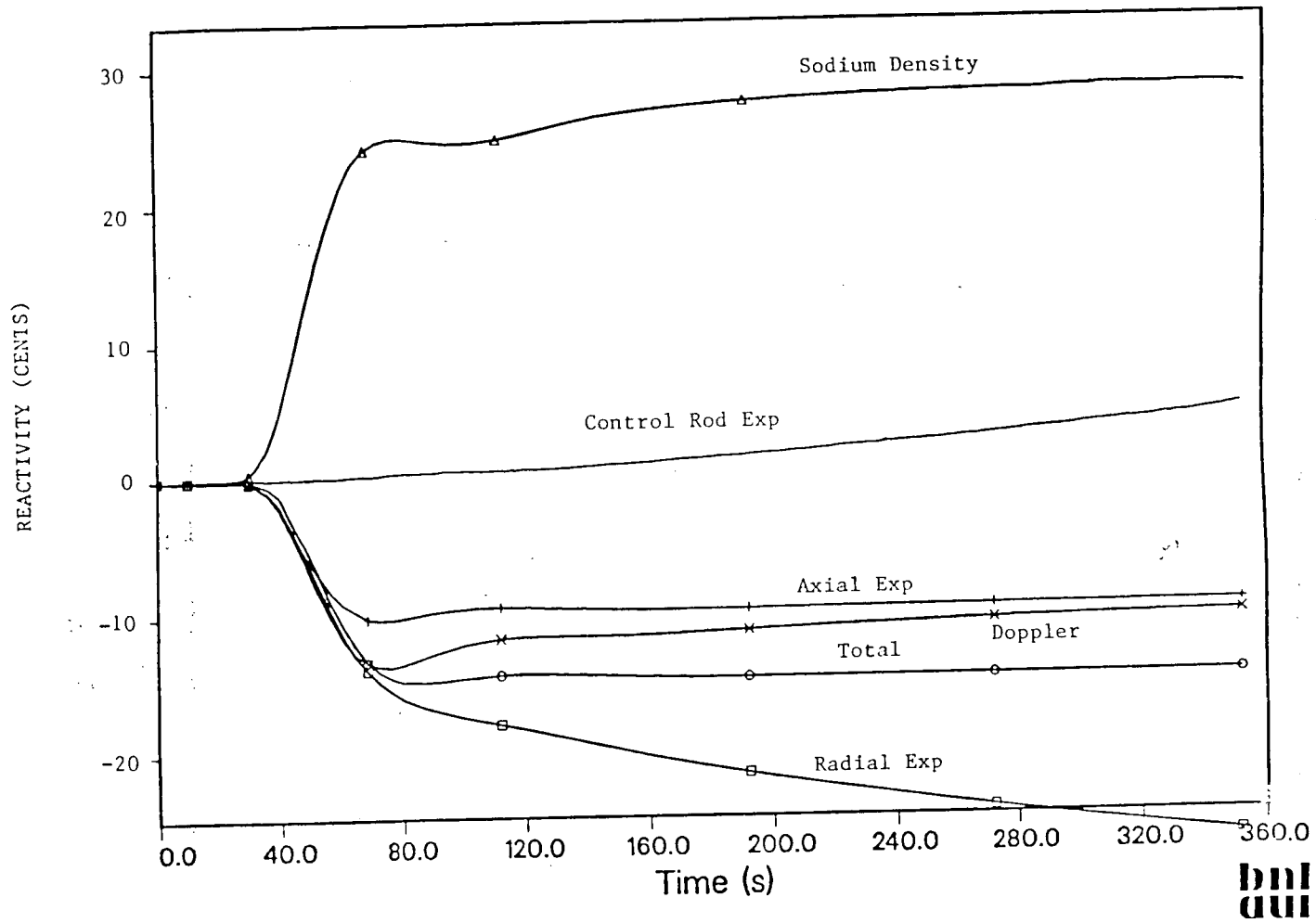


Figure 10 Reactivity Feedbacks for ULOHS from SSC



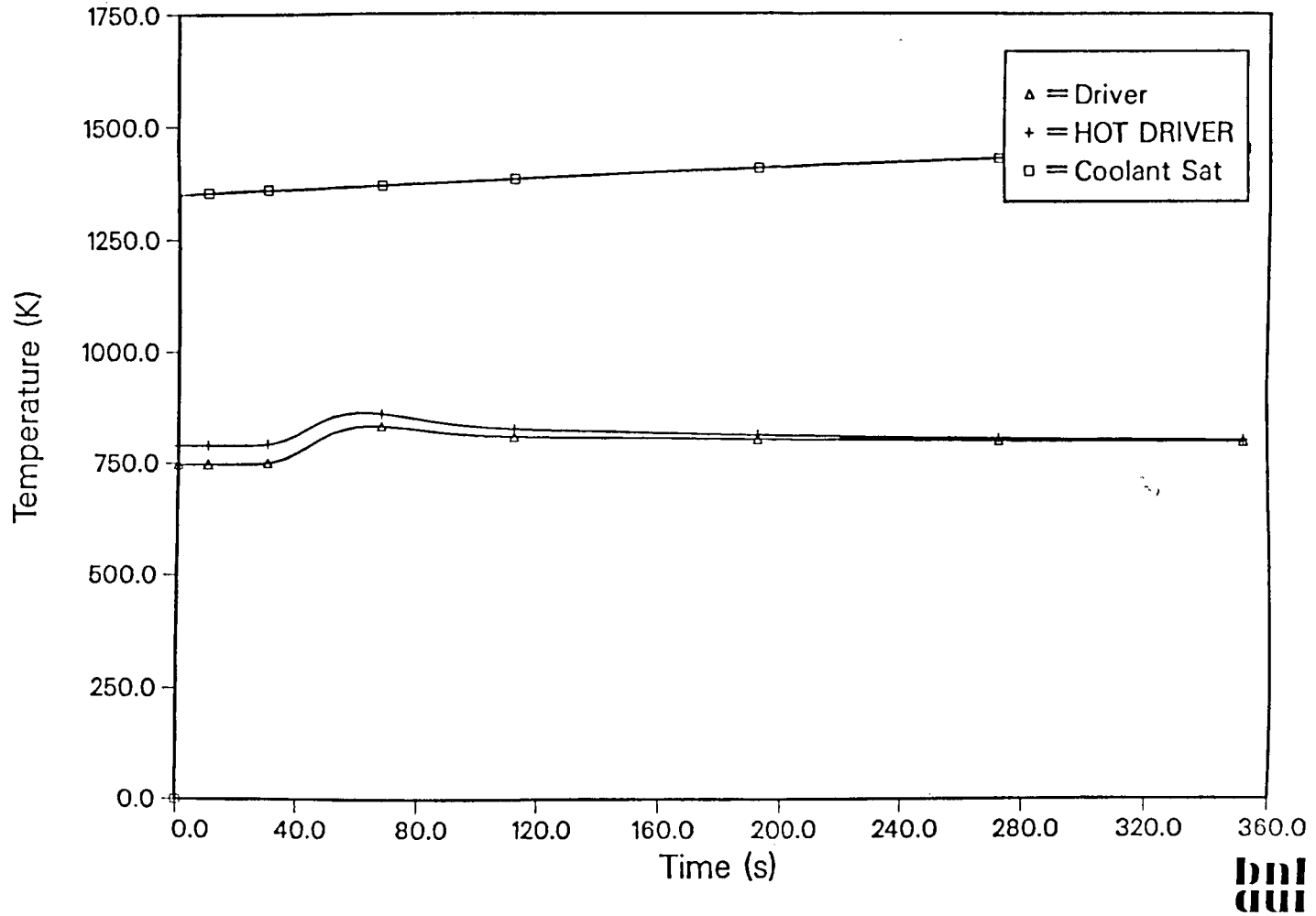


Figure 11 Peak Average and Hot Driver Assembly Coolant Temperatures Compared to the Saturation Temperature

bnl
at

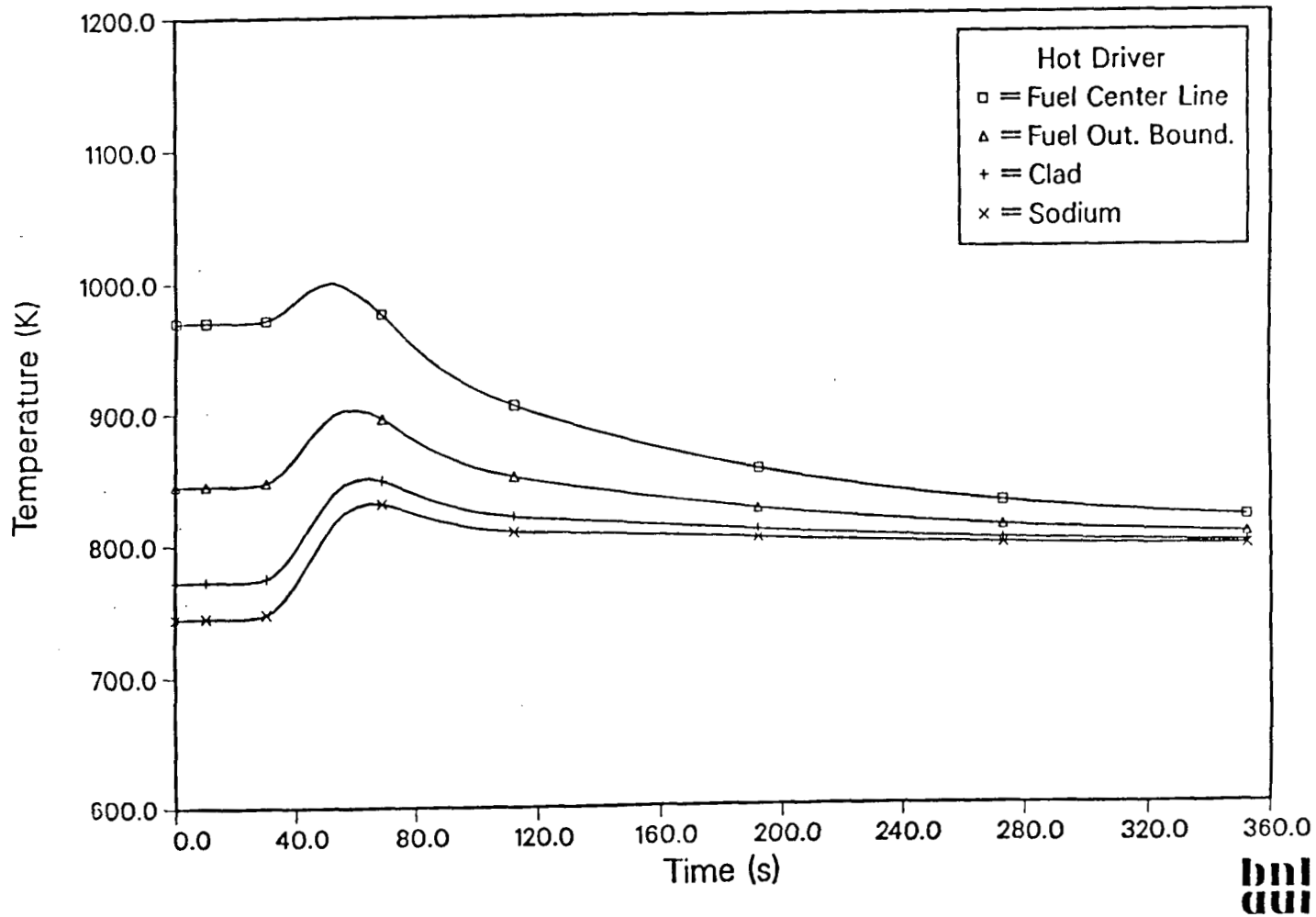


Figure 12 Fuel Temperature Distribution at Peak Location for ULOHS

4.2 Reactivity Insertion (TOP) BDBE Analysis Using SSC

A spurious signal is assumed to cause all six control rods to be withdrawn from the core, giving a reactivity insertion of 2 cents per second to a total of 35 cents. The rods are assumed to initially be positioned at about 8.5 inches inserted and are withdrawn to the lock-out position of 4 inches from the top of the fuel region. By forcing the control rods to be locked no further than 4 inches from the top of the fuel, the dead band region of the scram curve is removed.

The relative power curve predicted by SSC is shown in Figure 13. It reaches a maximum of 185% of rated by 60 s and drops to 161% by 350 s. The core flow stays constant. The added reactivity increases the reactor's power level and temperatures, which in turn activates the inherent feedbacks. As shown in Figure 14, the total reactivity reaches a maximum of 15 cents, with the reactivity insertion countered primarily by the Doppler and radial expansion feedbacks. These results are somewhat different from the GE ARIES results which predicted a peak power of 195% and a drop to 135% by 200 s. While both codes predicted the sodium density to add +15 cents, the Doppler feedback to insert about -17 cents, and the axial feedback to add about -7 cents, a big difference in the control rod drive line expansion was noted. The GE ARIES results showed the control rods being worth -20 cents by 120 s, while the SSC results showed only about -2 cents before the vessel expansion began withdrawing the rods. However, the overall results were similar because the radial expansion feedback was dominant, and the codes were generally in agreement on the dominant feedbacks.

The peak fuel and exit assembly sodium temperature had large margins to their respective safety limits. The peak sodium temperatures in the hot driver and average driver are shown in Figure 15. The closest approach to boiling occurs in the hot driver during the first 20 seconds, and is estimated to be 379 K (683°F). This is slightly less than the ARIES prediction of 409 K (737°F) for the margin to boiling. The maximum fuel centerline temperature is shown in Figure 16, and was found to be 1225 K (1746°F), which is below the 1283 K (1850°F) calculated by GE. No clad damage was indicated in either simulation.

4.3 SSC Analysis of PRISM LOF

The power supplied to the primary and secondary pumps was assumed lost at time zero. The loss of flow circulation was assumed to cause a stoppage in heat removal through the intermediate loop (needed for both SGS and ACS). Only the RVACS was assumed available to reject heat.

The power history predicted by SSC is shown in Figure 17. The flow coast down corresponds to the data supplied in the PSID. The power drops along with the flow to about 10% of rated by 350s, which is about the same as the GE ARIES prediction (Figure E.6-1a, Appendix F). In Figure 18 the reactivity feedbacks are plotted. The total feedback becomes negative within a few seconds and causes the reduction in power. The total reactivity predicted by SSC was similar to that estimated by GE, except for the sodium and the control rod drive line feedbacks. The sodium density feedback was predicted by SSC to have an average of about 20 cents during the first 350s, while the ARIES esti-

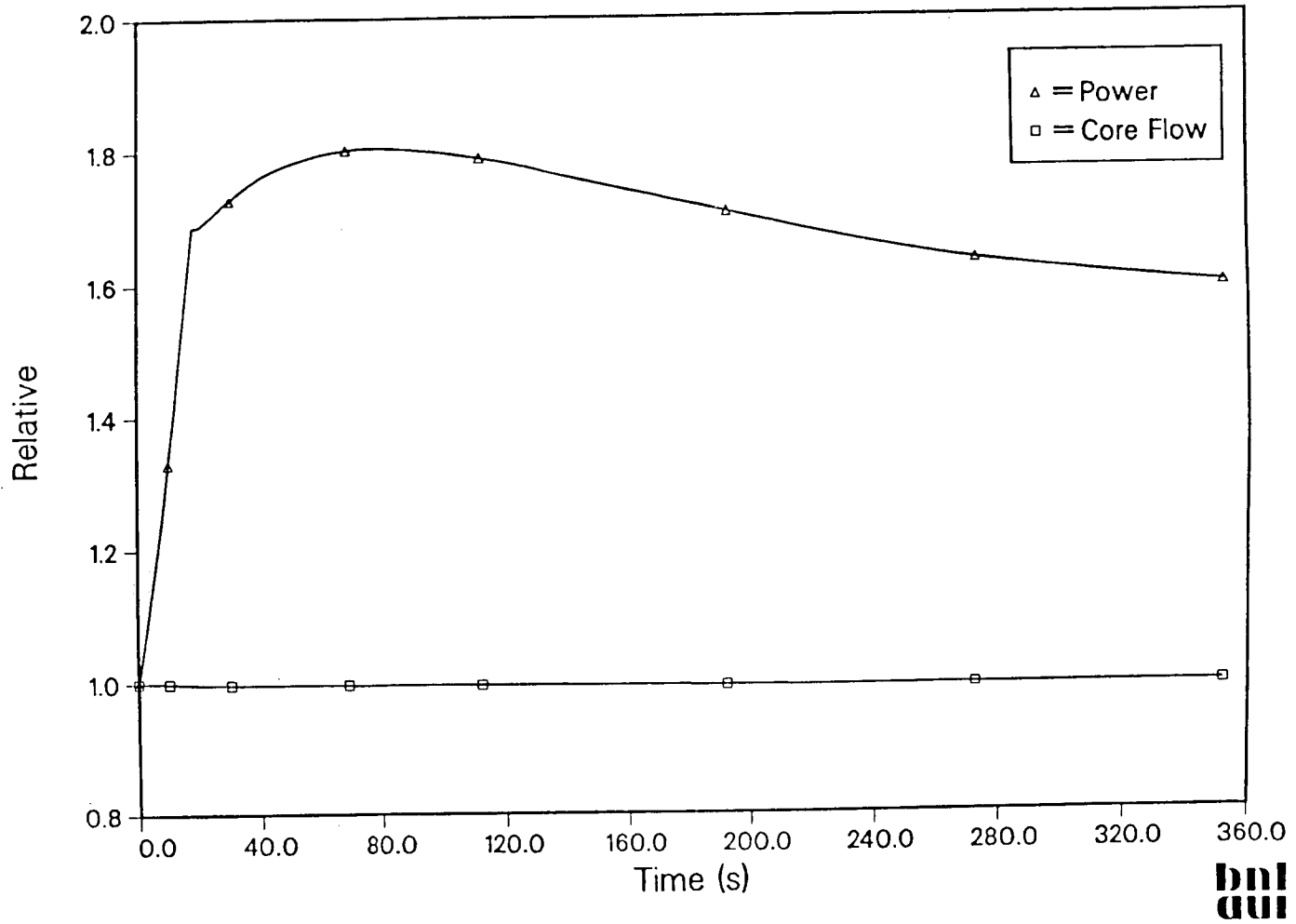


Figure 13 SSC Prediction for a 35 Cent UTOP for Power and Core Flow

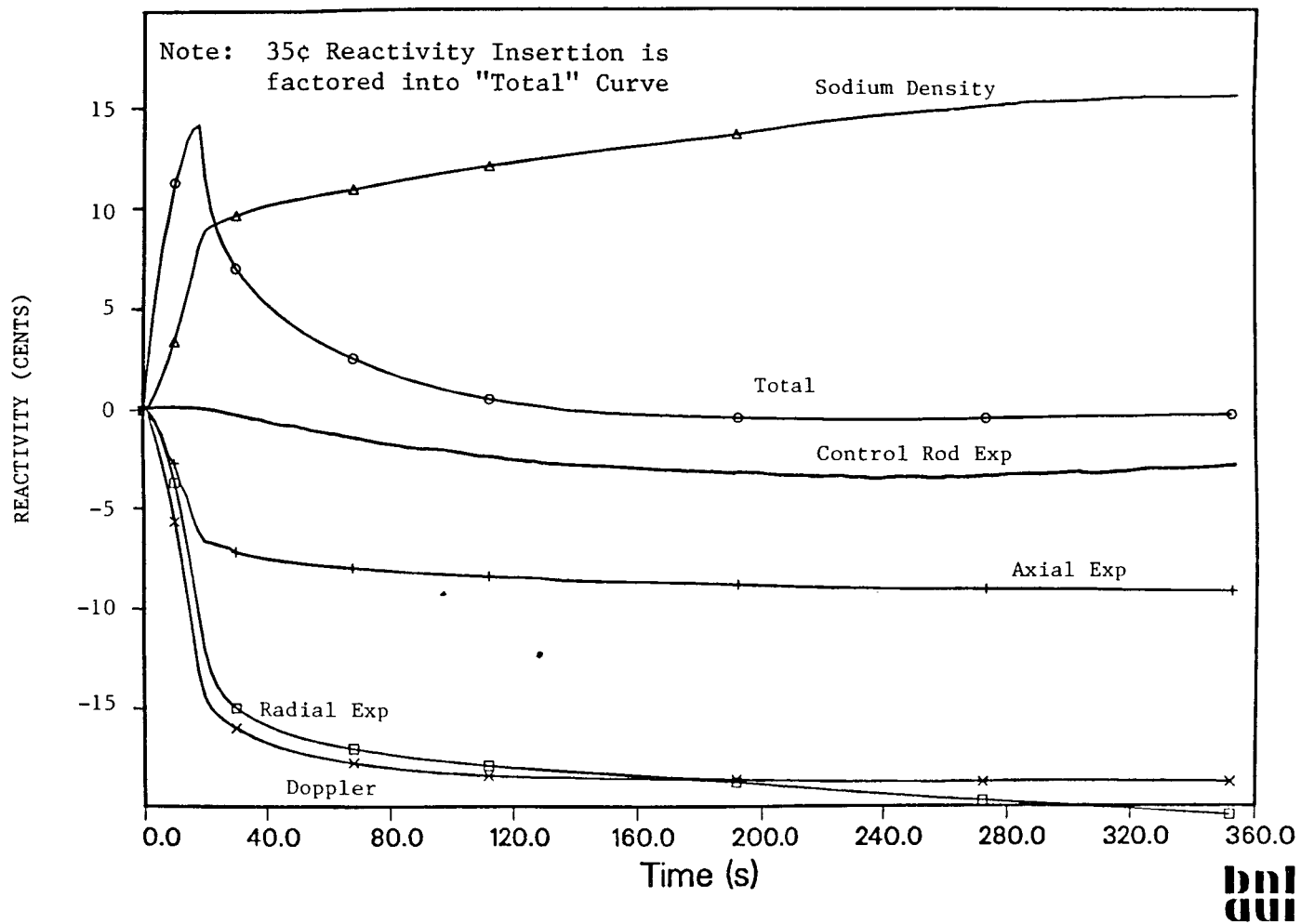


Figure 14 SSC Prediction of Reactivity Feedbacks for a 35 Cent UTOP

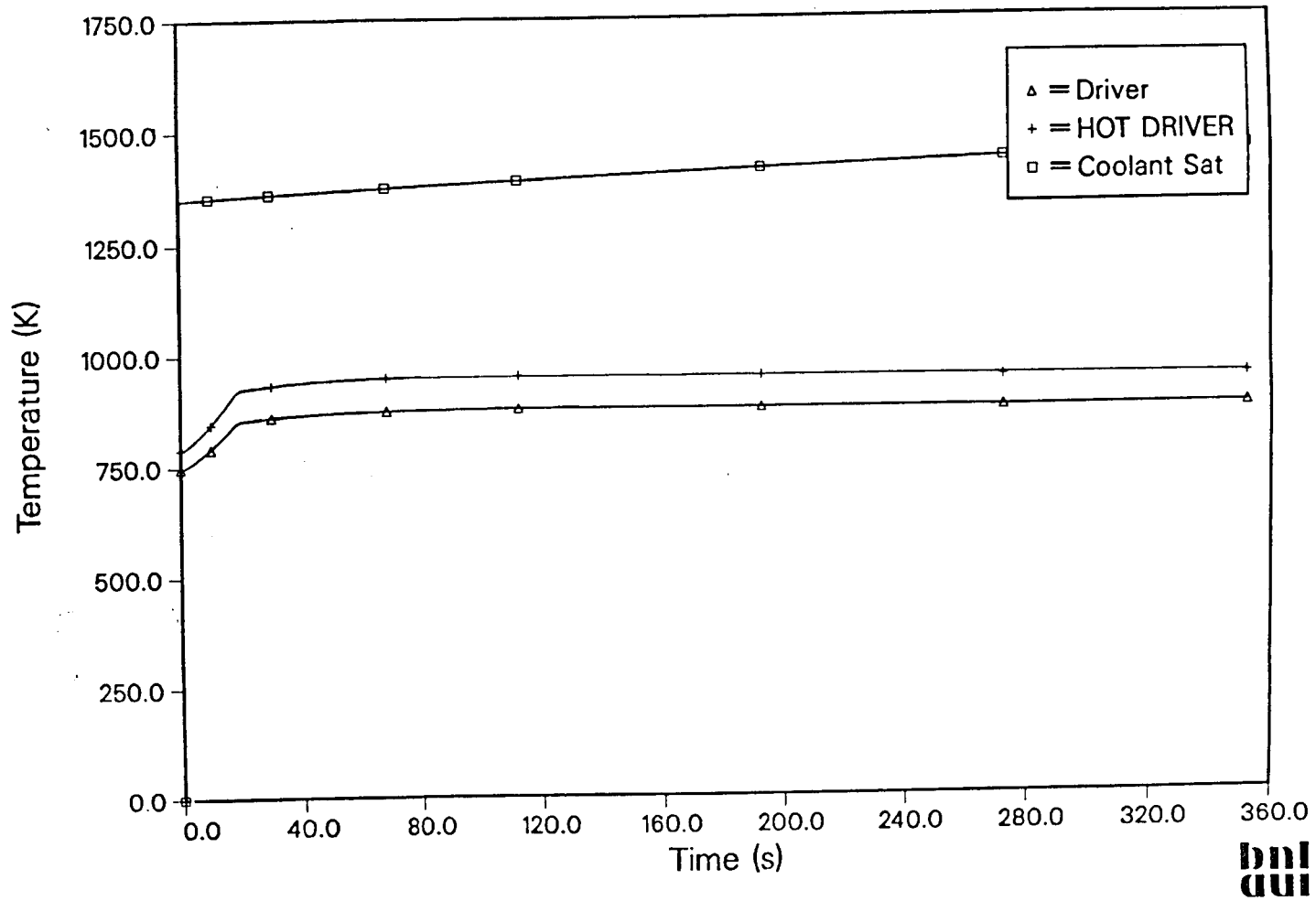


Figure 15 For 35 Cent UTOP: Peak Average and Hot Driver Assembly Coolant Temperature Compared to Saturation Temperature

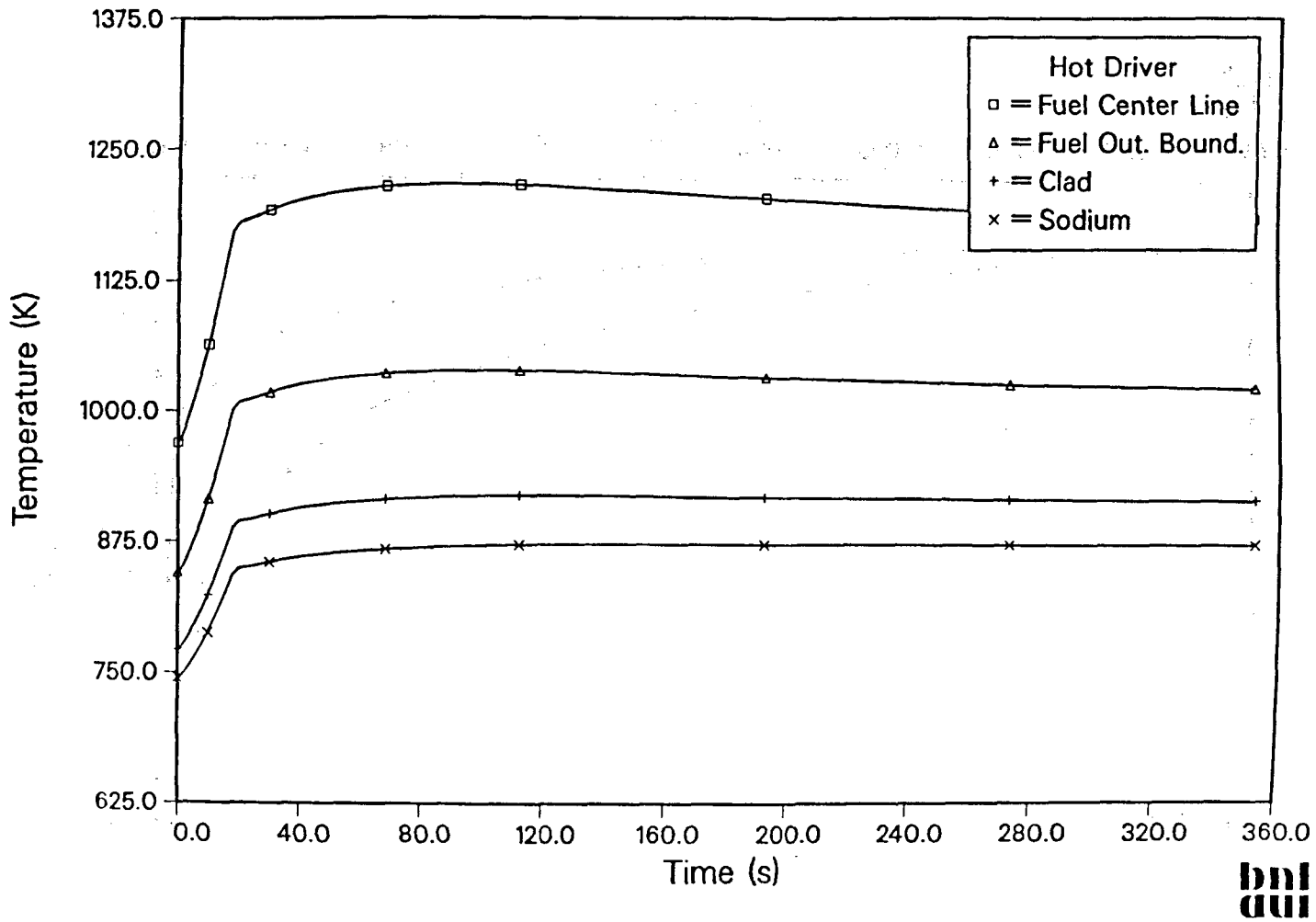


Figure 16 Fuel Temperature Distribution at Peak Location for 35 Cent UTOP



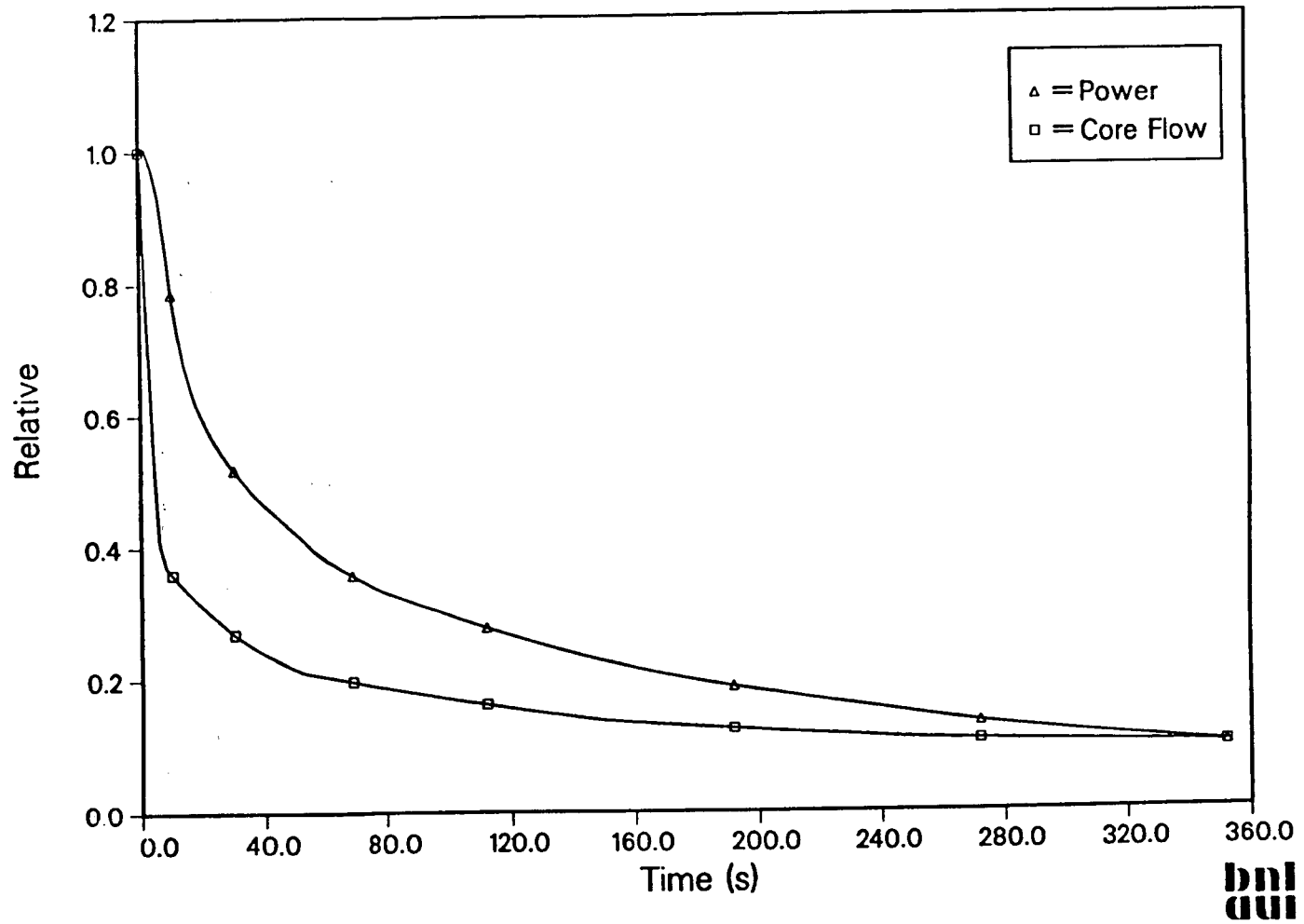


Figure 17 SSC Prediction for PRISM ULOF/LOHS: Relative Power and Core Flow

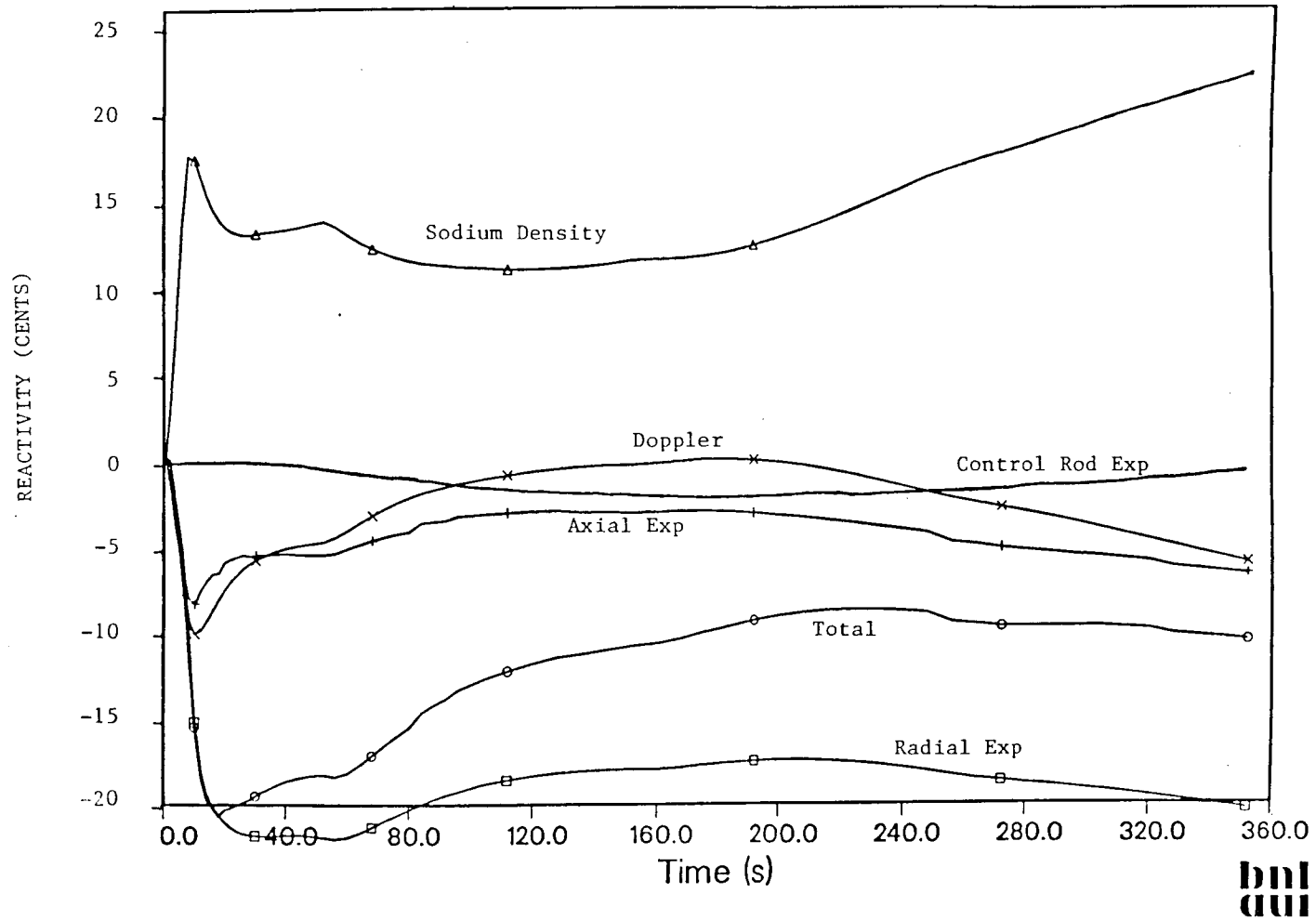


Figure 18 SSC Prediction for PRISM ULOS/LOHS: Reactivity Feedbacks



mation was 25 cents. Control rod expansion contributed only about -1 cent before turning positive in the SSC calculation, while the GE ARIES code predicted it to achieve a value of about -10 cents by 200s and not to turn positive until 700s. (It should be noted that the increasing sodium density feedback in the latter part of Figure 18 reflects fluid transport delays in the sodium pools. Thus, the changing feedback reflects the higher powers and temperatures from earlier in the transient. A careful review of the simulated PRISM reactor system conditions at 360 seconds indicates that the reactor inlet sodium temperatures are about to flatten out, and that the sodium density feedback in Figure 18 should reach a plateau within the next 20 to 30 seconds.)

The estimated peak temperatures were not high enough to be challenging during this event. In Figure 19, the peak assembly exit sodium temperature is presented, along with the associated saturation temperature. The values obtained were 1060 K (1449°F) for the peak and 946 K (1243°F) for the average driver assembly. The margin to sodium boiling was predicted by SSC to be 190 K (342°F), which is slightly less than the 217 K (391°F) calculated by ARIES. The peak fuel centerline temperature is shown in Figure 20, along with the fuel temperature distribution. The peak node temperature was found to be 1125 K (1565°F). Thus, the margin to fuel melting was 241 K (434°F). The ARIES predicted margin was 250 K (450°F). SSC calculated the peak clad temperature to be about 1000 K (1341°F), for only a few seconds. Thus, no significant fuel-clad interaction would occur.

Transient over Power with a Loss of Flow and LOHS Event

The TOP/LOF/LOHS transient is initiated by the withdrawal of all six control rods from their maximum position worth of 35 cents, with a ramp rate of 2 cents per second. Simultaneously, the pumps are assumed to trip and begin coasting down, and the heat rejection to the IHX is assumed lost.

The SSC results for this event are shown in Figures 21 through 24. The power (Figure 21) is shown initially to increase, since the combination of the added reactivity from the rod withdrawal and the sodium density feedback increases the power. The increase in reactor power and sodium temperature (from the drop in coolant flow in the core) activates the other feedbacks. Figure 22 shows that the 35 cents from the control rods and the 30 cents from the sodium density effect are effectively negated by the Doppler, axial expansion, and radial expansion feedbacks by 20 s into the event. The elevated temperatures result in the feedbacks producing a net negative value after 20 s, which reduces the power to 26% by 350 s and continues to reduce the power thereafter.

The peak temperatures during this event are very high, but they do remain below the critical values, at least over the short term. The margin to sodium boiling is shown in Figure 23. The hot driver has a margin of 33 K (59°F) while the average drive margin is 177 K (319°F). This indicates that even if the peak assembly did boil, the rest of the driver assemblies would be available to counteract the positive insertion. (Initiation of boiling would occur at the exit of the assembly and would produce an initially negative feedback because of the large increase in neutronic leakage. If time and circumstances allowed it to propagate down into the channel, the effect could become positive.) The margin to fuel melting is shown in Figure 24 to be 111 K

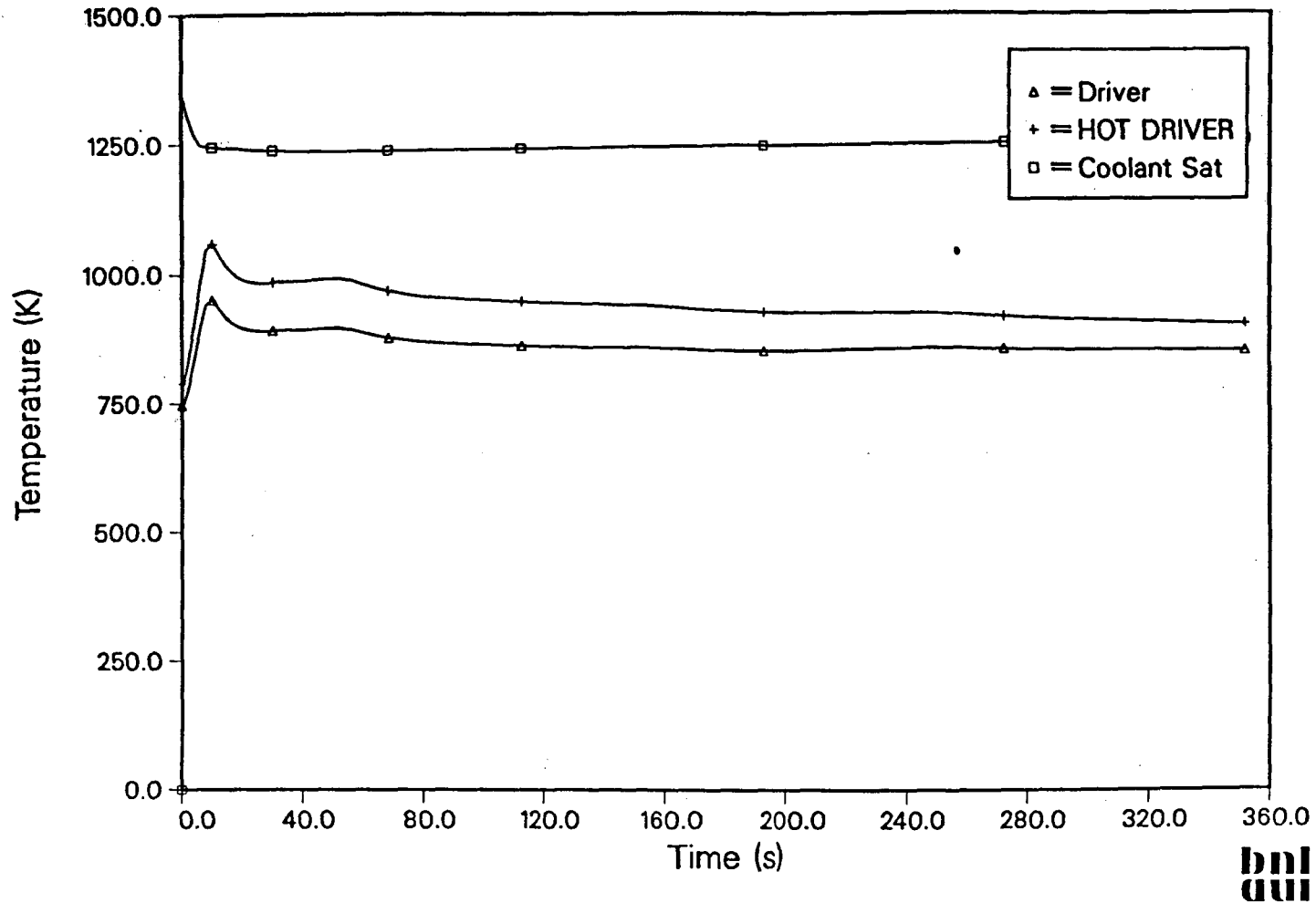


Figure 19 SSC Prediction for PRISM ULOF/LOHS: Peak Average and Hot Driver Assembly Coolant Temperatures Compared to the Saturation Temperature



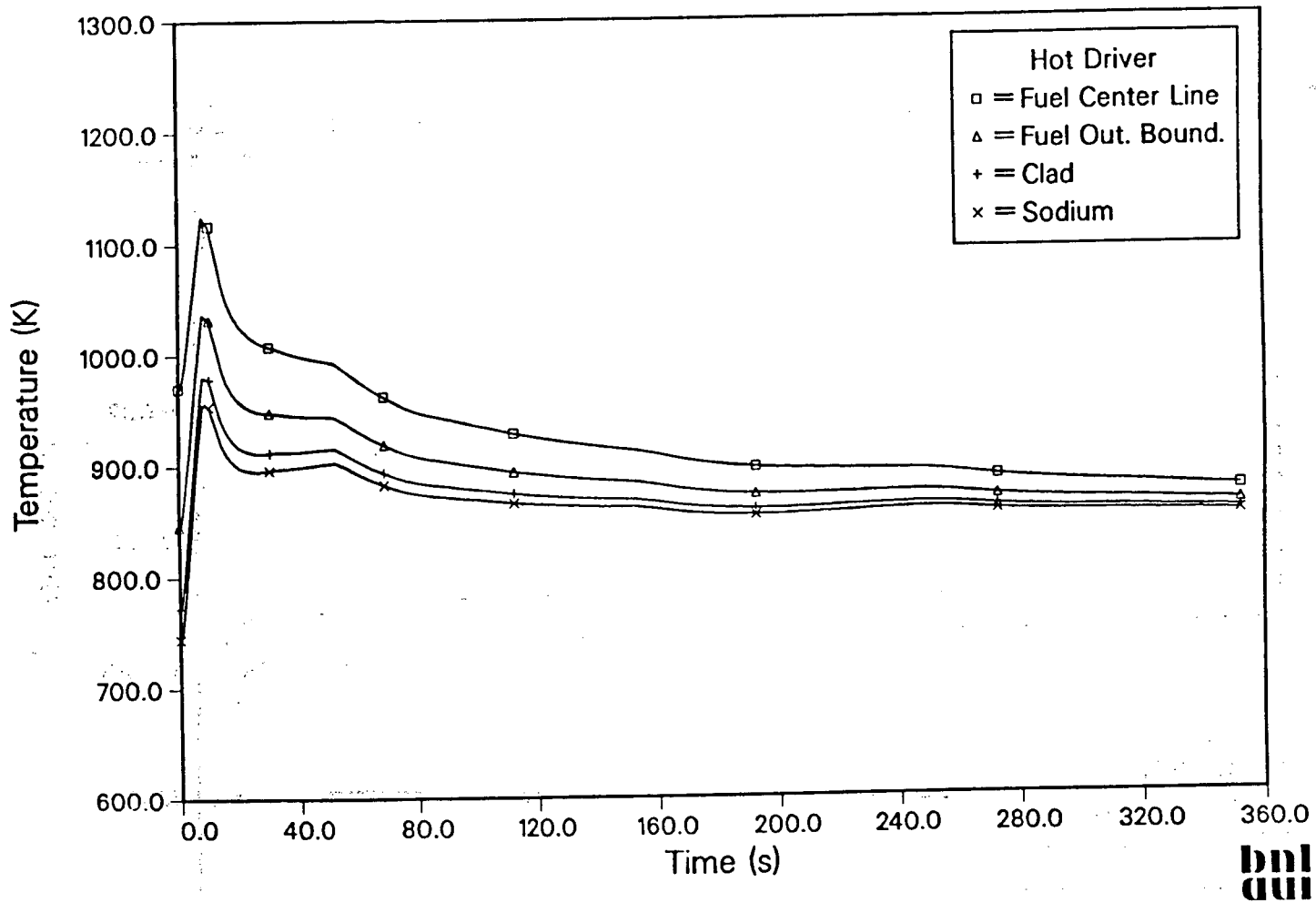


Figure 20 SSC Prediction for PRISM ULOF/LOHS: Fuel Temperature Distribution at Peak Location



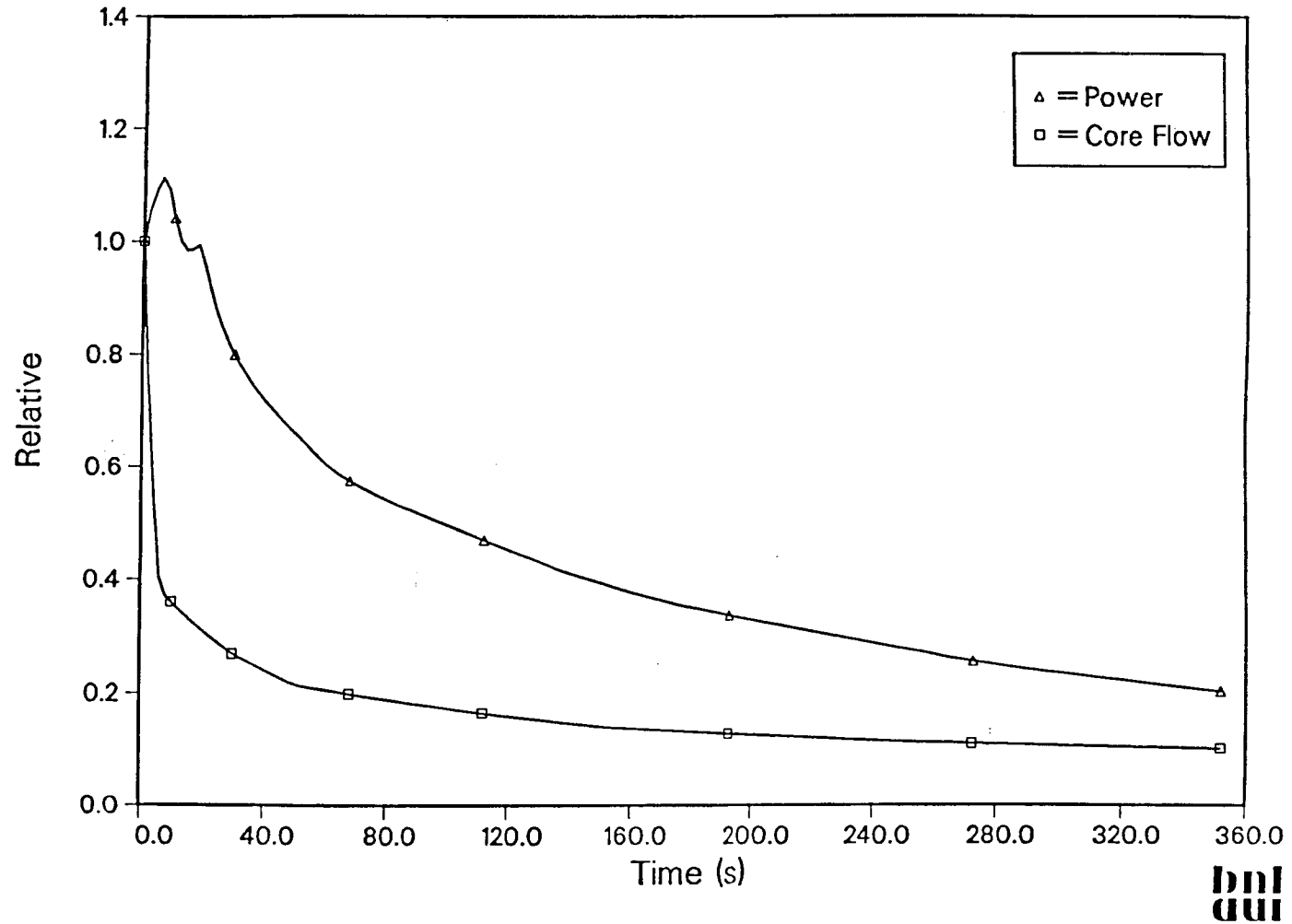


Figure 21 SSC Prediction for PRISM 35 Cent UTOP/LOF: Relative Power and Flow Rate



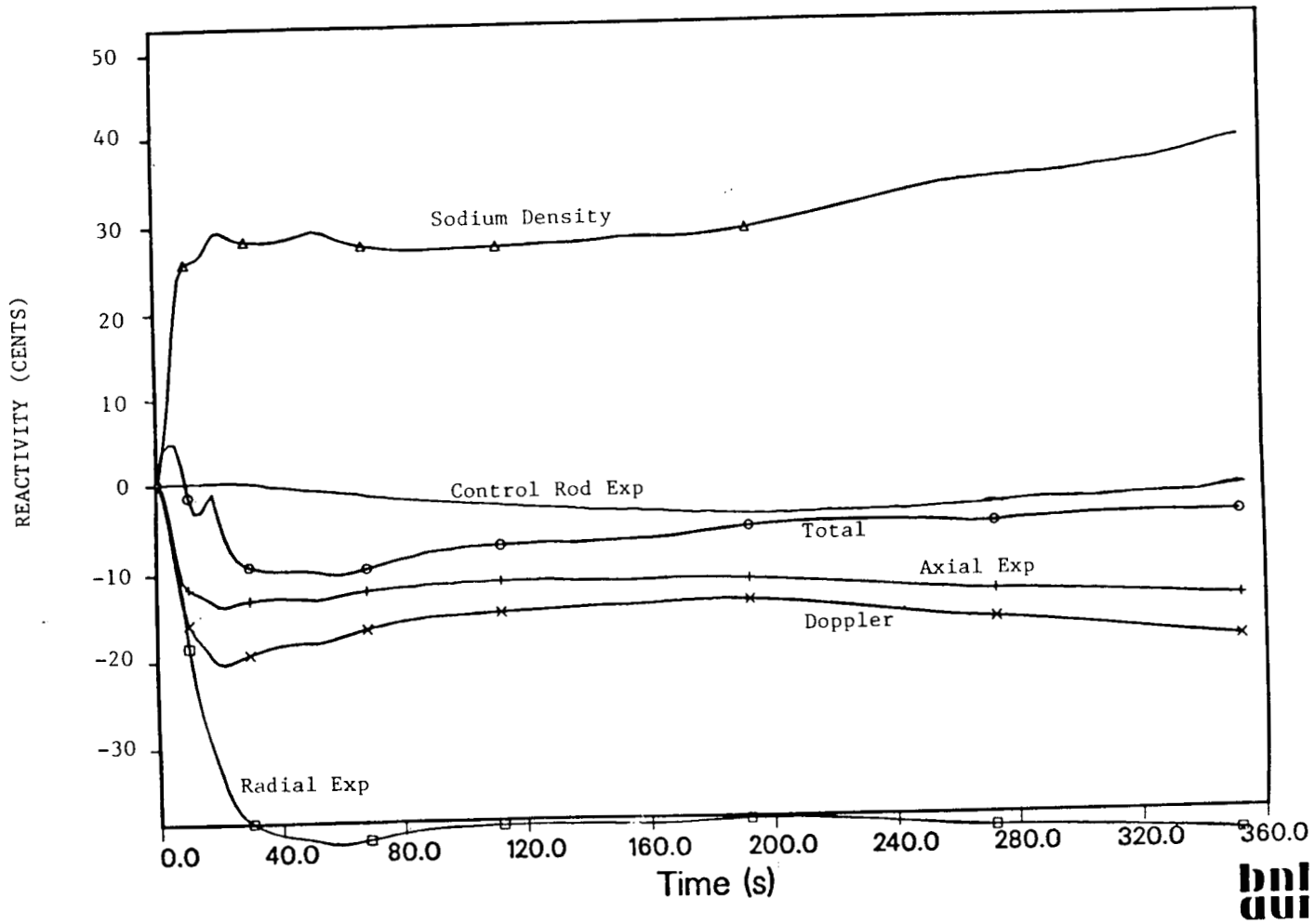


Figure 22 SSC Prediction for PRISM 35 Cent UTOP/LOF: Reactivity Feedbacks



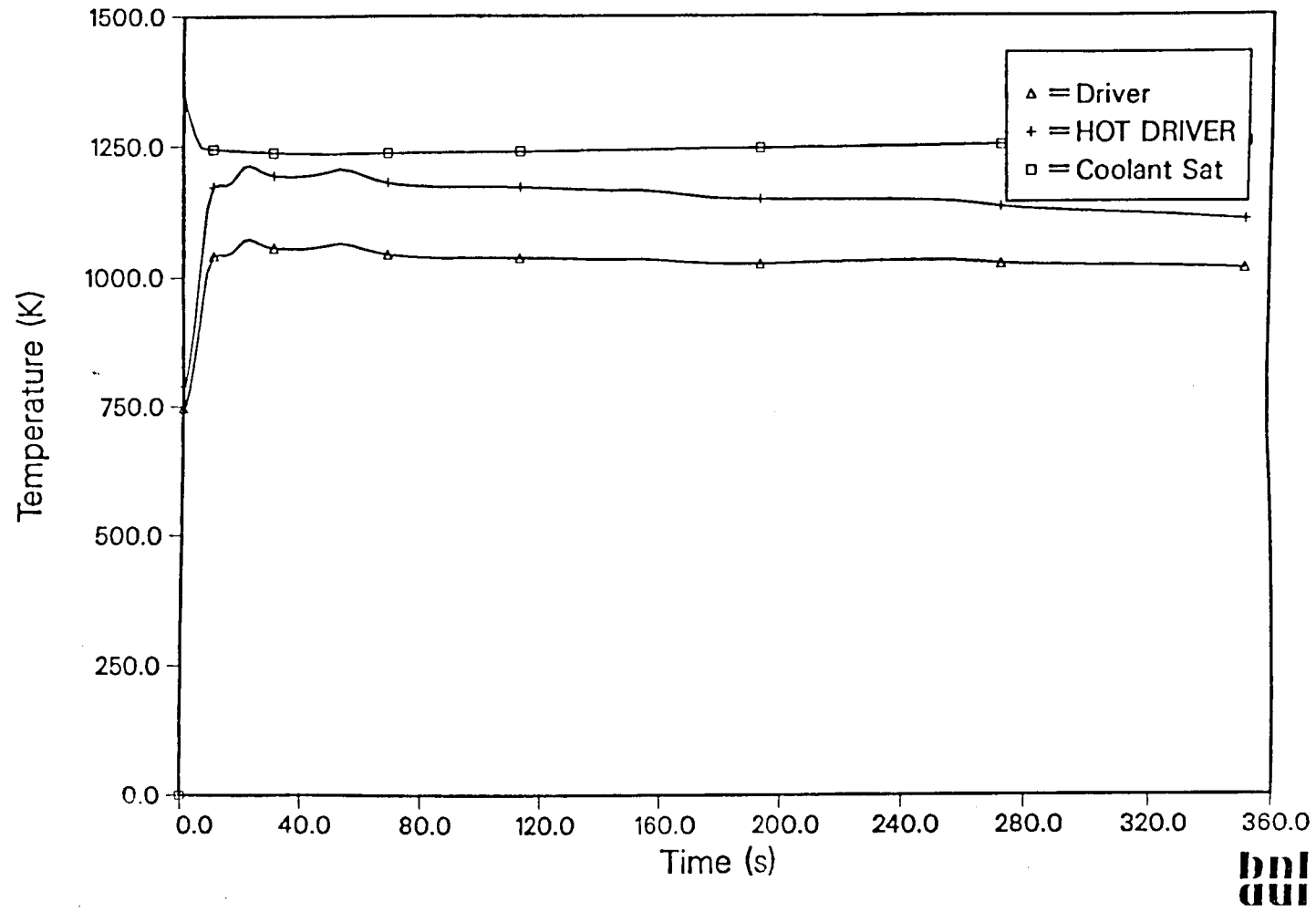


Figure 23 SSC Prediction for PRISM 35 Cent UTOP/LOF: Peak Average and Hot Driver Assembly Temperatures Compared to the Saturation Temperature

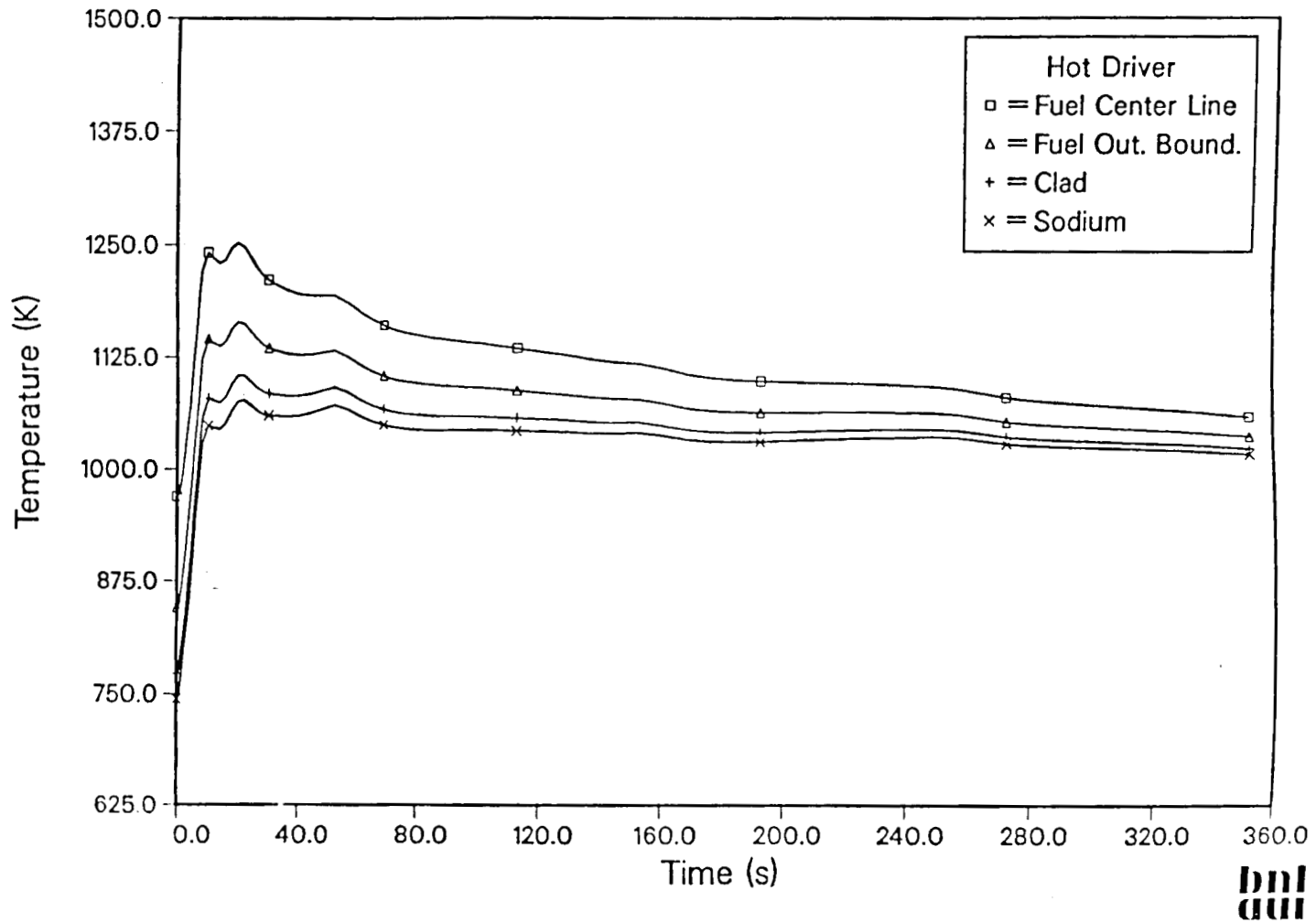


Figure 24 SSC Prediction for PRISM 35 Cent UTOP/LOF: Fuel Temperature Distribution at Peak Location



(200°F). From this figure (deduced by interpolating between the fuel outer boundary node temperature and the fuel clad midwall temperature in Figure 24) it is also apparent that fuel-clad interactions would occur and that the eutectic would begin penetrating the clad. The peak fuel clad temperature was found to be about 1116 K (1549°F), at which level penetration through 10 mils would take .9 hours (3300 s). By 350 s, the fuel-clad interface temperature reaches 1045 K (1422°F) which has a corresponding penetration rate of 2.1 hours for 10 mils. The definition of clad "penetration" is the wastage of 10 mils, although the clad thickness is actually 22 mils. For this event, the reactor would have to be scrammed within 2 hours or the clad integrity would be lost. As seen in Figure 25, the transient also causes the core average outlet temperature to pass the ASME code limit D, since the temperature reaches 1050 K (1431°F) and levels off near 1029 K (1393°F). However, the average upper plenum temperature stays below the service limit C (i.e. 922 K/1200°F) since the average temperature has only just reached 845 K (1062°F) at the IHX inlet, as shown in Figure 26.

In summary, SSC was used to analyze a 35 cents TOP/LOF/LOHS event on the PRISM reactor and has shown that PRISM could survive for 2 hours before clad penetration in the hot channels would occur. The ASME service limit D would be reached since the core exit temperature goes to 1050 K (1431°F) and the limit is 978 K (1300°F). However, the operator has been given considerable time to respond since he has two hours to enact a scram before the first boundary layer is lost (i.e., the clad). While this transient is obviously a severe challenge to PRISM, it is believed to be exceedingly unlikely and should be considered a worst-case or a bounding event.

4.5 Unscrammed Pipe Break in PRISM

While the tripping and coasting down of the PRISM pumps is the most likely LOF, there are variations that could be more troublesome - if there is a failure to scram. The reactor flow rates in cases where a pipe breaks or one, two, three, or all four EM pumps stop instantaneously ("seize"), as calculated using MINET, are shown in Figure 27. In all cases except normal coastdown, a rapid drop in flow is predicted, and the drop is severe for two or more pump "seizures". For the two more likely events, i.e., the breakage of one pipe or the "seizure" of one pump, the drop in flow is about 50%. The pipe break, resulting in 49% normal reactor flow, is more limiting than the pump "seizure" case (53%), so that event was analyzed using SSC.

Results of the SSC simulation of the PRISM unscrammed pipe break event are given in Figures 28-32. The relative reactor flow rate was specified to be 49%, based on the MINET analysis. As shown in Figure 28, the reactor power also dropped quickly, but leveled out around 75% after a few minutes (the core temperature rise increased). The reason for the rapid change in power can be seen in Figure 29, where the reactivity feedbacks shift quickly, particularly the sodium density, the radial and axial expansion, and the Doppler. As a result, the core outlet temperature increases sharply at first, but peaks at acceptable levels before ten seconds pass. Similar trends are shown in the fuel and cladding temperatures.

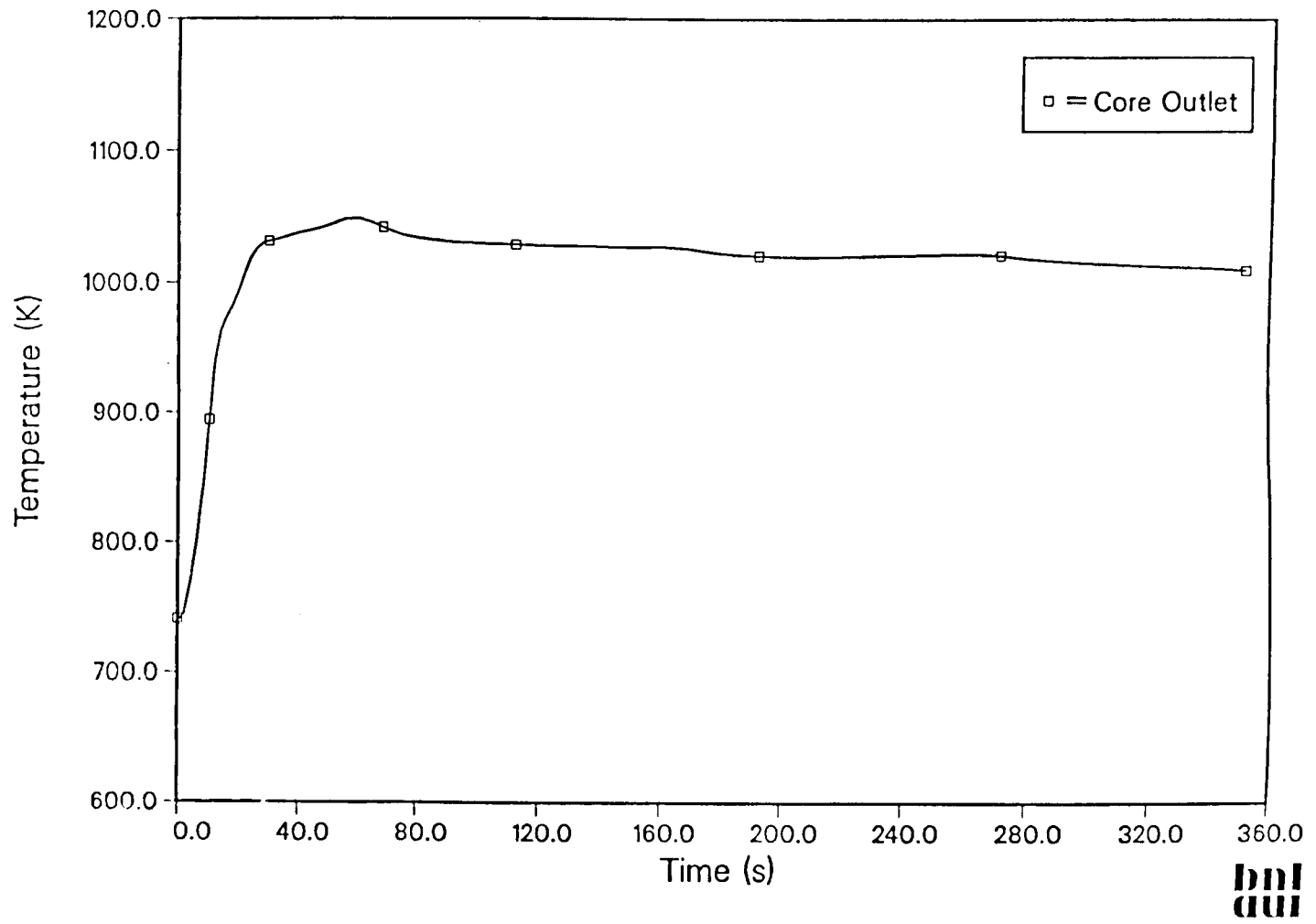


Figure 25 SSC Prediction for PRISM 35 Cent UTOP/LOF: Core Exit Temperature

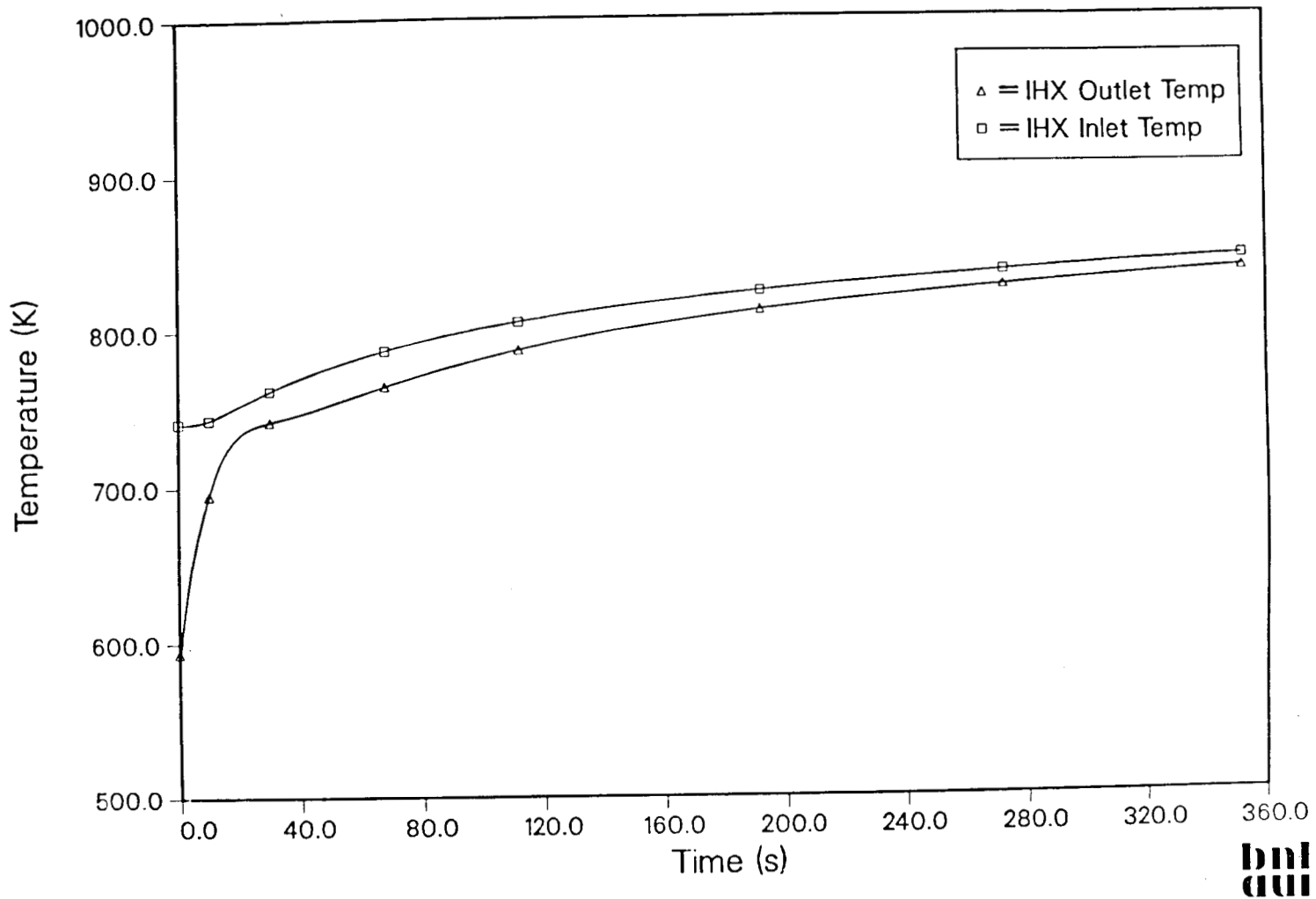


Figure 26 SSC Prediction for PRISM 35 Cent UTOP/LOF: IHX Inlet and Outlet Temperatures



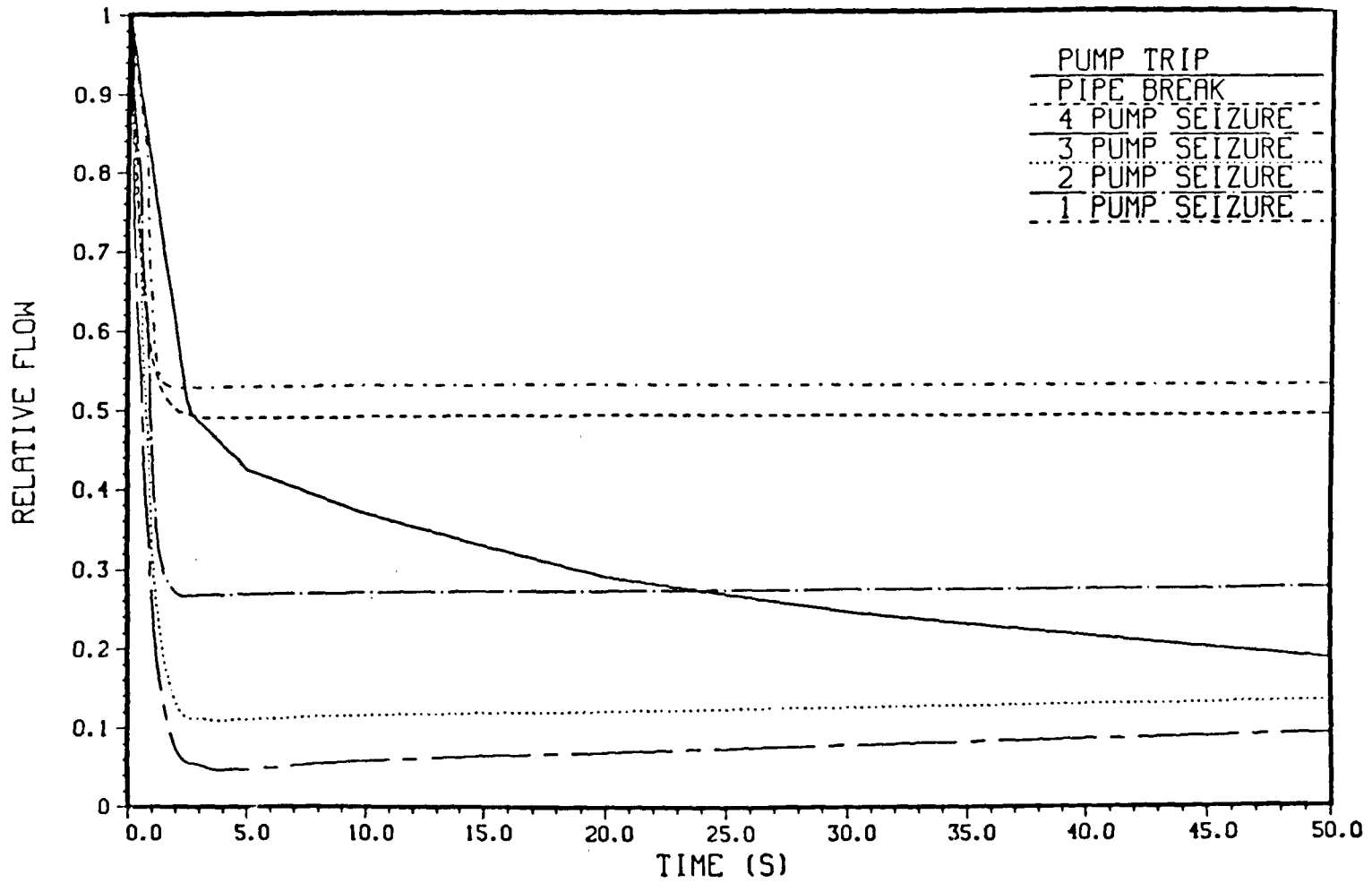


Figure 27 PRISM-MINET Analysis - Core Inlet Flow Rate vs. Time

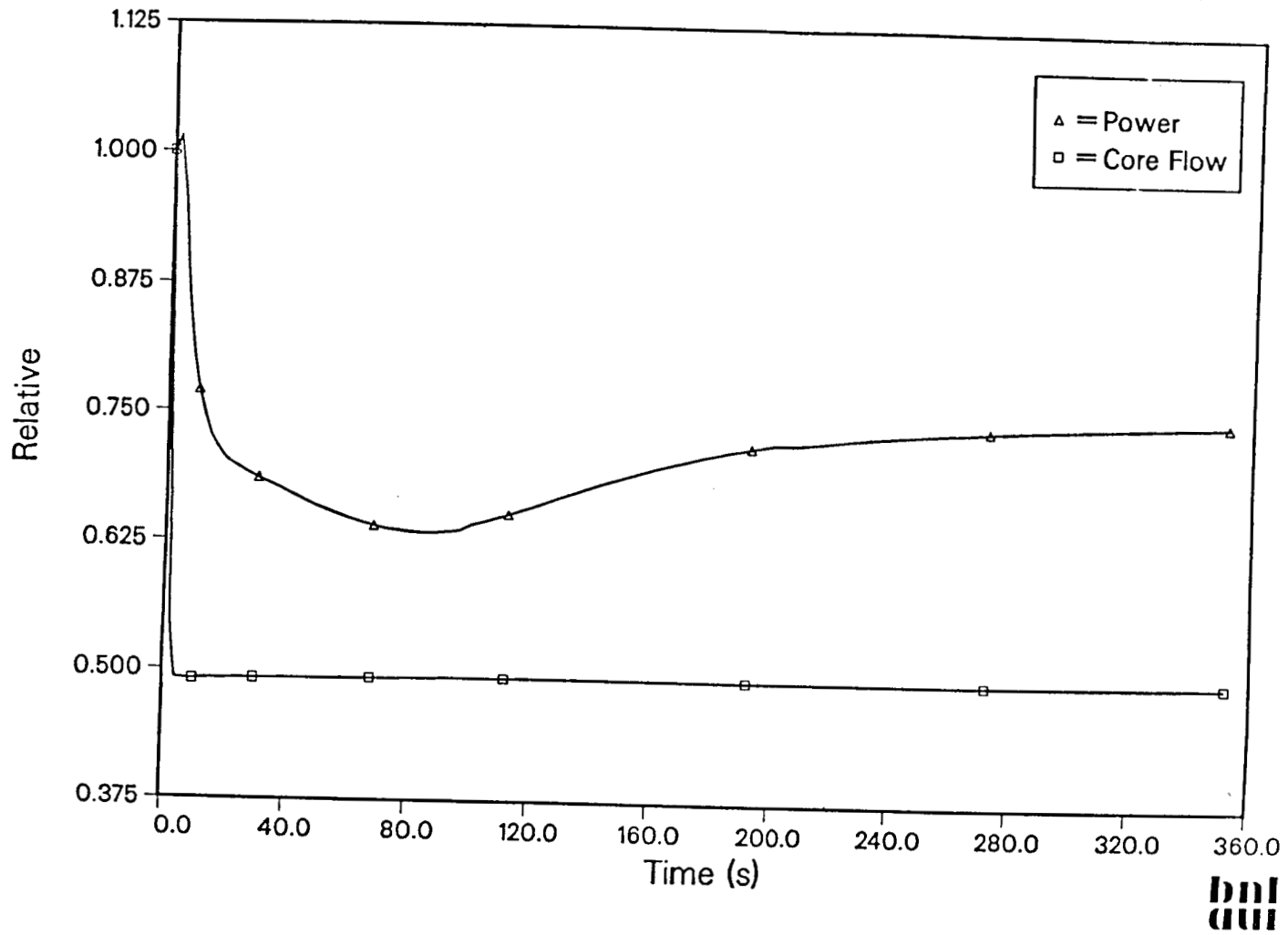


Figure 28 SSC Prediction for PRISM Pipe Break: Relative Power and Core Flow

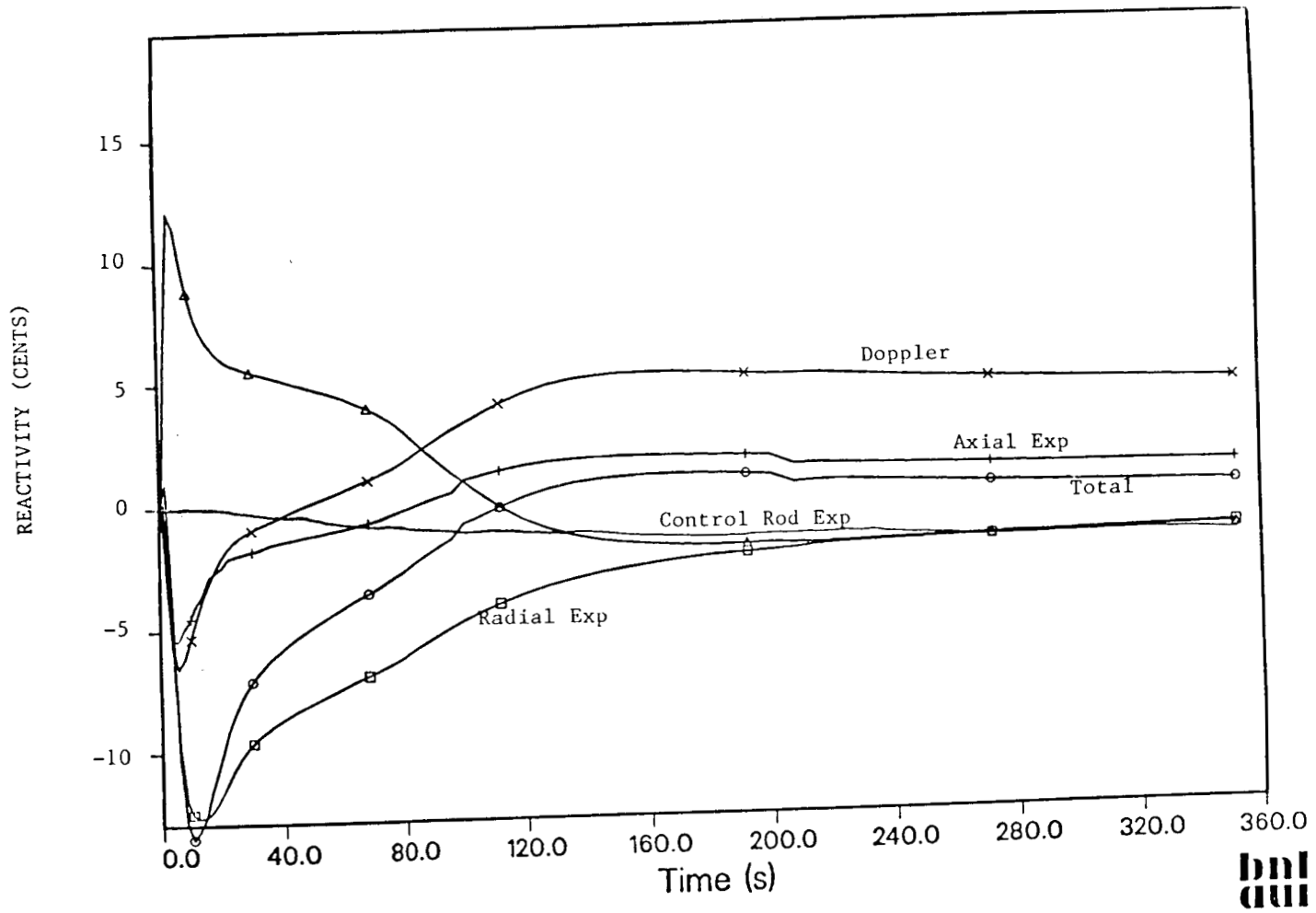


Figure 29 SSC Prediction for PRISM Pipe Break: Reactivity Feedbacks

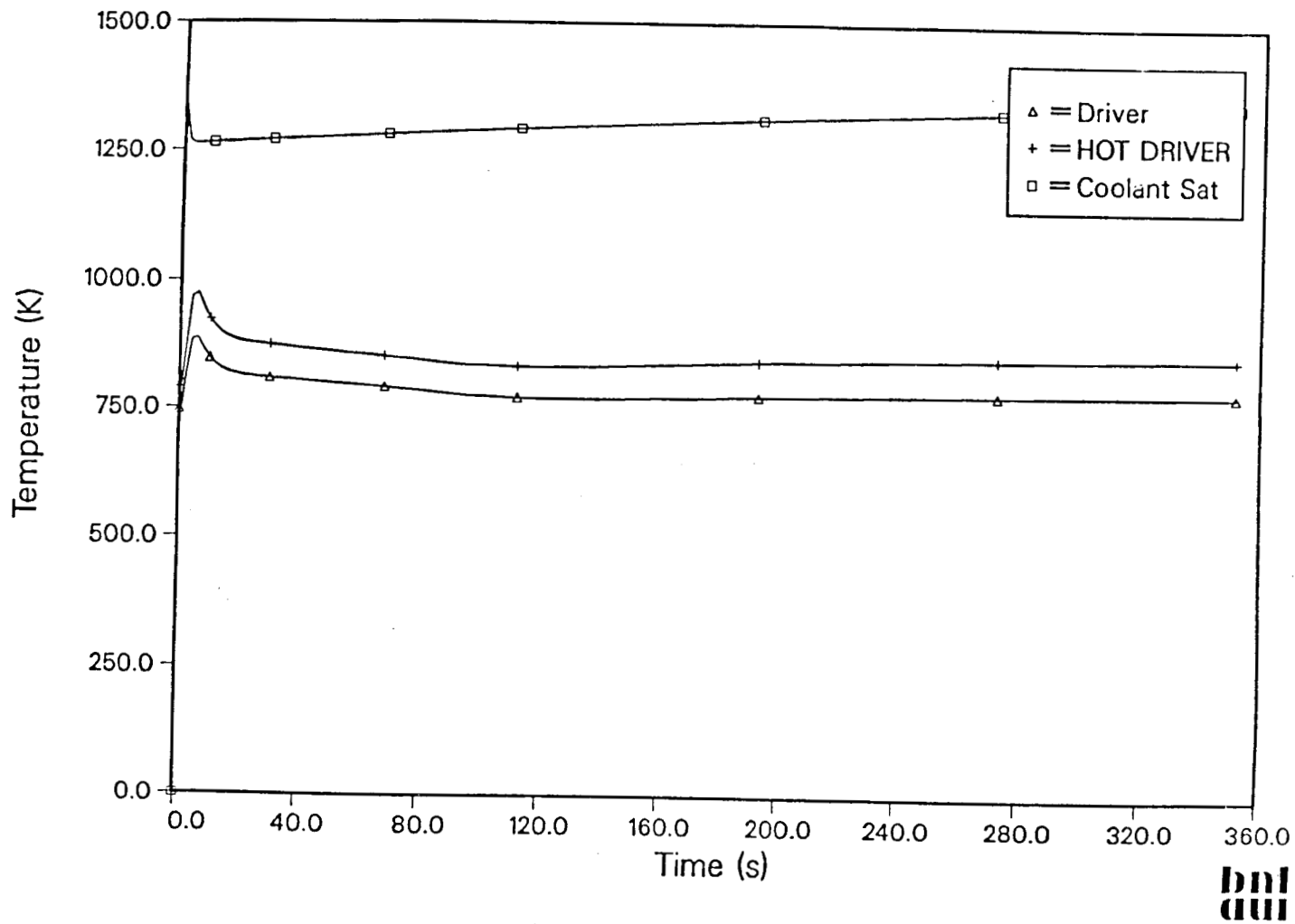


Figure 30 SSC Prediction for PRISM Pipe Break: Core Outlet Temperatures and Saturation Temperature



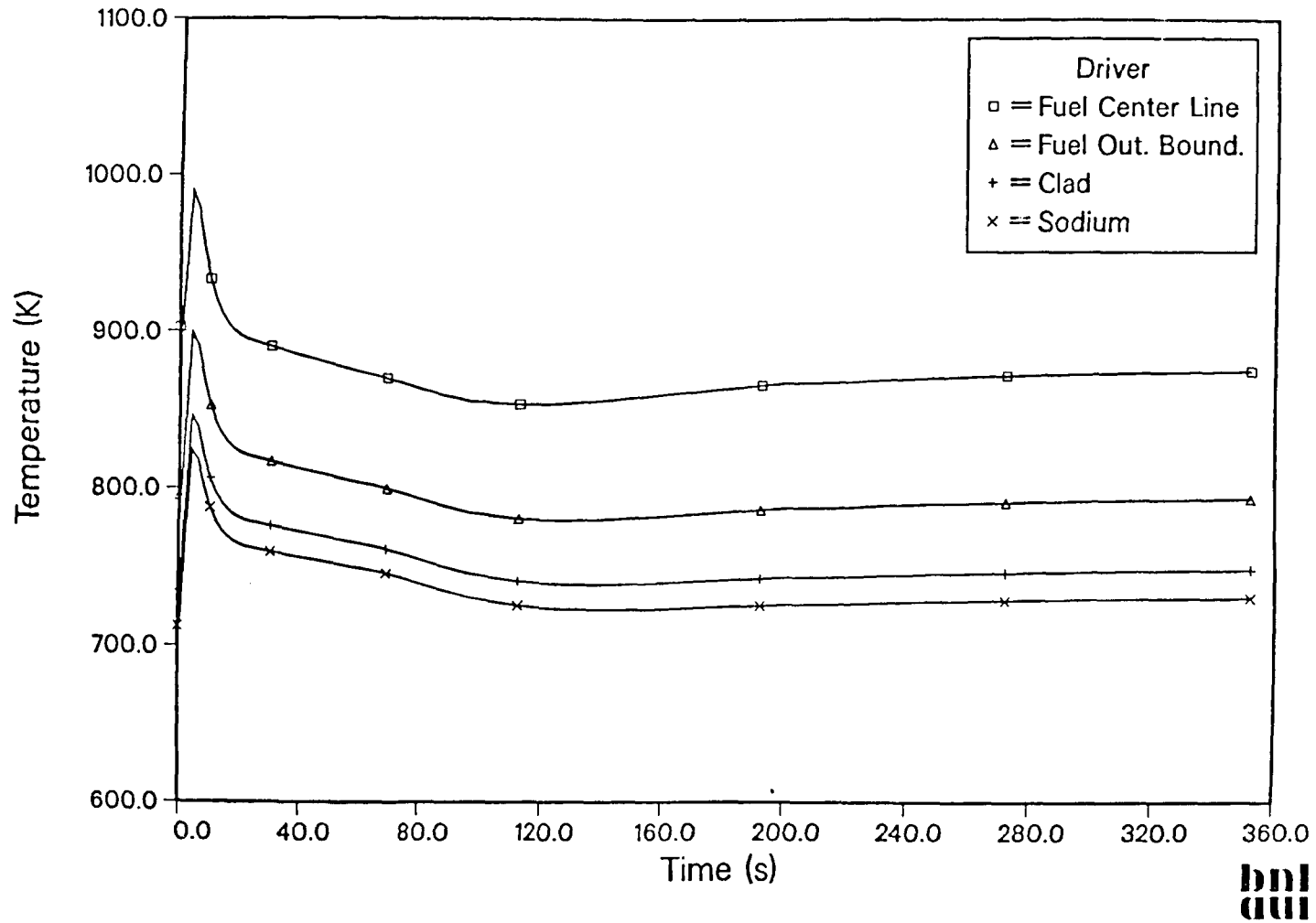


Figure 31 SSC Prediction for PRISM Pipe Break: Driver Temperatures

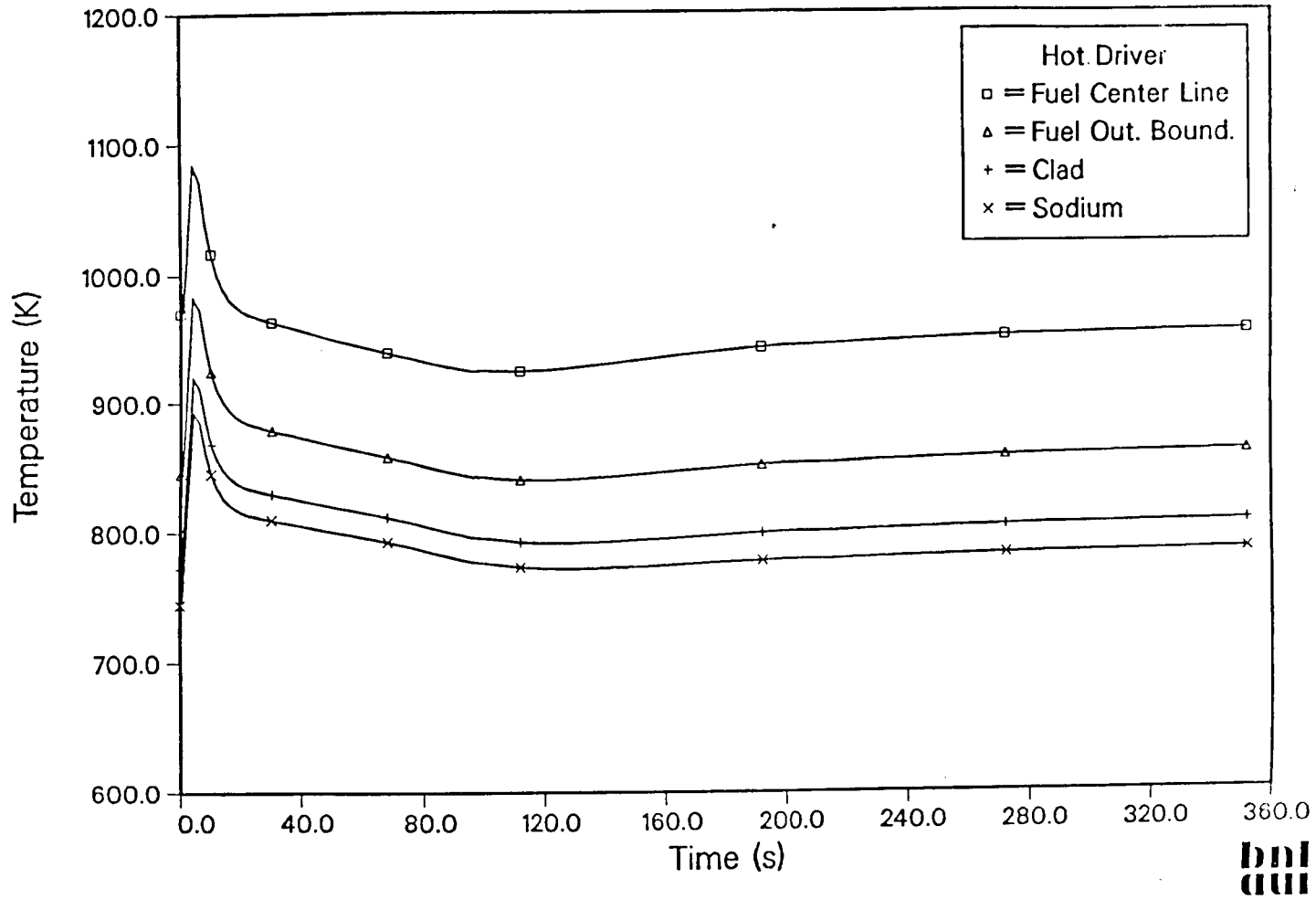


Figure 32 SSC Prediction for PRISM Pipe Break: Peak Temperatures



4.6 PRISM Unscrammed LOF Missing One Coastdown

Our effort to analyze this event involved two codes, SSC and MINET. We used MINET to estimate the reactor flow rate versus time, with pump behavior inferred from the normal coastdown event. Thus, we cut the voltage to one pump and "coasted" the voltage downward for the other three. The calculated reactor coolant flow decreased somewhat faster than it did in the GE calculation. This was traced to an assumption on GE's part that the flow conditions in the reactor do feed back to the synchronous machines via the impedance "sensed" by the EM pumps. Information received from GE thus far has not be sufficient to allow us to make a judgement regarding this behavior.

The second step in the analysis was to input the reactor coolant flow curve into SSC and calculate the resulting power transient. The GE flow coastdown curve was utilized. Results of the SSC calculations are illustrated in Figures 33 through 37. The SSC results for the (average) driver were very similar to GE's calculations, particularly with respect to peak temperatures. However, some localized sodium boiling was observed in the hot driver (pin) channel - which includes peaking factors and 2-sigma uncertainties on geometric parameters. Thus, there appears to be little safety margin for this event. Further, if the coastdown curve we calculated using MINET is utilized, we would expect even higher temperatures.

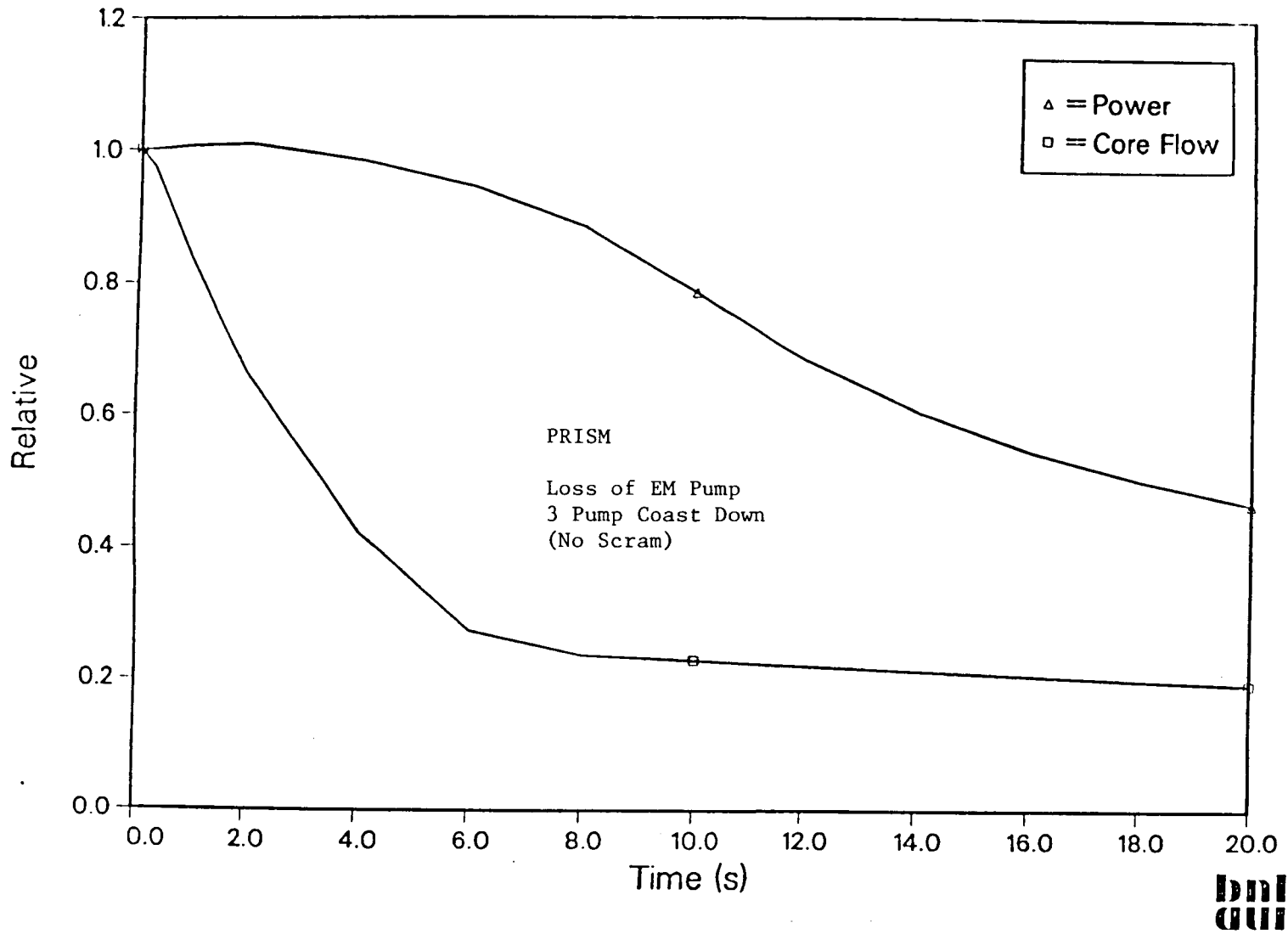


Figure 33 SSC Prediction for PRISM 3 Pump Coastdown: Relative Power and Core Flow

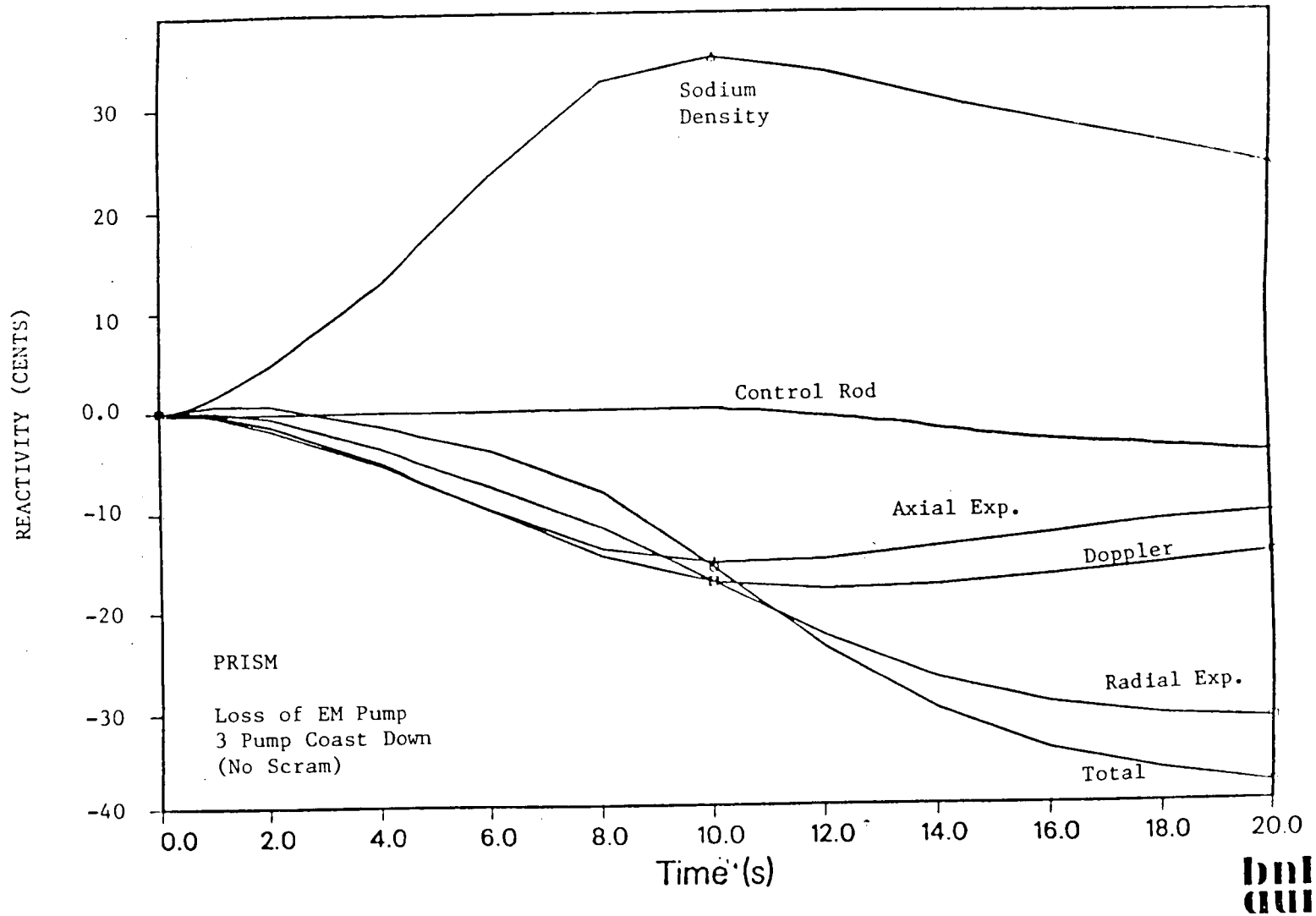


Figure 34 SSC Prediction for PRISM 3 Pump Coastdown: Reactivity Feedbacks

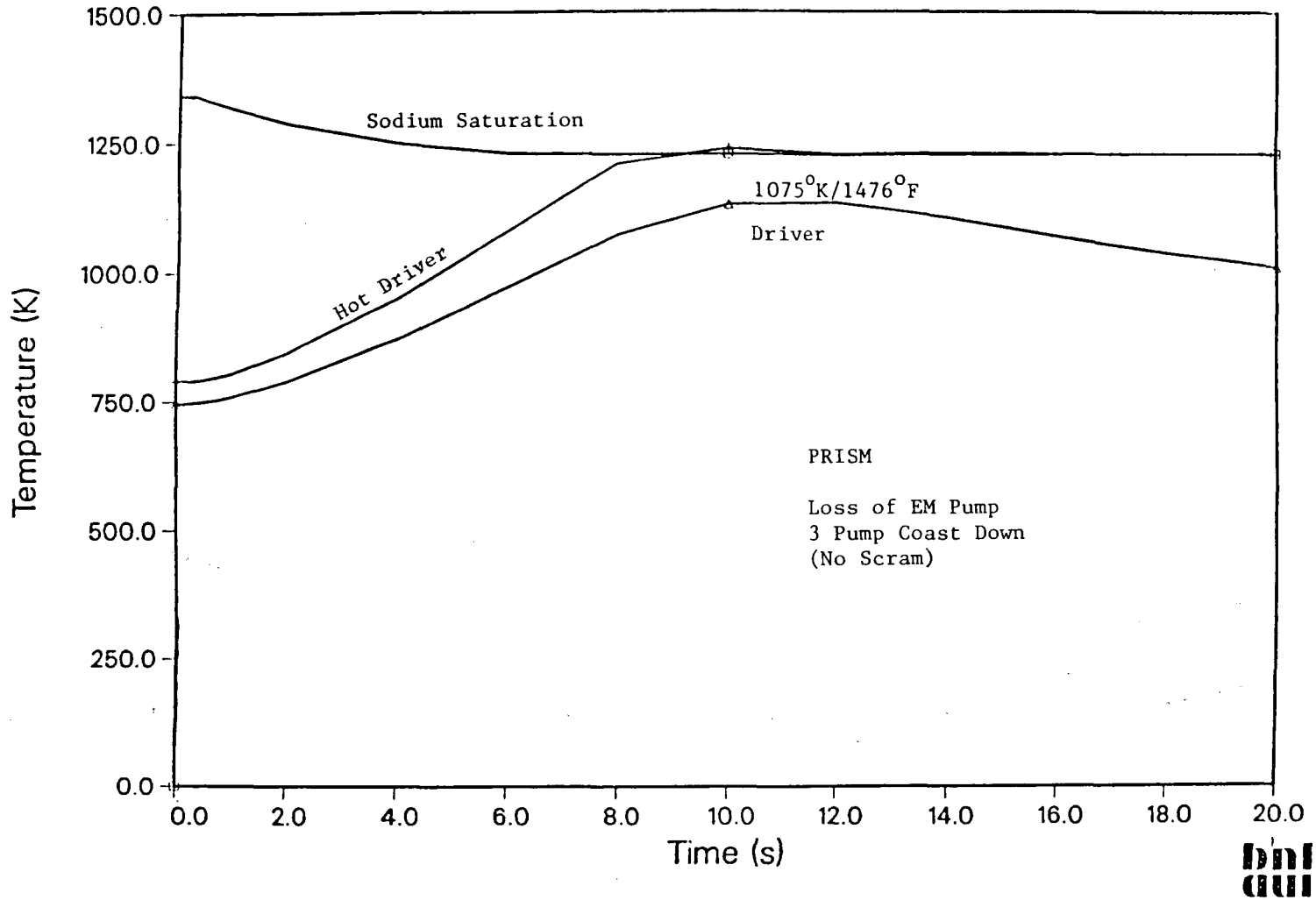


Figure 35 SSC Prediction for PRISM 3 Pump Costdown: Outlet and Saturation Temperatures

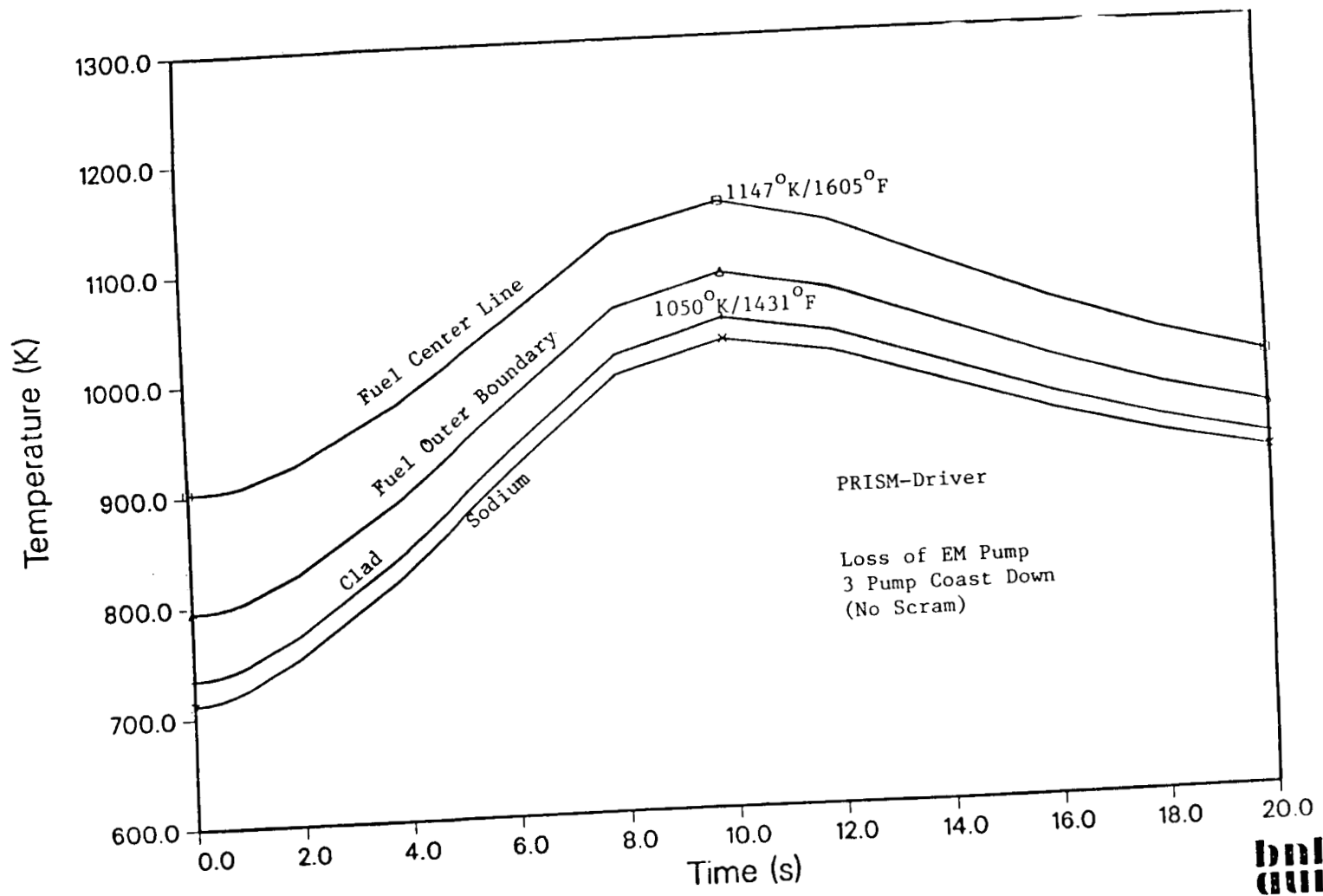


Figure 36 SSC Prediction for PRISM 3 Pump Coastdown: Driver Temperatures

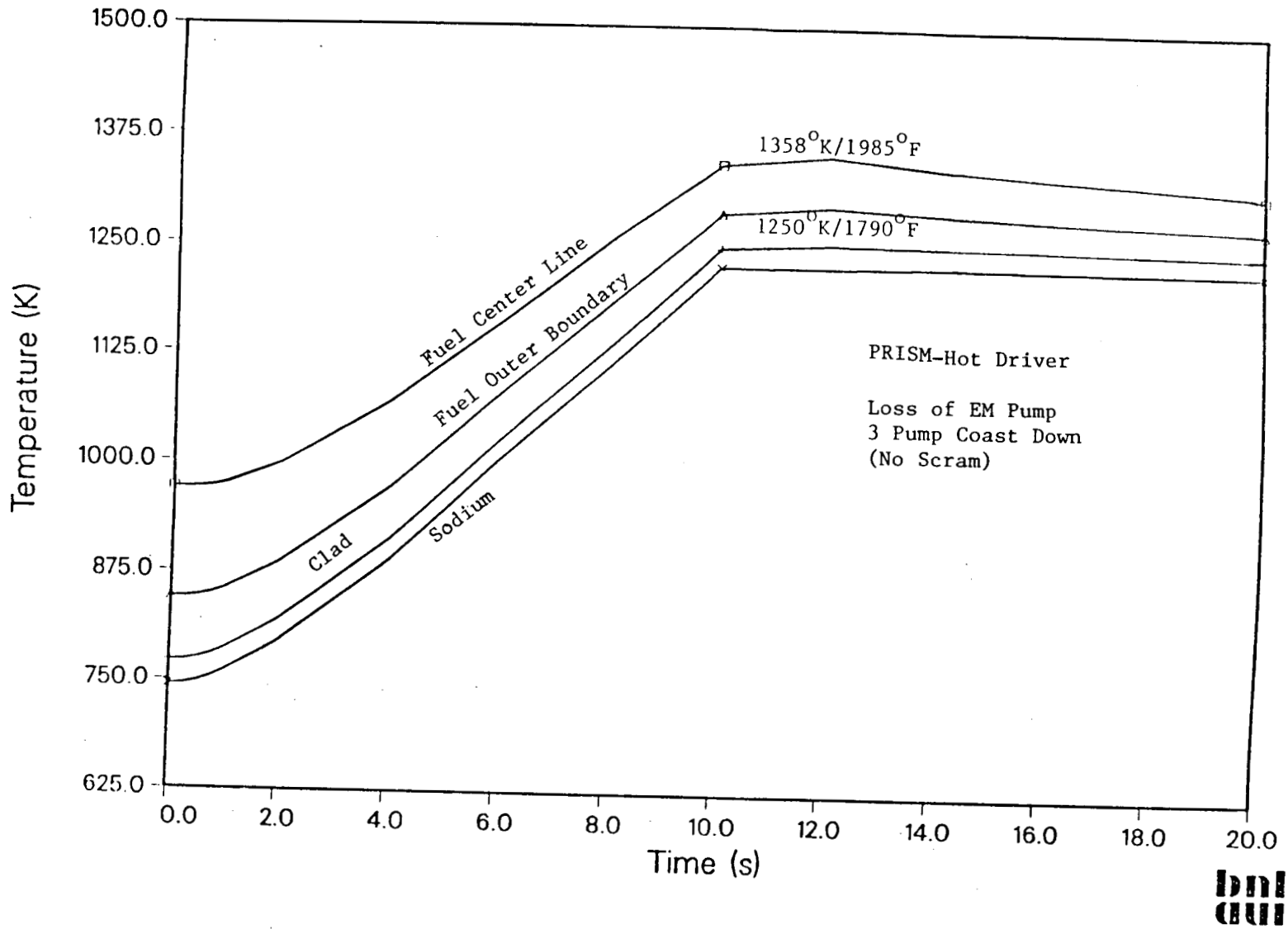


Figure 37 SSC Prediction for PRISM 3 Pump Coastdown: Peak Temperatures



5. SAFR UNSCRAMMED EVENTS

The transient responses of the SAFR reactor system to various unscrammed events were evaluated using SSC and, to a lesser degree, MINET. In nearly every case, the BNL calculated results were very similar to those submitted by RI/ANL.

Five types of unscrammed events are covered in this section. The first three, i.e., the loss of heat sink (LOHS), the transient-over-power (TOP), and the loss of flow, are the more likely events and form the basic group of BDBE events (design basis events without scram). Two less likely events were also analyzed, including a combined TOP/LOF and an unscrammed pump seizure event.

5.1 SAFR Loss of Heat Sink (LOHS)

The feedwater pumps providing water to both of the two steam generators are assumed to lose power, causing the steam generators to dry out in 20 s. Heat rejection is lost except for the small amount that is leaving through the RVACS (about 2.5 MWt). The rest of the SAFR module continues to operate as normal.

The SSC predictions are shown in Figures 38 through 41. The power, as shown in Figure 38, drops from rated conditions to about 6% by 400 s. In Figure 39, the reactivity feedbacks are shown. The positive feedback from the sodium is initially nullified by the negative feedback from the radial expansion. (This is expected since the heat rejection is lost at the steam generators allowing the heat to be dissipated throughout the system. Having such a large thermal dump dampens out the thermal front.) By 40 s, the combined effects of all the negative feedbacks outweigh the positive, and the net negative response reduces the power. The radial expansion feedback is the dominate feedback causing the power to transition to a low level.

From Figure 39 it can be seen that the control rod drive line feedback starts out a few cents negative. The time constant for this is 28 s. However, the reactor vessel also begins to thermally expand due to increased temperatures at a rate corresponding to its 750 s time constant. This withdraws the control assemblies somewhat from the core and causes a positive feedback. SSC predicts this to be worth +10 cents by 400 s.

The peak temperatures for this event do not appear to challenge the system. Figure 40 shows the peak sodium temperature plotted against the saturation temperature, and shows that the temperature increase during the event is small. The margin to boiling for this event is, on the average, 507 K (913°F). The resultant peak fuel temperature history during this event is presented in Figure 41 where it is shown that fuel center line (as well as the rest of the fuel slug) reduces its temperature as the power falls.

The SSC results for the LOHS do differ somewhat from those predicted by ANL. The reactivity trends are reasonably similar, but the SSC timing seems compressed when compared to theirs. The discrepancy has been traced to the fact that the ANL model apparently utilizes a user-specified core inlet sodium

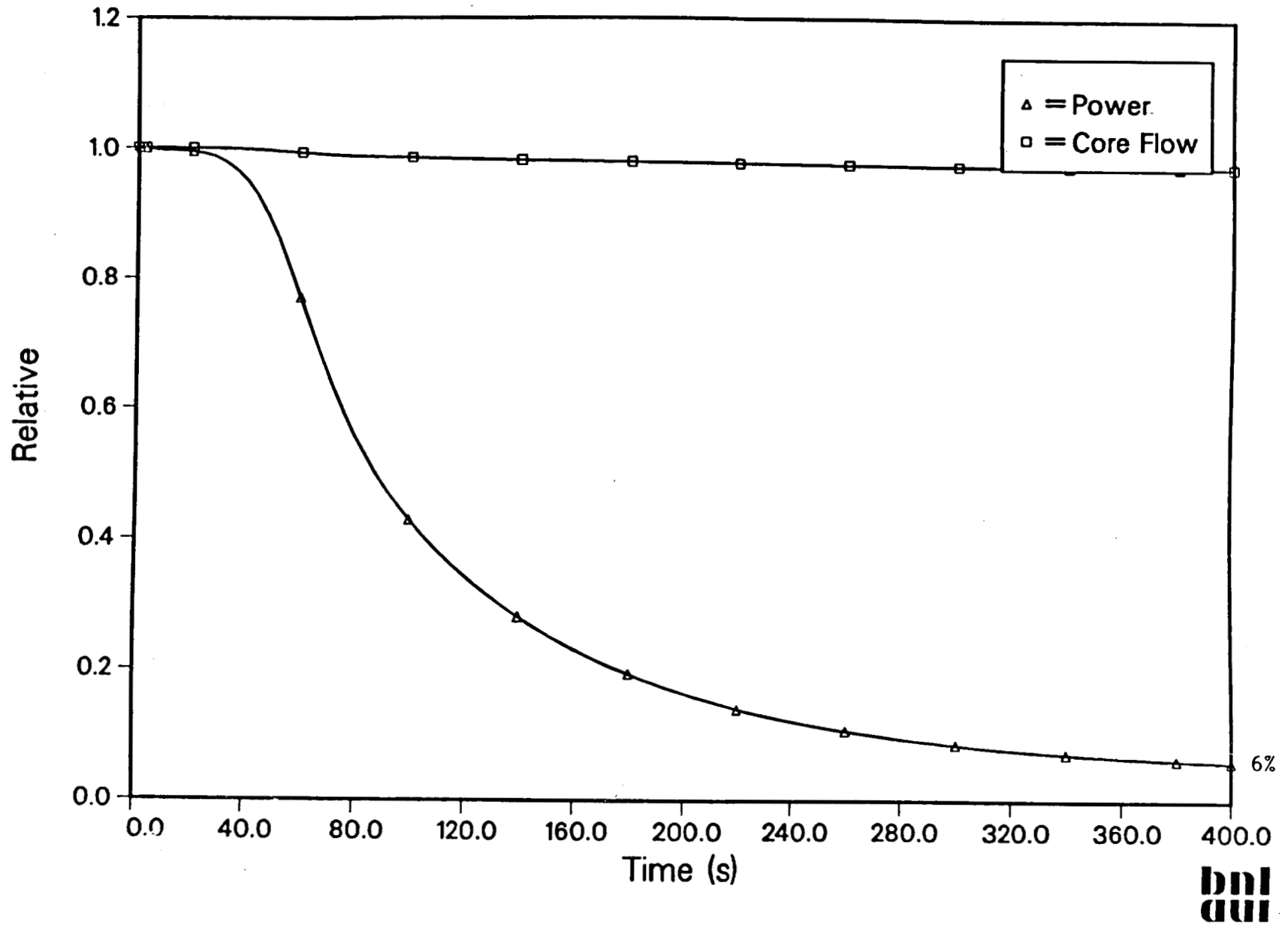


Figure 38 SSC Prediction for SAFR ULOHS: Relative Power and Core Flow

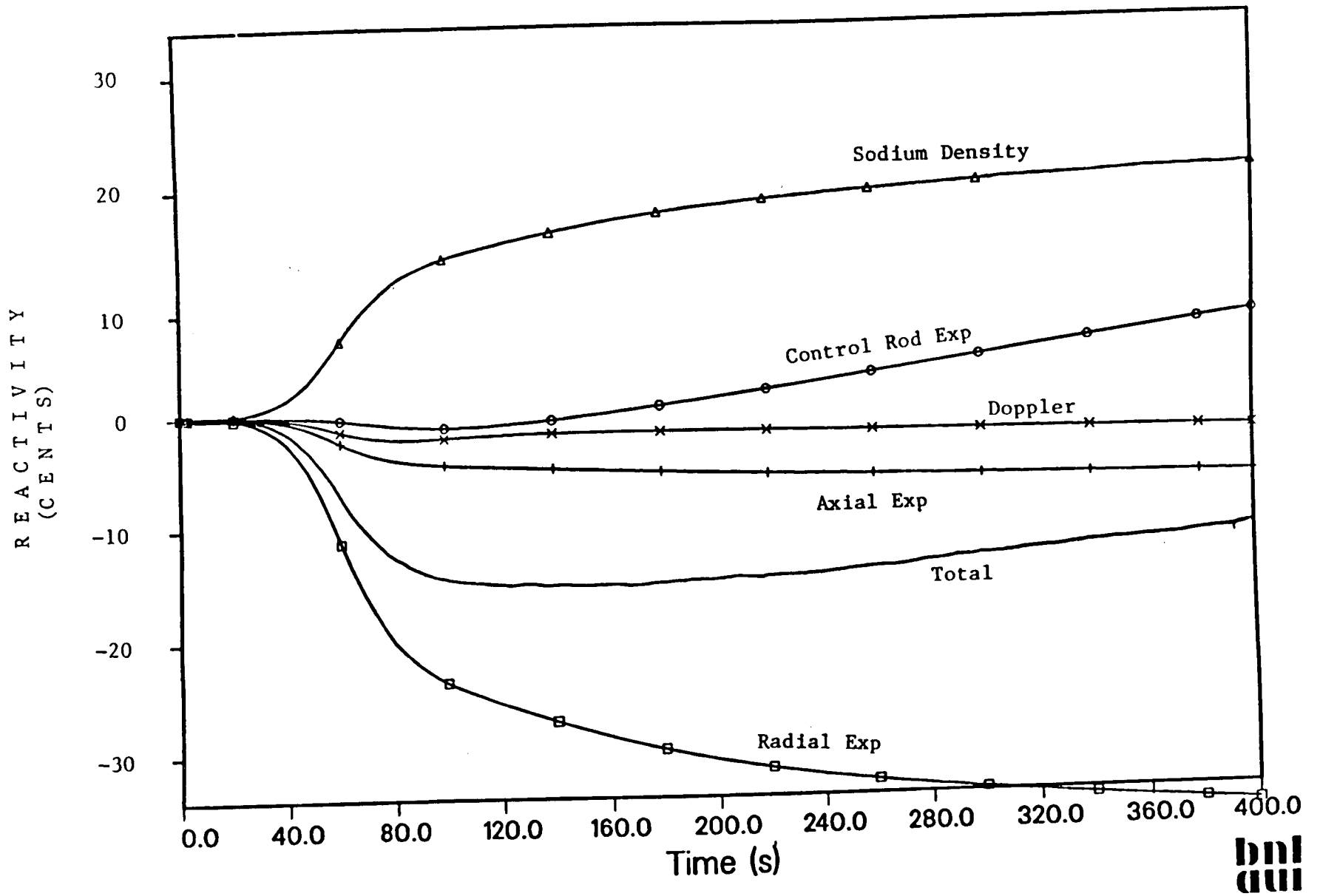


Figure 39 SSC Prediction for SAFR ULOHS: Reactivity Feedbacks



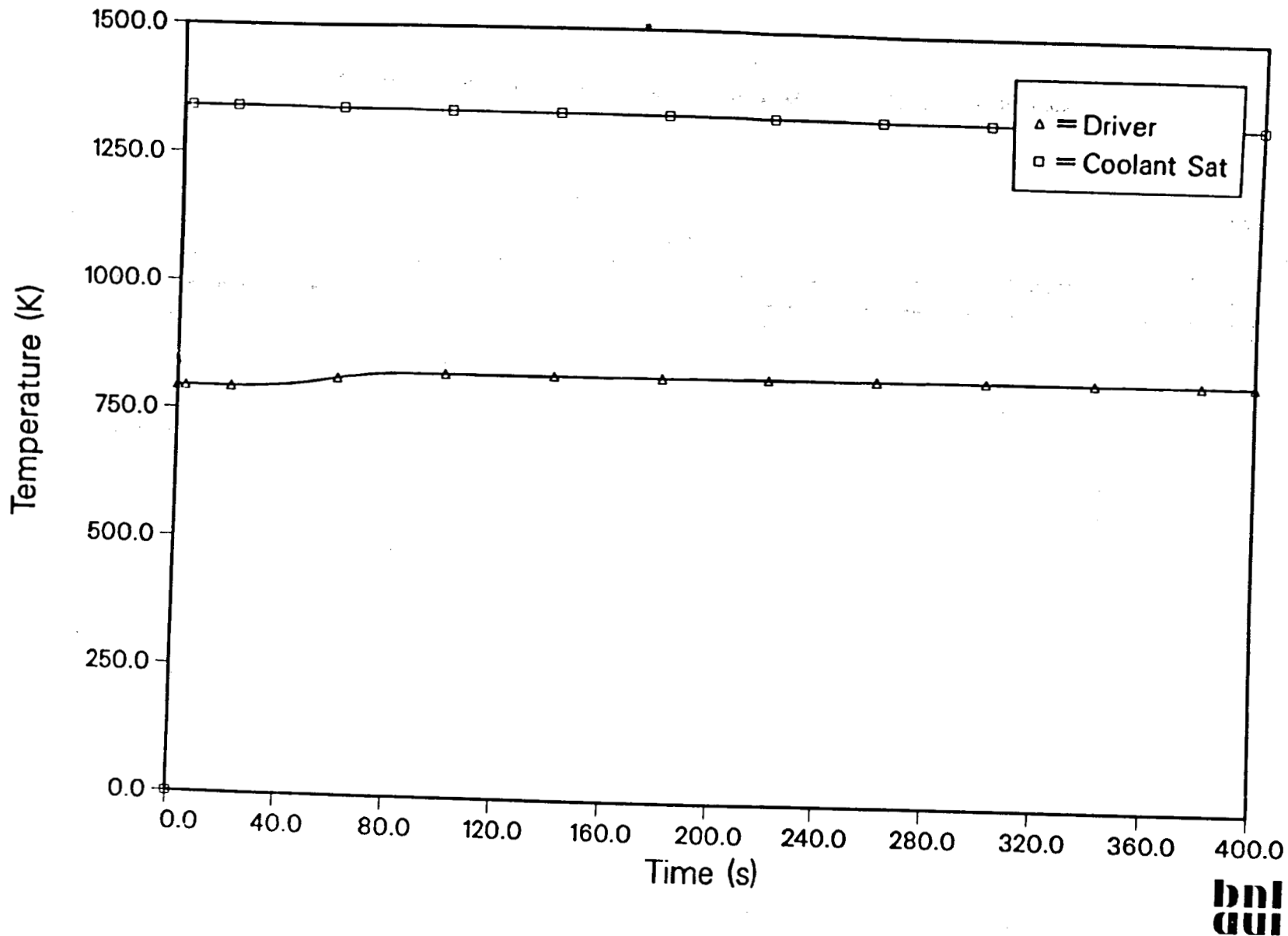


Figure 40 SSC Prediction for SAFR ULOHS: Peak Sodium and Saturation Temperatures



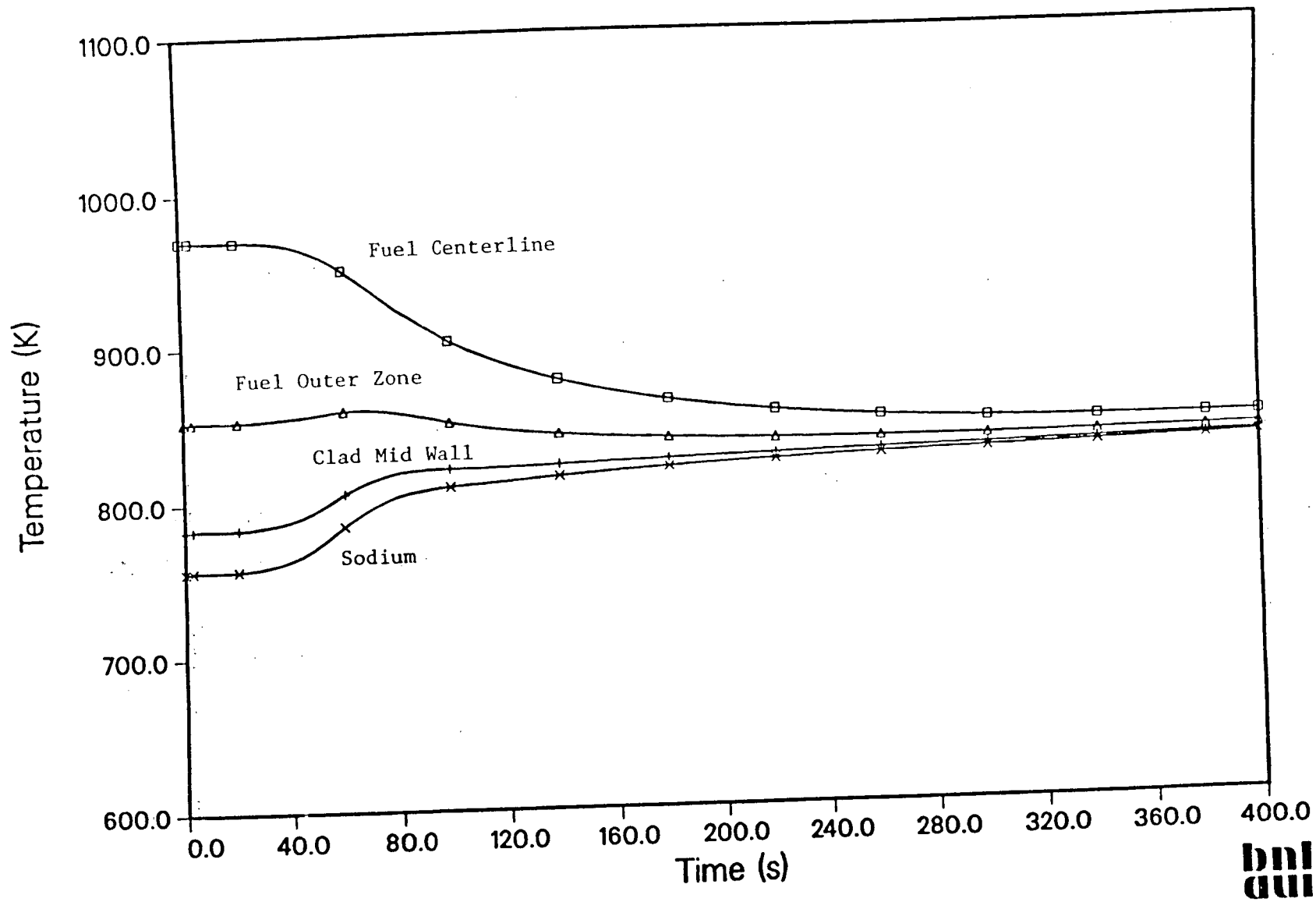


Figure 41 SSC Prediction for SAFR ULOHS: Fuel Temperatures



temperature (as a function of time), while the SSC version actually calculated it dynamically (it increases with time). The SSC version (which modeled the IHX, cold pool, and intermediate loops) predicted higher core inlet sodium temperatures which resulted in the power dropping faster. ANL predicted the power to be about 19% at 800 s, while SSC calculated it to be 6% at 400 s. However, both codes predicted the same general outcome, which is that the power will transition to a lower level and will pose as no threat to the reactor system.

5.2 SAFR Transient Over Power Events

Doppler feedback in a metal fuel LMR is significantly smaller than for an oxide core. This is due to the fact that the metal core has a very hard spectrum, with few neutrons in the Doppler resonance region. This attribute works in a favorable manner for fuel loading (need less) and minimizing the temperature defect (makes it smaller), but during an event when the power increases, the Doppler isn't as effective in stopping the power rise. Thus, the designer must rely on other feedbacks to limit a power increase.

The SAFR TOP event is limited principally by the activation of the radial expansion feedback, although other negative feedbacks contribute. These feedback have time constants of a few seconds and lack the prompt response of Doppler. However, the metal fuel core also has a small TOP initiator because the control rods worth is minimized. This is possible because the breeding ratio is high enough to place the burnup swing near zero which allows the designer to minimize the rod worth. Only enough excess reactivity is added to the fuel cycle to overcome the temperature defect and the expected burnup swing.

To analyze the response of the SAFR module to the TOP, two different initiators were used. The following calculations using SSC were performed to independently verify those performed by ANL.

20 Cent TOP

The reactivity ramp rate for this event is .65 cents/s to a total 20 cents. The plant is assumed to continue operating as normal except for the withdrawal of about three of the six primary control rods. (This quantity is also suppose to correspond to worst case seismic-induced insertion.) The ramp rate corresponds to a withdrawal speed of 0.2286 m/min (9 in/min). In the SAFR module each control rod is operated individually, i.e., they are not ganged together.

The results are shown in Figures 42 through 45. The power is shown in Figure 42 to rise to 130% and to return to a quasi-static power level of 115% by 160 s when criticality is re-established (see Figure 43). The ANL prediction had the power peak at the same level; but the power then drifted down to 104%. The difference comes from the control rod drive line expansion feedback, where ANL shows it to initially go to -7 cents while the SSC predictions goes to -4 cents and decreases from vessel expansion. The other feedbacks match very closely with their counter parts in the ANL calculations.

The sodium and peak fuel centerline temperature are comparable in both

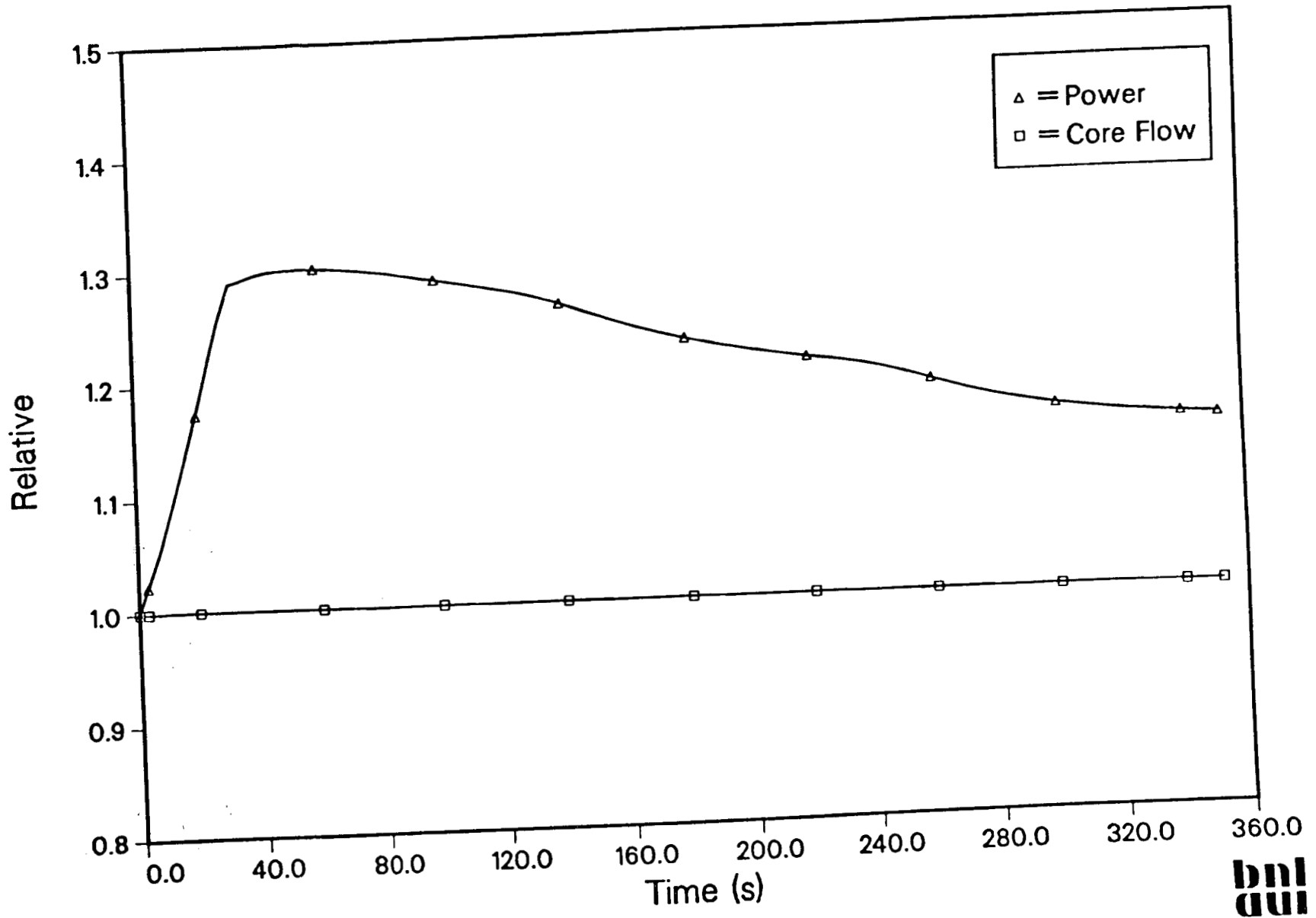


Figure 42 SSC Prediction for SAFR 20 Cent UTOP: Relative Power and Core Flow



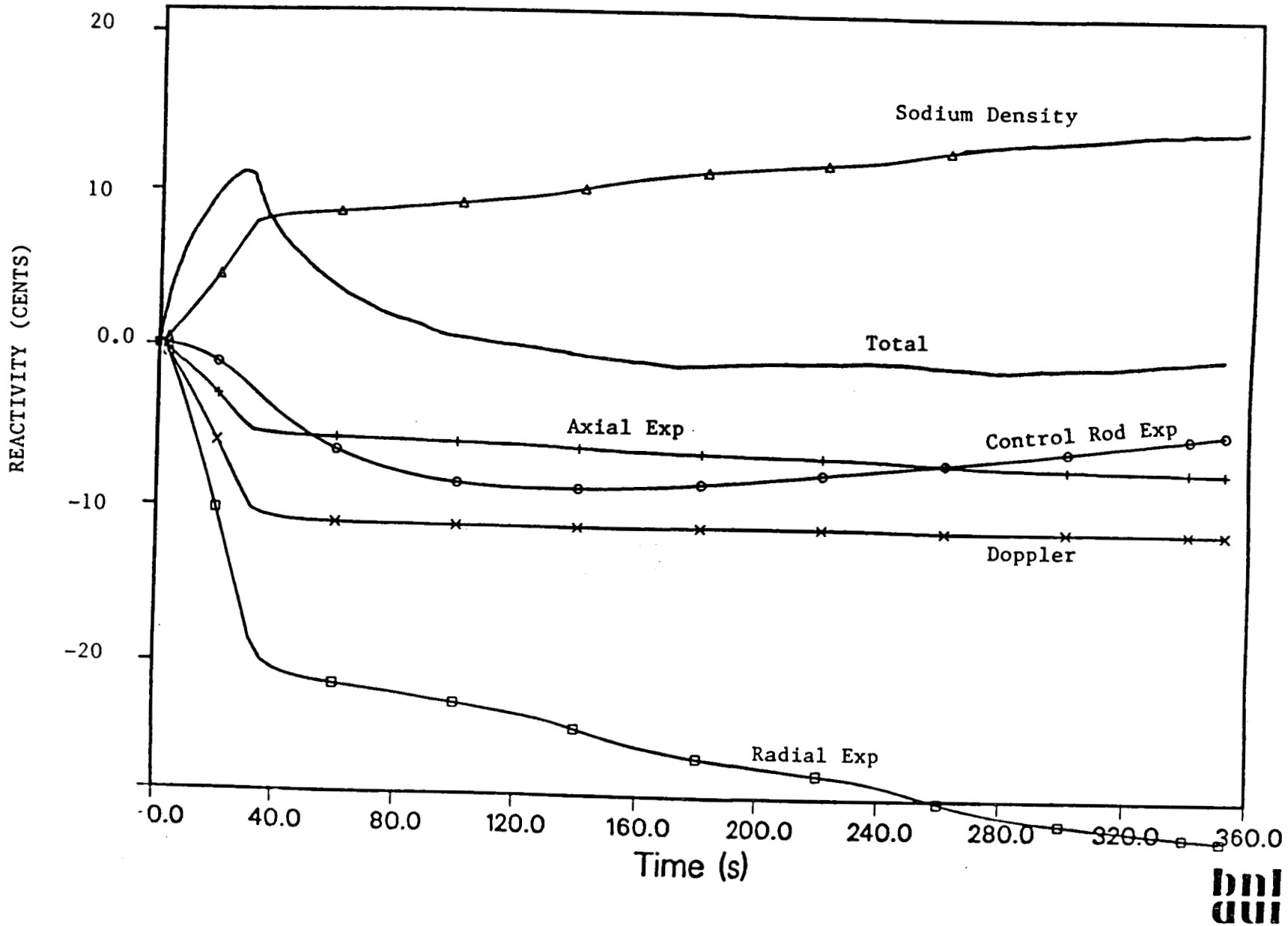


Figure 43 SSC Prediction for SAFR 20 Cent UTOP: Reactivity Feedbacks



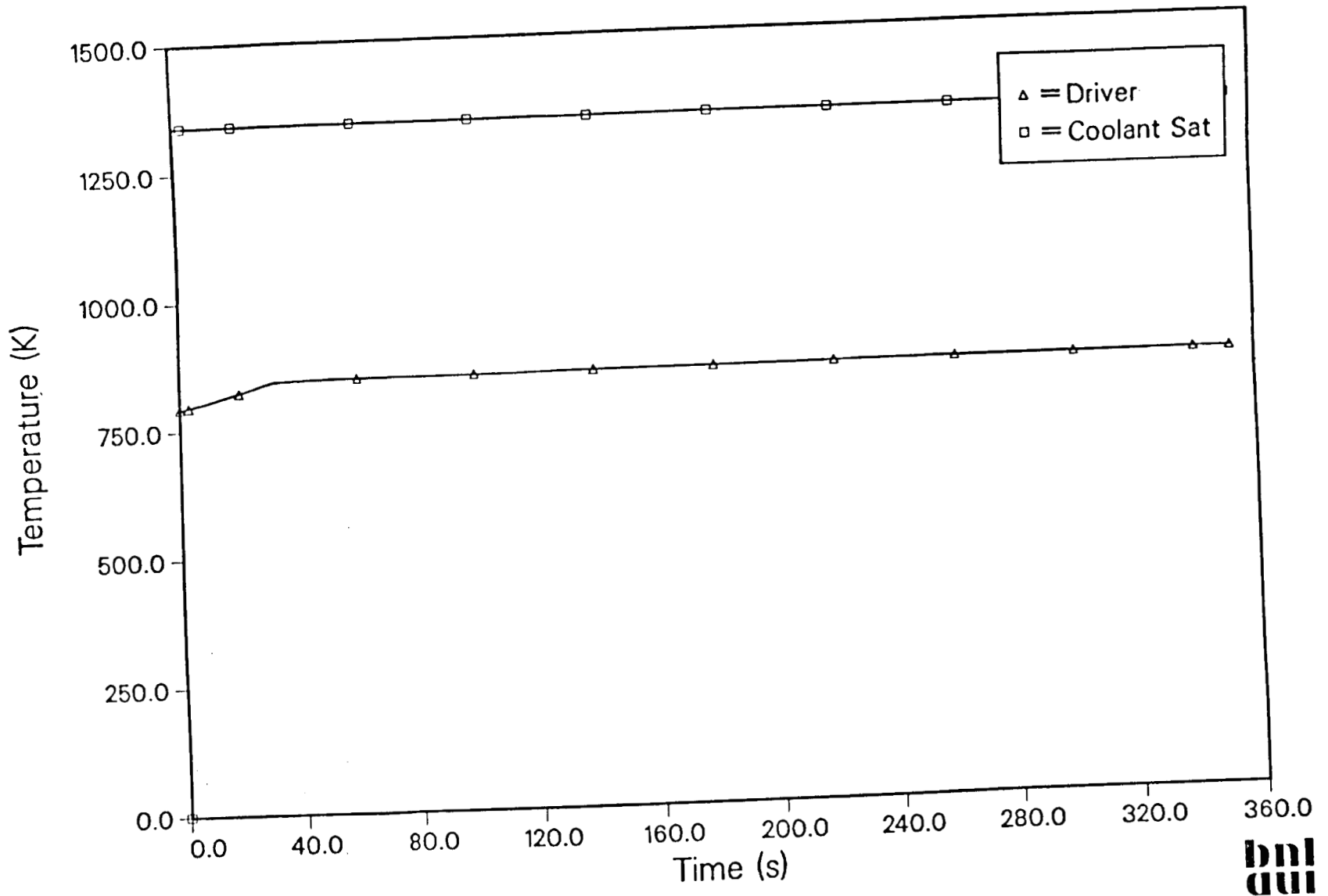


Figure 44 SSC Prediction for SAFR 20 Cent UTOP: Sodium Saturation and Outlet Temperatures



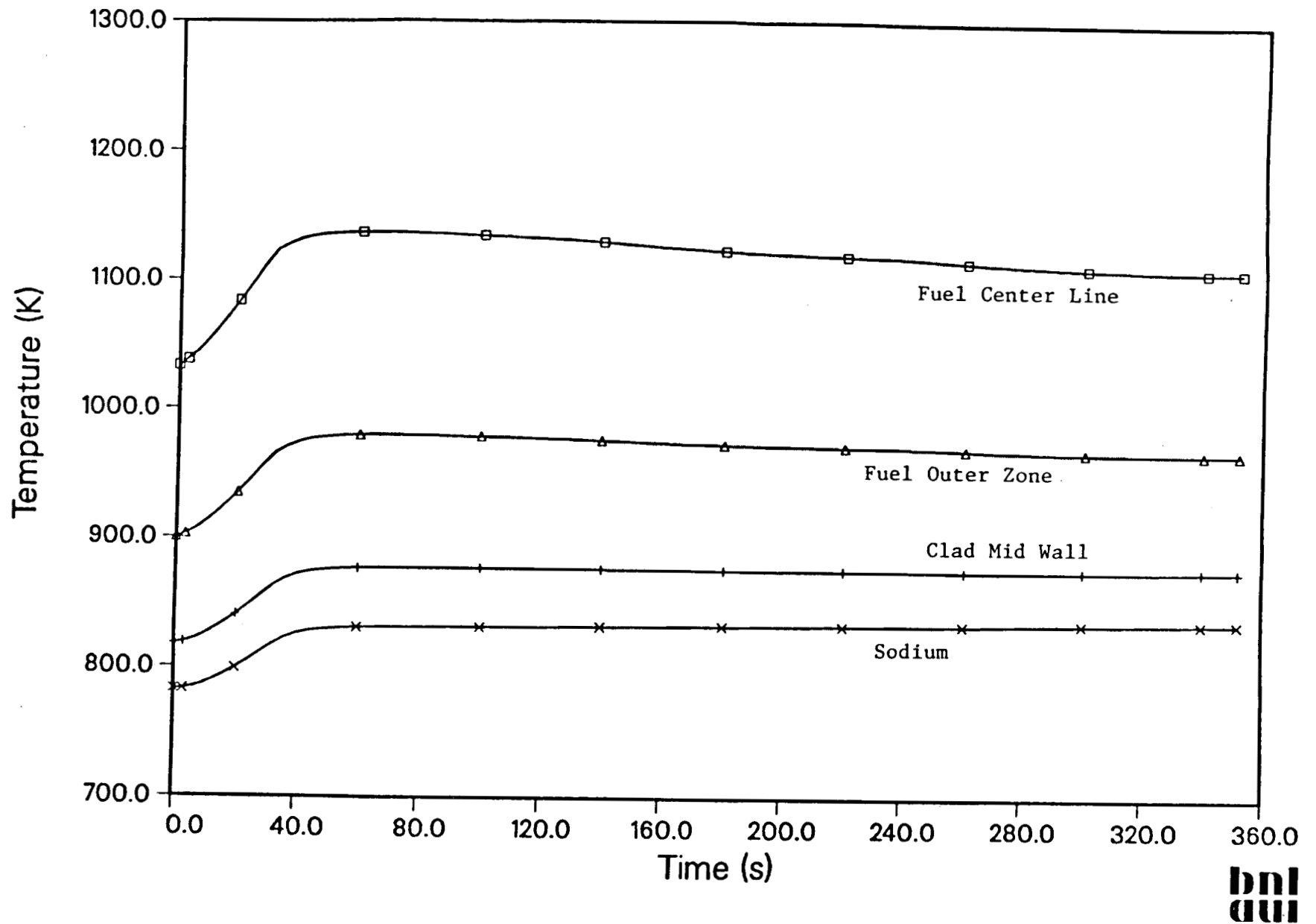


Figure 45 SSC Prediction for SAFR 20 Cent UTOP: Fuel Temperature



calculations. In Figure 44 the peak sodium temperature in the core is shown to reach a value of 870 K (1107°F) while the ANL results go to 872 K (1110°F). The margin to boiling is predicted by both codes to be about 470 K (846°F). The peak fuel centerline temperature is shown in Figure 45 to be 1138°K (1589°F), which compares well with the 1111 K (1540°F) predicted by ANL. The margin to fuel melting (not including Zr migration effects) is 228 K (411°F). All margins are thus predicted to be quite significant.

In summary, the SAFR module appears capable of withstanding a 20 cent TOP indefinitely, since the elevated power and temperature don't pose a problem. It should be noted (see Figure 43) that the Doppler feedback inserted about -6 cents for this event while the radial expansion feedback supplied around a -15 cents by 300 s and is clearly the dominate negative feedback mechanism. This suggests that TOPs can be mitigated as long as the rate of reactivity insertion is within the response time of the time constant for the radial feedback.

36 Cent TOP

The second SAFR TOP event is based on a ramp rate of 5 cents/s to a total of 36 cents. This amount of reactivity corresponds to the withdrawal of all six of the primary control rods at a rate of 1.02 m/min (40 in/min). Again, the rest of the plant is assumed to function as normal.

The SSC results are shown in Figures 46 through 49. The power, as shown in Figure 46, is predicted to reach 156% of rated and slowly drift back toward rated conditions. These results closely match those of ANL, since their power peaked at 154% and was at 120% by 350 s. For the same times, SSC predicted the power to be at 156% and 125%. The transient simulation was terminated at 350 s since the peak fuel and clad temperatures had already been passed, and the power level was continuing to decrease. The reactivities plotted in Figure 47 also match within a few cents with those predicted by ANL except for the control rod drive expansion feedback. The SSC predictions indicated that the reactor vessel was elongating and withdrawing the control rods from the core while the ANL plots indicate no vessel expansion since their control rod feedback plot remained flat. This effect caused the different rates of power reduction between the calculations. However, this effect is small, and both codes show the same trends.

Radial expansion is the dominate feedback. In Figure 47, the total reactivity is the accumulation of all the components. The radial feedback is the largest of the negative feedback effects, while the second largest is the sodium density effect - which is the only major positive feedback. The Doppler feedback only generated about -7 cents, while the radial expansion was providing -25 cents by 350 s. Thus, the power history of the TOP is basically controlled by the response of the radial expansion feedback.

The margins to sodium boiling and fuel melting were substantial in this calculation. The peak sodium temperature in the core is shown in Figure 48, where it is plotted against the saturation temperature. The results show that the temperature is about 895 K (1152°F) which gives a margin of 445 K (801°F). The ANL peak sodium temperature prediction was 908 K (1175°F). The peak fuel center line temperature was calculated to be 1221 K (1738°F) using

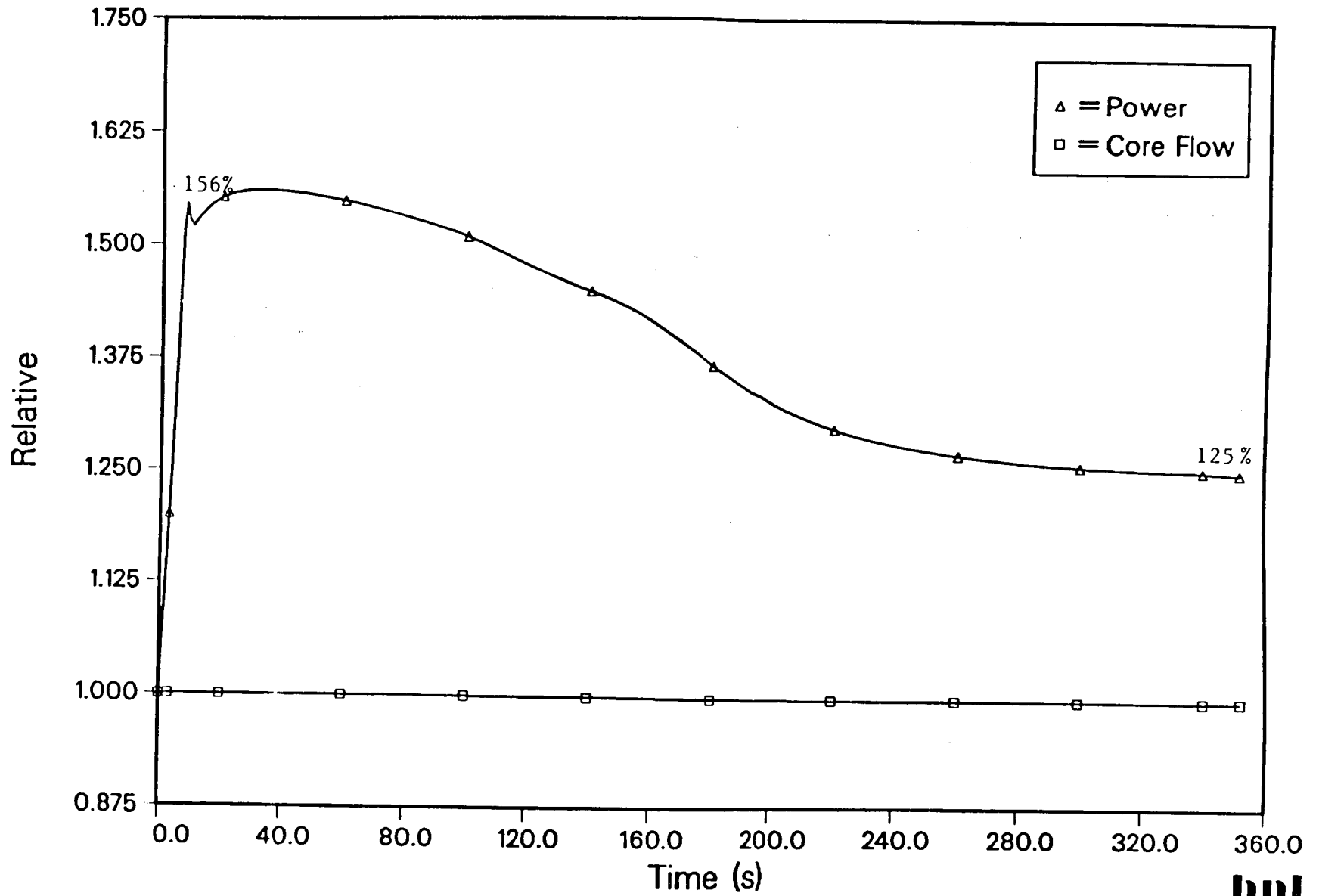


Figure 46 SSC Prediction for SAFR 36 Cent UTOP: Relative Power and Core Flow



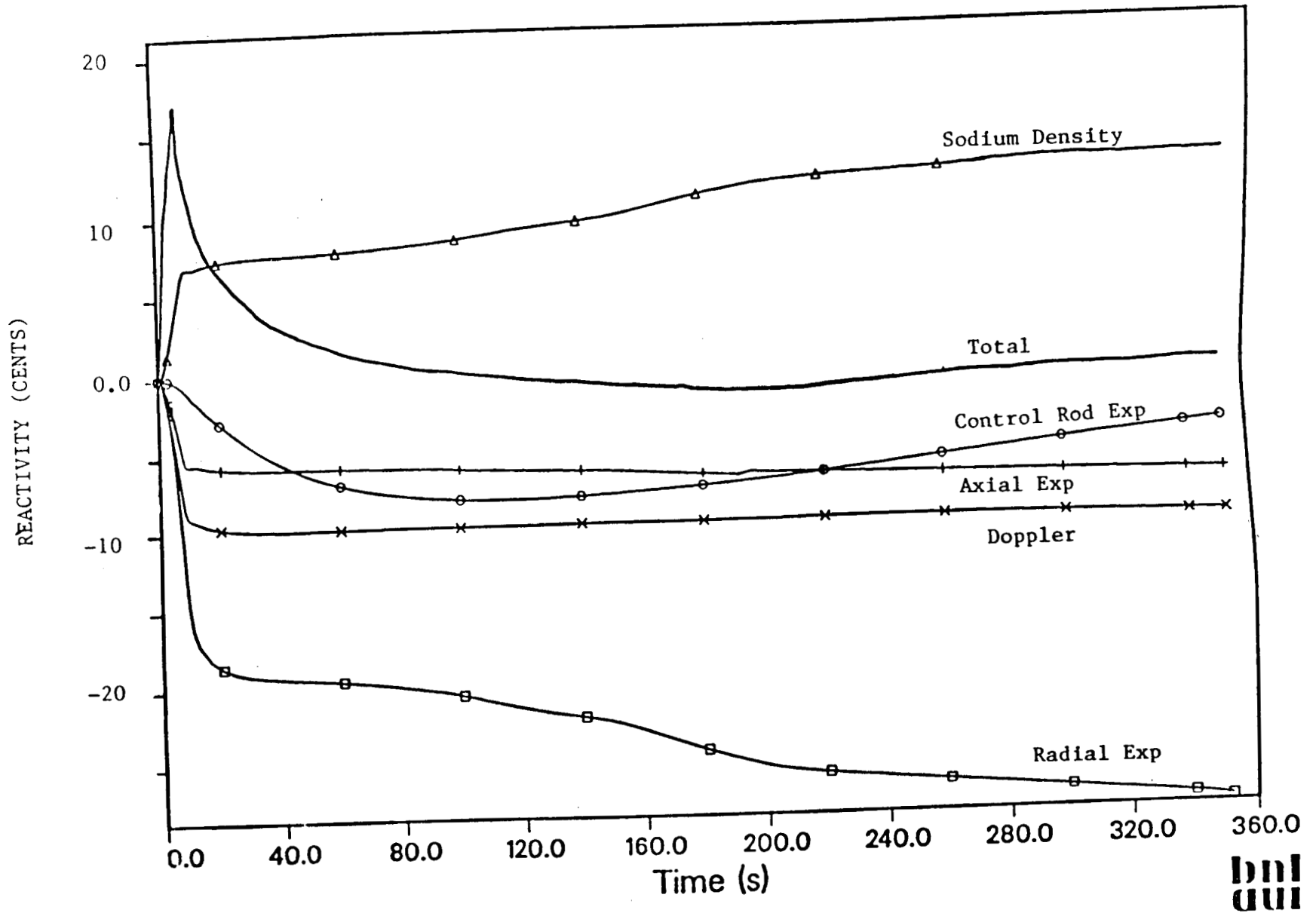


Figure 47 SSC Prediction for SAFR 36 Cent UTOP: Reactivity Feedbacks



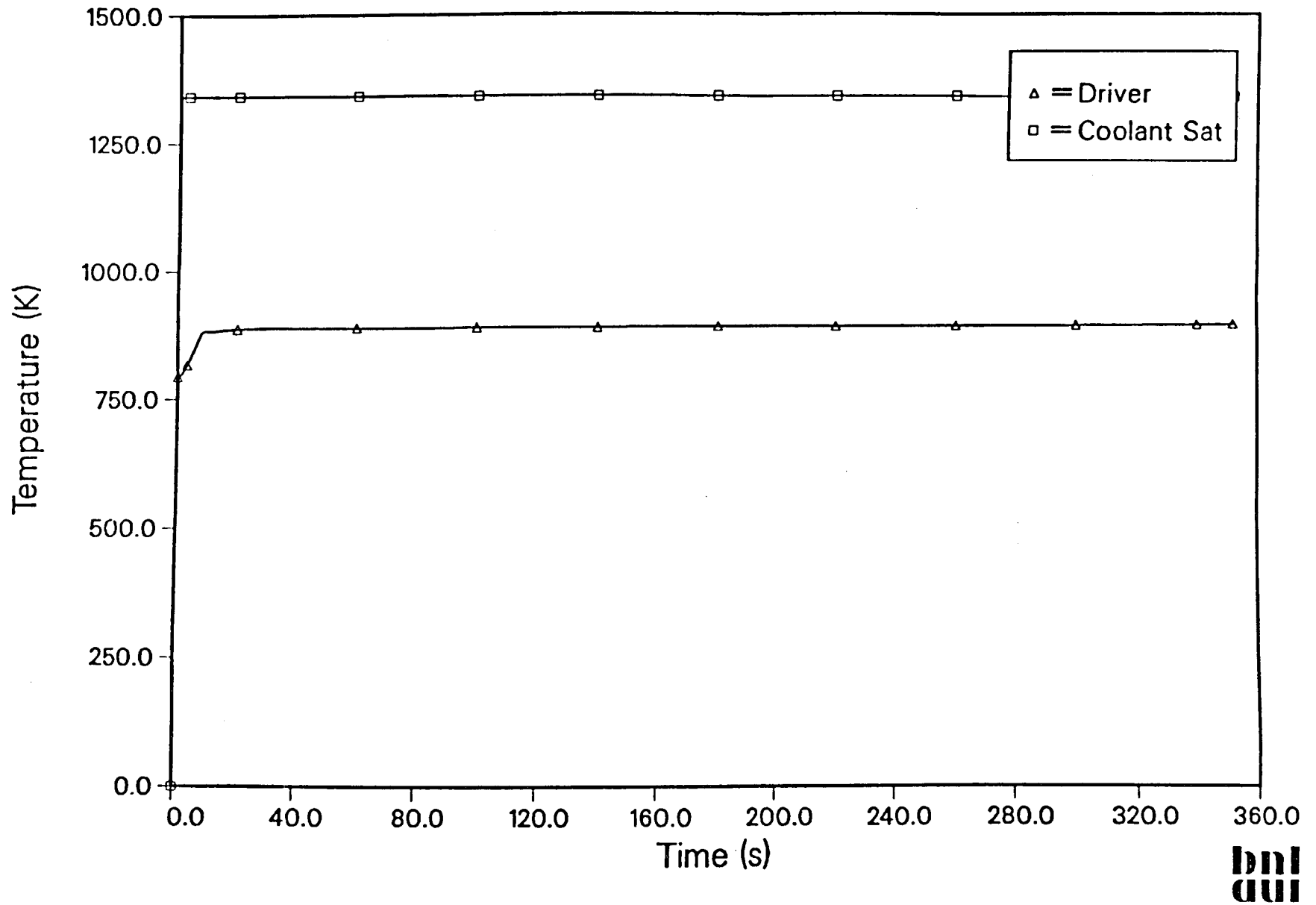


Figure 48 SSC Prediction for SAFR 36 Cent UTOP: Sodium Saturation and Outlet Temperatures

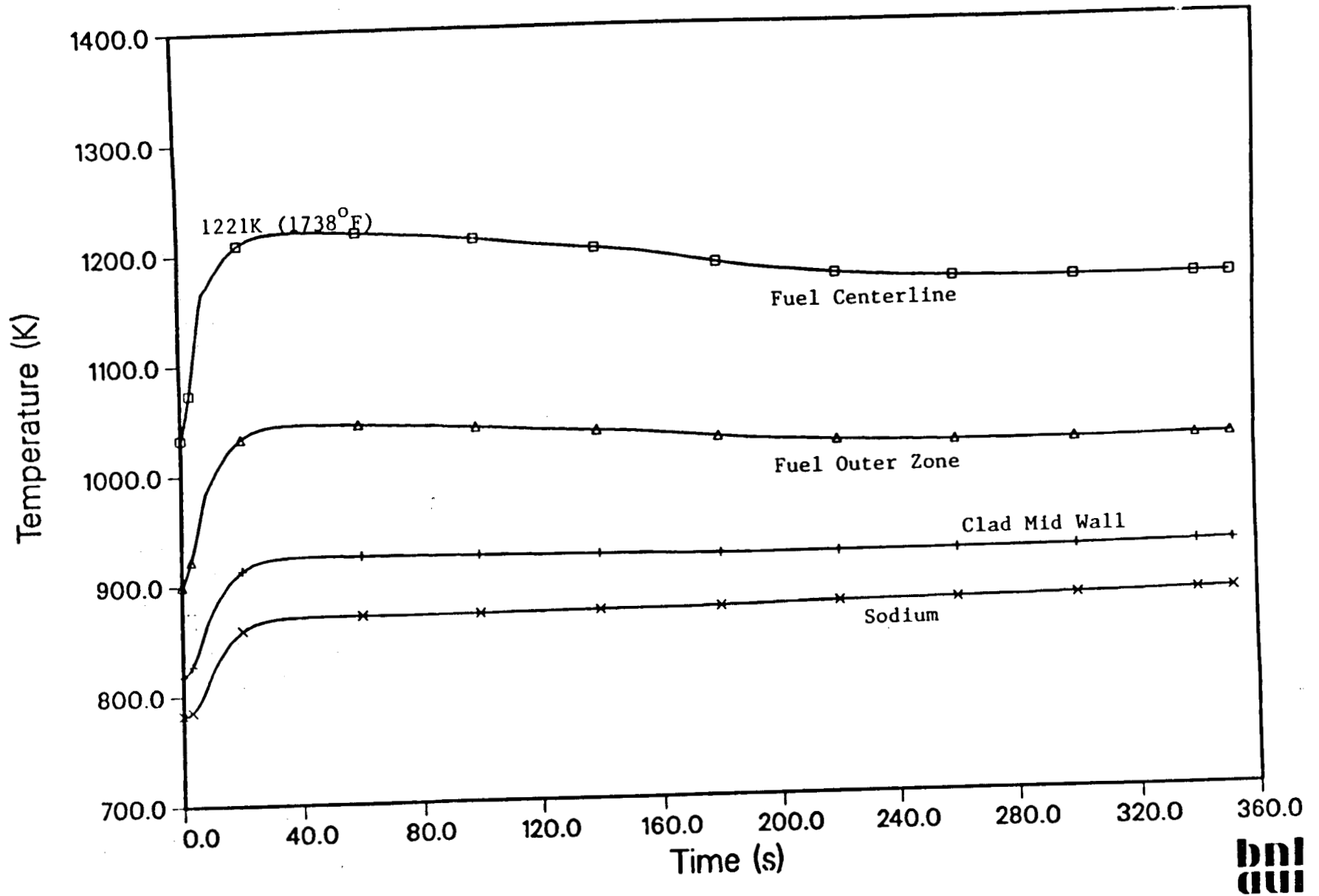


Figure 49 SSC Prediction for SAFR 36 Cent UTOP: Fuel Temperatures

SSC, which is higher than the 1130 K (1575°F) estimated by ANL. However, neither code predicted that the fuel melting temperature of 1366 K (2000°F) would be approached by closer than 145 K (261°F). The peak fuel-clad interface temperature momentarily reached the eutectic threshold of 972 K (1290°F) around 20 s, but it settled back to about 944 K (1240°F) and will continue to decrease as the power descends. Consequently, no fuel damage is expected during this event.

5.3 SAFR Loss of Flow Event

The event is initiated by an instantaneous loss of power to the primary, intermediate loop and steam generator pumps. No scram is assumed and the inertially-controlled coastdown of the primary pump is characterized by an initial 6 second flow halving time. Around 135 s after the loss of power, the sodium coolant flow goes into natural circulation and the pump rotor stops rotating.

Key results are presented in Figures 50 through 52. In Figure 50, it is shown that the power level drops off as the flow decreases. The fuel temperatures increase because of the reduced coolant flow in the core, activating the Doppler and axial expansion feedbacks. The reduction of coolant flow in the core also causes the sodium temperatures to increase. This inserts positive reactivity because of the hardening of the neutron spectrum. However, once the sodium begins to heat up, it disperses the heat throughout the system and activates the radial dilation at the ACLPs, which in turn activates the radial expansion feedback. In Figure 51 it is shown that the radial expansion feedback dominates, causing a reduction in power. By 140 s the power level reaches a quastatic level at about 10% of rated power, where the reactivity feedbacks are balanced and power remains steady. The peak channel sodium exit temperature is shown in Figure 52 to be 1020 K (1377°F) and has a 180 K (324°F) margin to boiling. The peak fuel center line temperature was found to be 1050 K (1431°F) which gives a margin of 316 K (569°F) to the fuel melting point. (The reduction in the solidus or fuel melting temperature is not considered here since the effect of Zirconium migration and its effect were not simulated.)

These results are quite similar to those predicted by ANL. The SSC prediction for the peak coolant temperature was 1020 K (1377°F), while ANL calculated 1037 K (1407°F). The peak fuel centerline temperature was predicted by SSC to be 1050 K (1431°F) while ANL calculated 1069 K (1465°F). The reactivity feedbacks were predicted by both to reduce the power level to a much lower level and avoid damage to the fuel. Also, the margin to sodium boiling is large in both calculations.

The eventual result is that the reactor power level transitions to a much lower level. However, the feedbacks which initially started out strongly negative ultimately re-established a critical state after a few hundred seconds. The feedbacks were able to reduce the power level significantly because the temperature defect in a metal fuel core is small, about \$1.6. Hence, the negative feedbacks were able to overcome the Doppler and decrease the power, while maintaining the core at elevated temperatures. The results indicate that the reactor could maintain this state for quite an extended

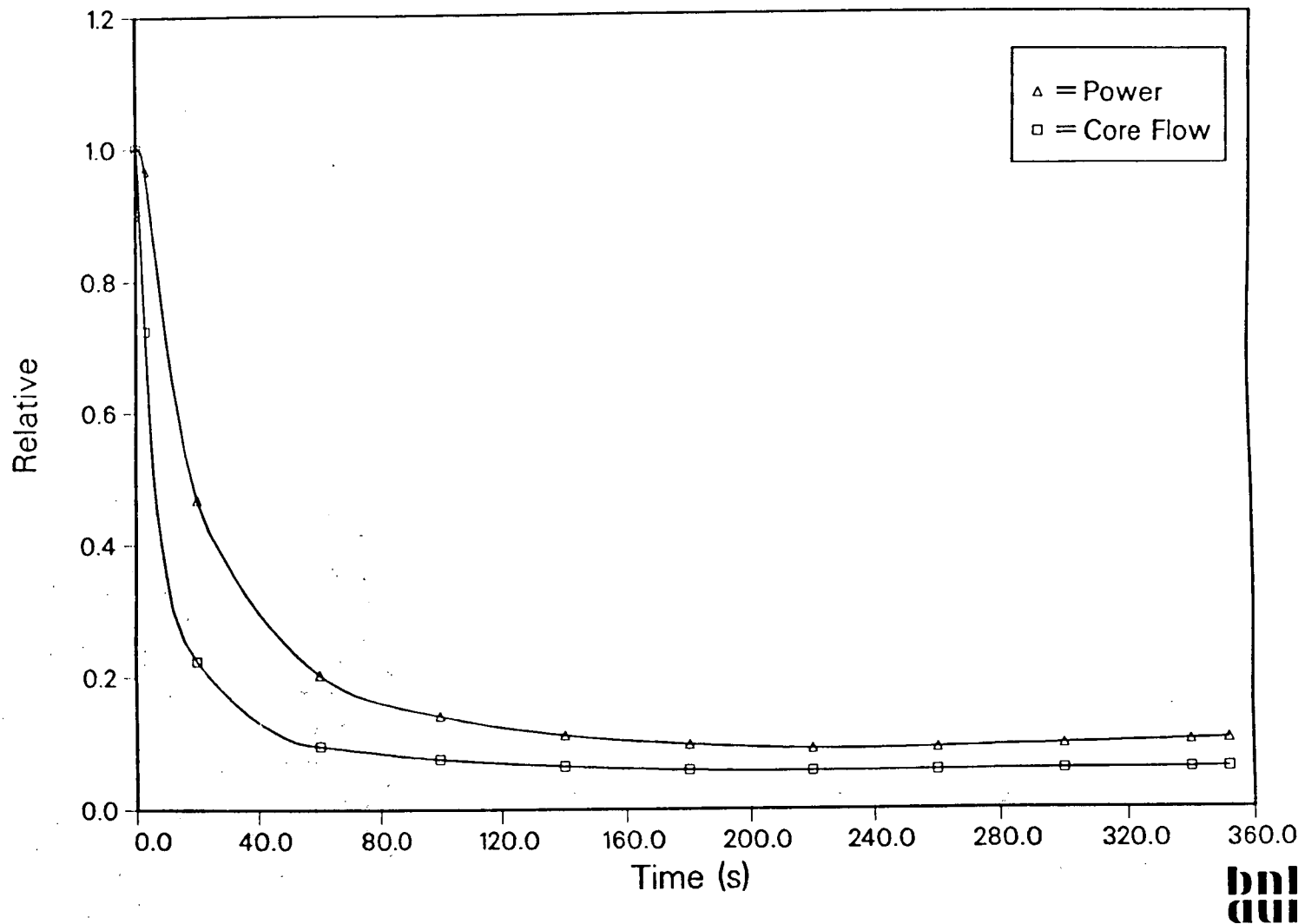


Figure 50 SSC Prediction for SAFR ULOF: Relative Power and Flow

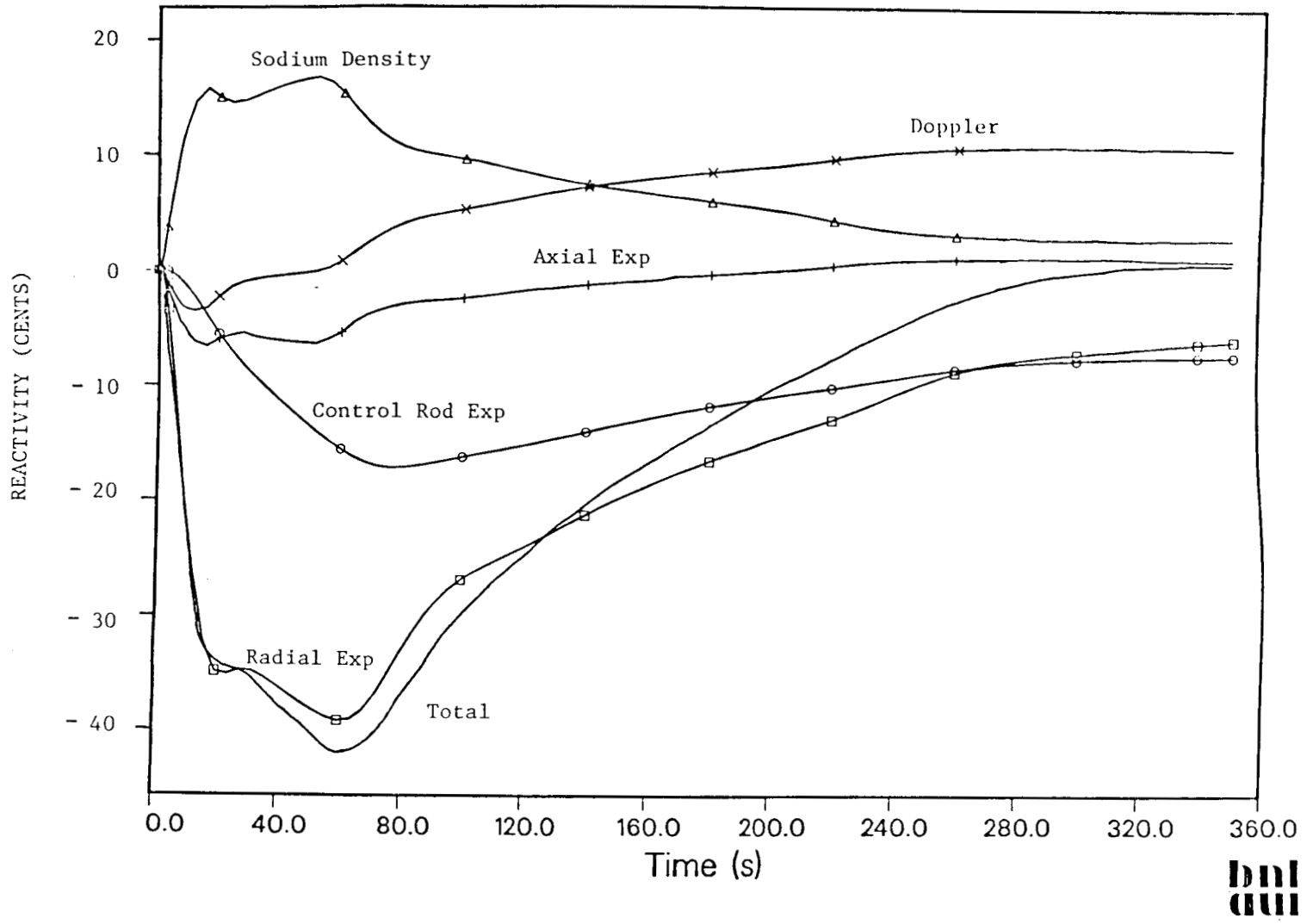


Figure 51 SSC Prediction for SAFR ULOF: Reactivity Feedbacks



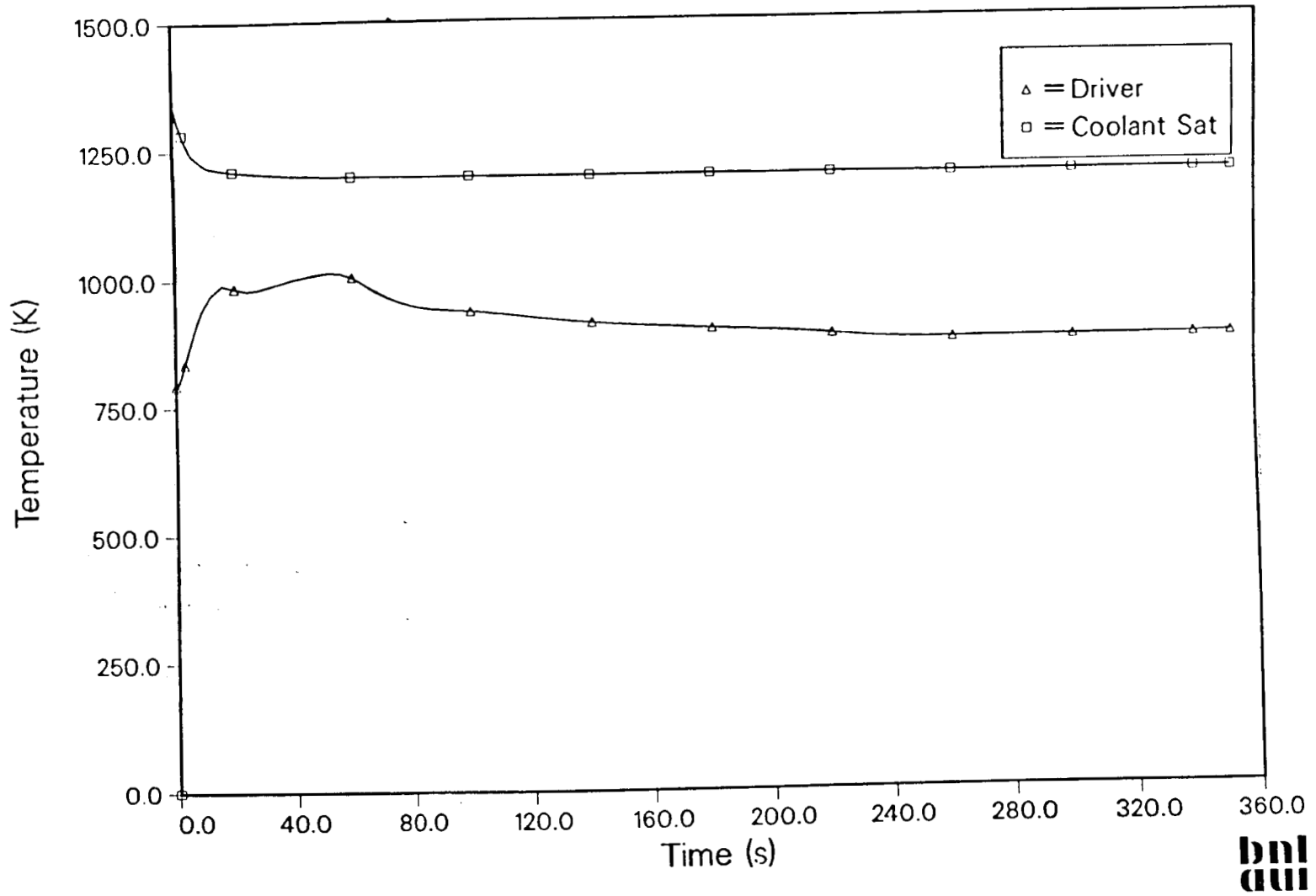


Figure 52 SSC Prediction for SAFR ULOF: Sodium Saturation and Outlet Temperatures



period without danger. However, the plant must be scrammed to shut the fission process down completely; furthermore, the operator doesn't have to make a fast decision or take quick action to avoid damage to the core.

5.4 Combined TOP/LOF in SAFR

The 20 cent TOP with a ramp rate of 0.65 cents/s (9 inch/min or 13.72 m/s) was rerun with a LOF added. The purpose of this simulation was to encompass the reactivity insertion that could accompany a SSE. The 20 cents actually corresponds to the worth of three primary rods, and should be conservative for the SSE since the reactivity insertion from assembly movement was estimated by RI to be a maximum of 13 cents. The event is initiated by tripping the pumps (with their associated reference coast downs, and ramping in the reactivity).

The SSC results are shown in Figures 53 through 55. The power and flow history are shown in Figure 53. The power increases a few percent and then drops off. By 200 s, the power is down to 14%, and will continue to drop due to the total reactivity remaining negative, see Figure 54. The plot of the reactivities demonstrate that the radial expansion feedback dominates the initial response of the core and therefore drives the drop in power. The control rod expansion and the radial expansion are the two most significant negative feedbacks by the end of the 200s transient. The power is able to transition to a lower level because the system average temperature increases (which activates the radial expansion, control rod drive line expansion, and axial expansion for the negative feedbacks, while causing a positive response only from the sodium density) generating a net negative feedback. The more dominant Doppler phenomena in an oxide core would hinder or stop a power reduction because it has the potential to insert far more positive reactivity as the power and temperatures fall. The problem doesn't exist in the metal core.

The safety margins for this event are significant. The peak sodium temperature was found to be 1060 K (1449°F), which leaves a 150 K (270°F) margin to sodium boiling, see Figure 55. The peak fuel centerline temperature was calculated to be below 1089 K (1500°F), which makes the margin to fuel melting greater than 277 K (499°F). No clad damage would be expected from eutectic penetration. These are significant margins for such a severe event.

5.5 Pump Seizure without Scram

One of the two centrifugal pumps in the SAFR plant is assumed to seize during full power operation. The other pump continues to operate, and the plant protection system fails to SCRAM. A pump seizure at full speed is considered to be a very unlikely event. The only known full speed seizure in the U.S. was a pump in the Sodium Pump Test Facility (SPTF) at ETEC. All other seizures have occurred during the coast down phase.

The MINET code was used to model the flow network around the core. The most important aspect of this analysis is the modeling associated with the behavior of the (1) operating, and (2) seized pumps. This ultimately determines how much flow will continue through the core. The seizure causes a drop in system impedance, and the unfailed pump will experience a large flow increase

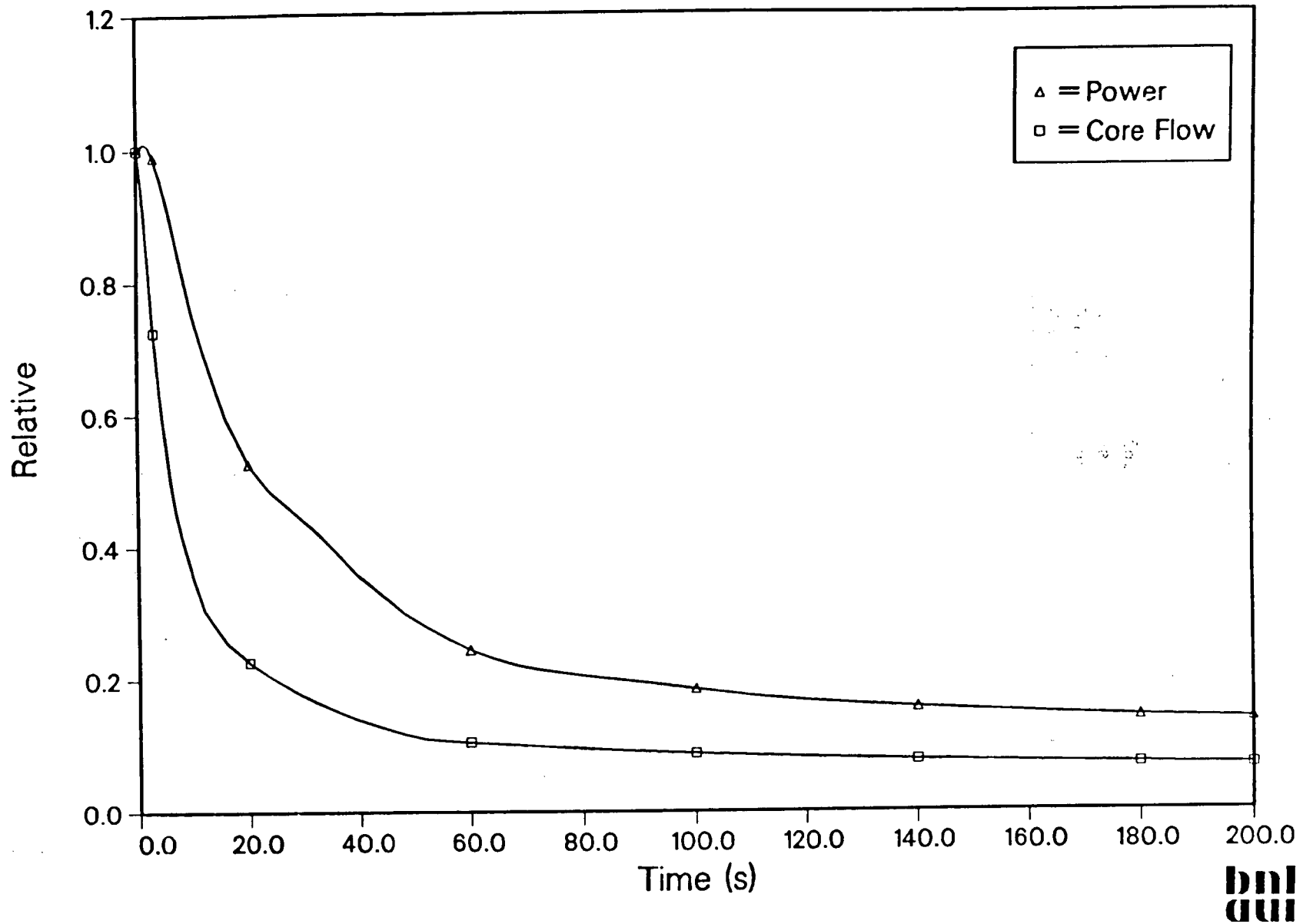


Figure 53 SSC Prediction for SAFR 20 Cent UTOP/LOF: Relative Power and Flow



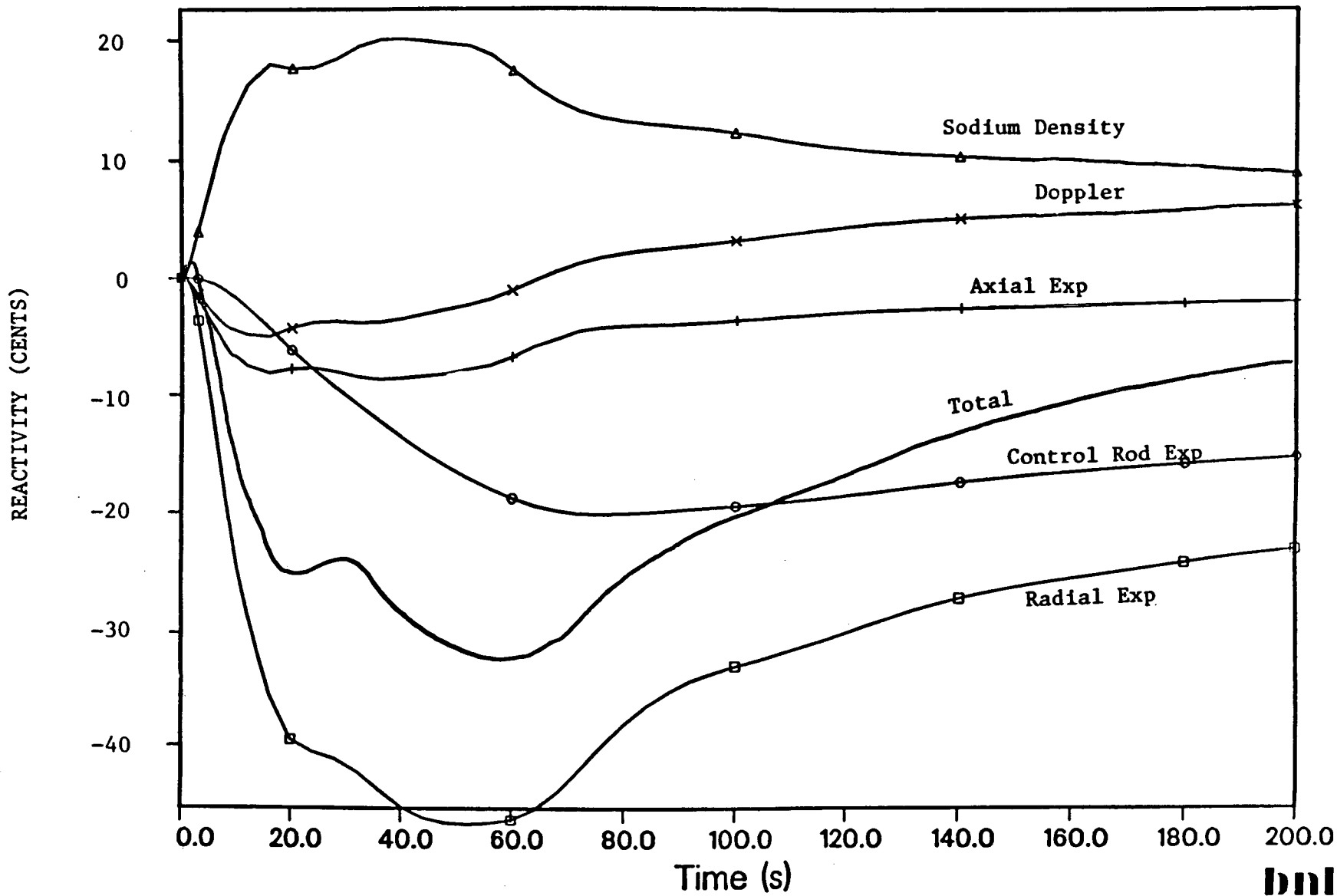


Figure 54 SSC Prediction for SAFR 20 Cent UTOP/LOF: Reactivity Feedbacks

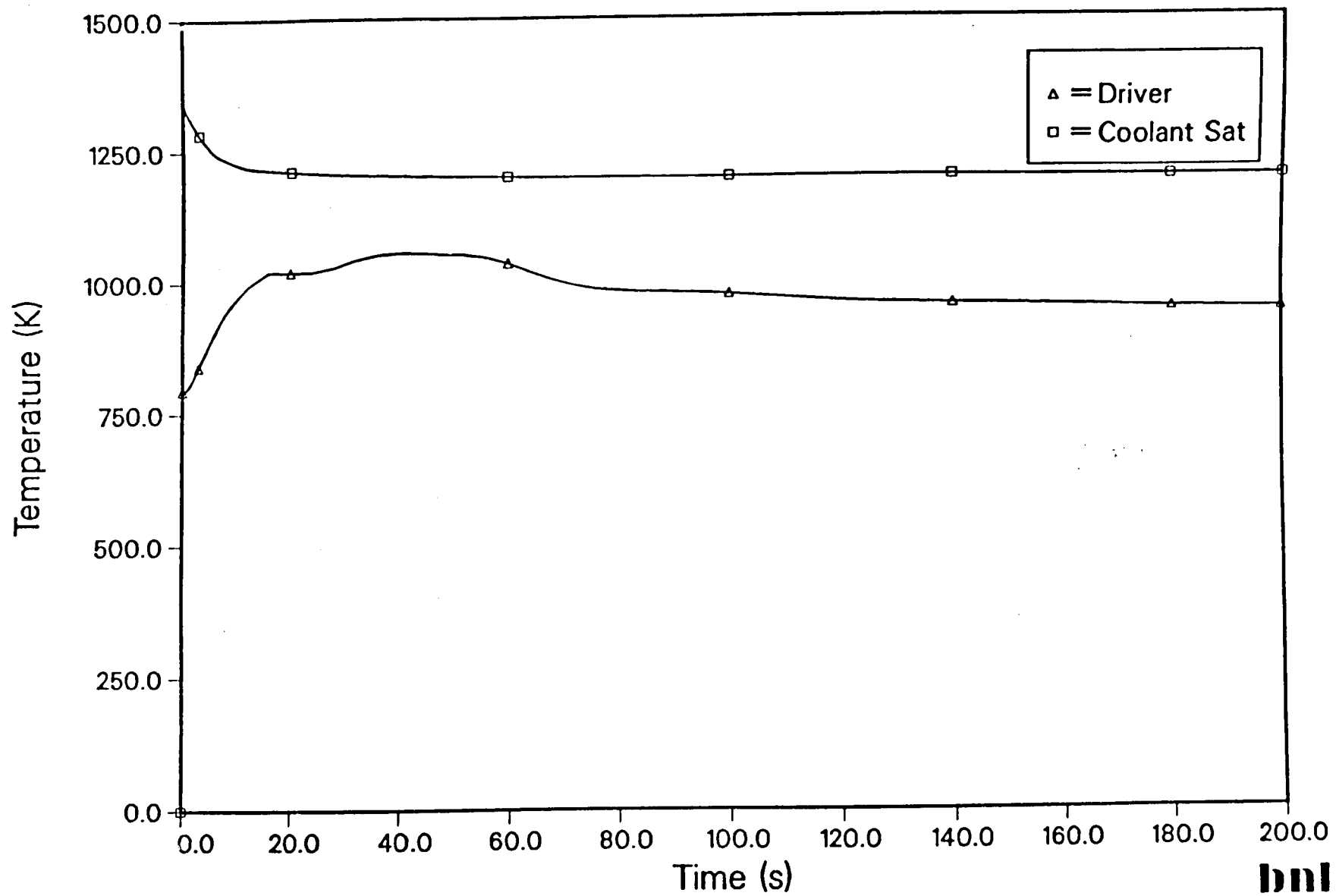


Figure 55 SSC Prediction for SAFR 20 Cent UTOP/LOF: Sodium Saturation and Outlet Temperatures



up to 128% of its rated condition. The pump will cavitate in this mode. (The designers are fully aware of this problem and believe that they can design a pump to operate in this regime.) The resistance through the locked rotor directly determines the amount of flow that will bypass the core and feed back into the cold pool. The MINET model accounted for all the above effects and found that 65% of the system flow will bypass the core through the locked rotor. As shown in Figure 56, the remaining 35% of the system sodium flow will still continue to flow through the core.

The prescribed flow condition from MINET was simulated in SSC and the results are presented in Figures 57 and 58. The power in Figure 57 drops immediately to 50% and re-establishes a critical condition at about 52% of rated power. In Figure 58, the reactivity feedbacks that make up the inherent response to a sudden loss of flow in a metal fueled core are shown. The initial reaction comes from the Doppler and axial expansion feedback, since the reduction in coolant flow induces them to heat up first. This generates a negative feedback, as both give a negative feedback for a temperature increase. Within the first few seconds, Doppler and axial expansion insert -6 and -9 cents, respectively. The drop in sodium flow, coupled with the increase in fuel temperatures, leads to increased sodium temperatures which generates a positive feedback. This added about +17.5 cents of reactivity at its peak, and then slowly returned to zero around 200 s when the reactor re-established criticality. Hotter sodium temperatures increase temperatures in the surrounding structures and the load pads, which activates the radial expansion. From Figure 58, it is clear that the radial expansion feedback is the dominant mitigating factor, and that this is the most significant feedback in terminating the event.

It should be noted that the Doppler reactivity only inserts about +7 cents of reactivity after the power is re-established at 52%, as shown in Figure 58. A negligible Doppler, and the correspondingly reduced temperature defect, makes it possible for the small reactivities generated in the metal fuel core to force the power to a much lower power level.

While this event is challenging, the safety margins are still large. The peak fuel center line temperature was calculated by SSC (see Figure 57) to be 1134 K (1581°F), which leaves a 232 K (419°F) margin to the solidus temperature. The peak assembly outlet temperature was calculated to be 1050 K (1431°F) which is well below the saturation temperature of 1222 K (1740°F). Furthermore, the feedbacks reduced the power level to a point where the maximum fuel centerline temperature and the maximum sodium temperature in the core is low enough at the new quasi static condition that the system could endure this situation indefinitely without serious consequences.

The ANL prediction for this event was only calculated out to 18 s and a comparison is not practical. One difference between the two analyses was that ANL estimated that the core would receive 40% of the system flow even after the pump seized, while the MINET results indicate the value to be 35%. Both calculations, however, predicted that this event would be mitigated by the feedbacks in the core with no fuel damage or requirements for immediate operator action.

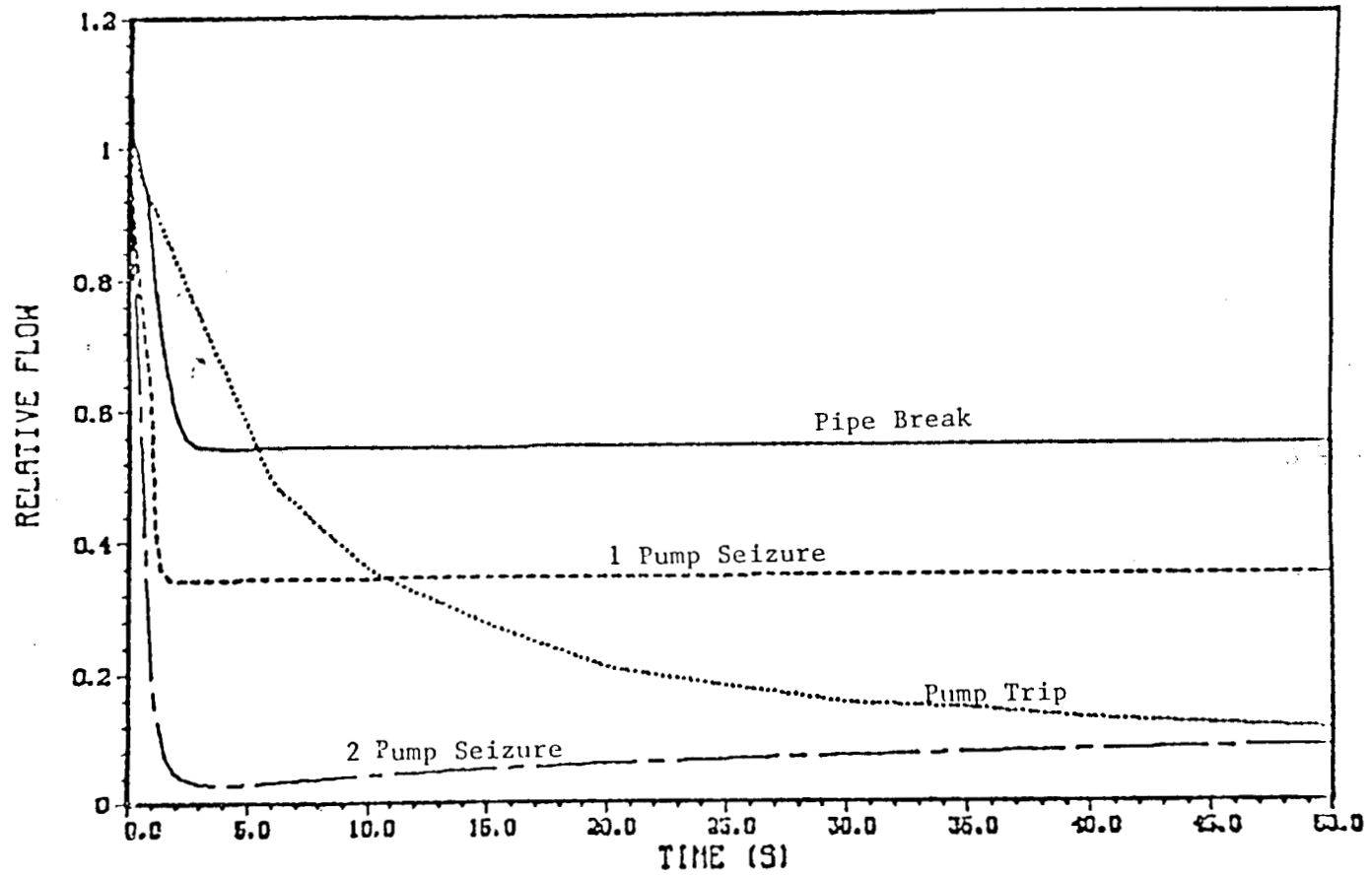


Figure 56 MINET Prediction of SAFR Core Flow Rate for Various LOF Cases

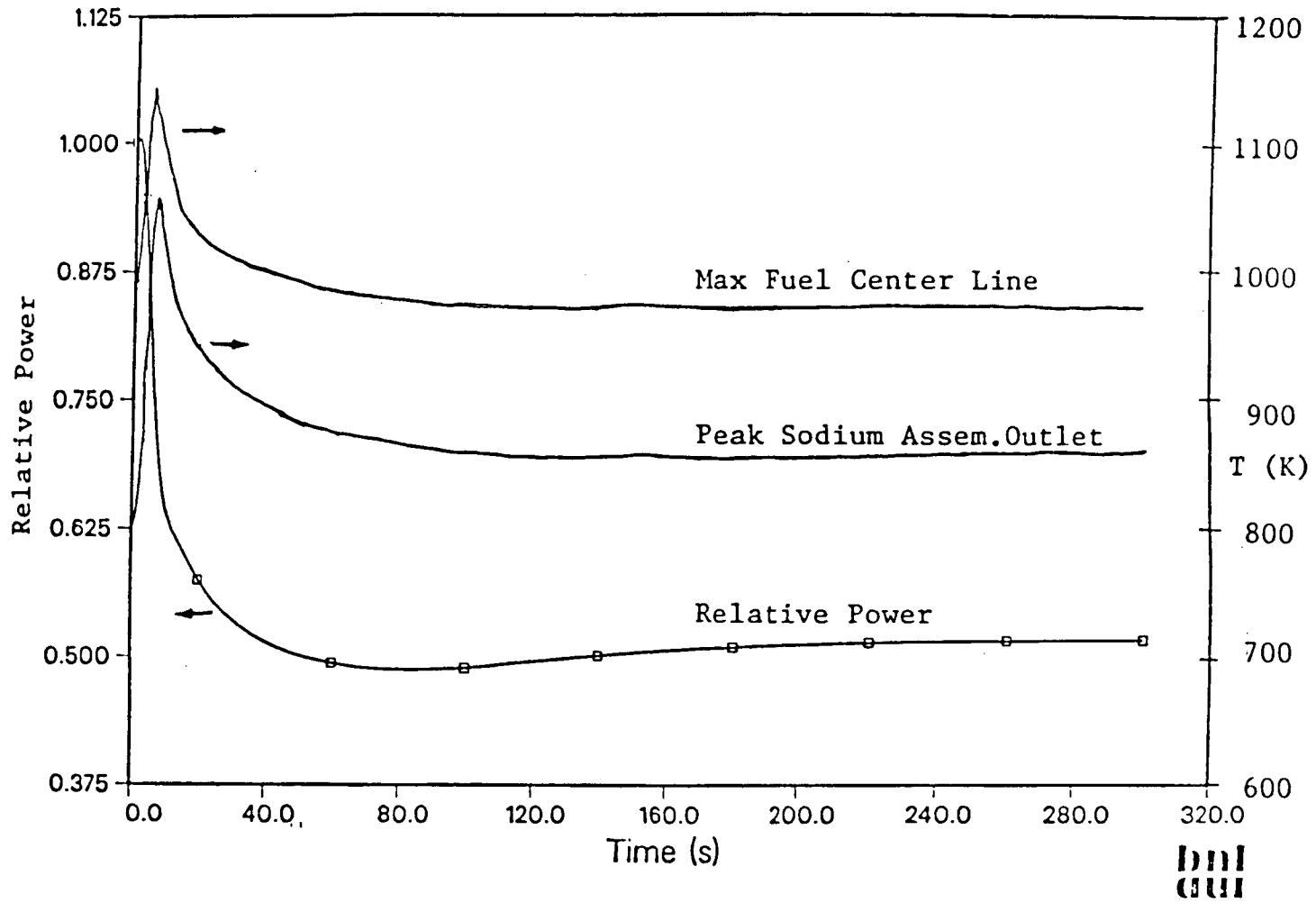


Figure 57 SSC Prediction for SAFR Pump Seizure: Relative Power and Key Temperatures

-85-186

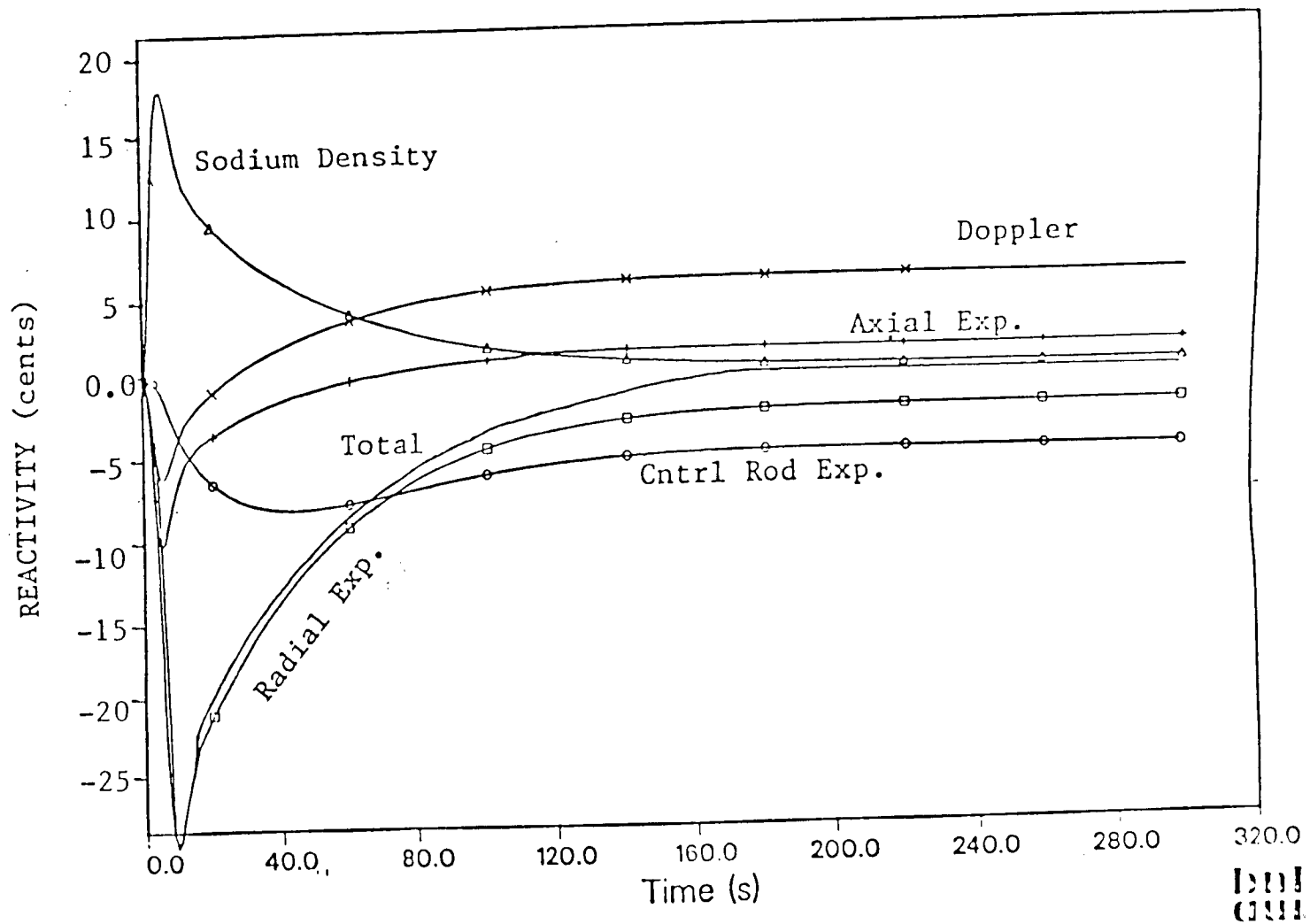
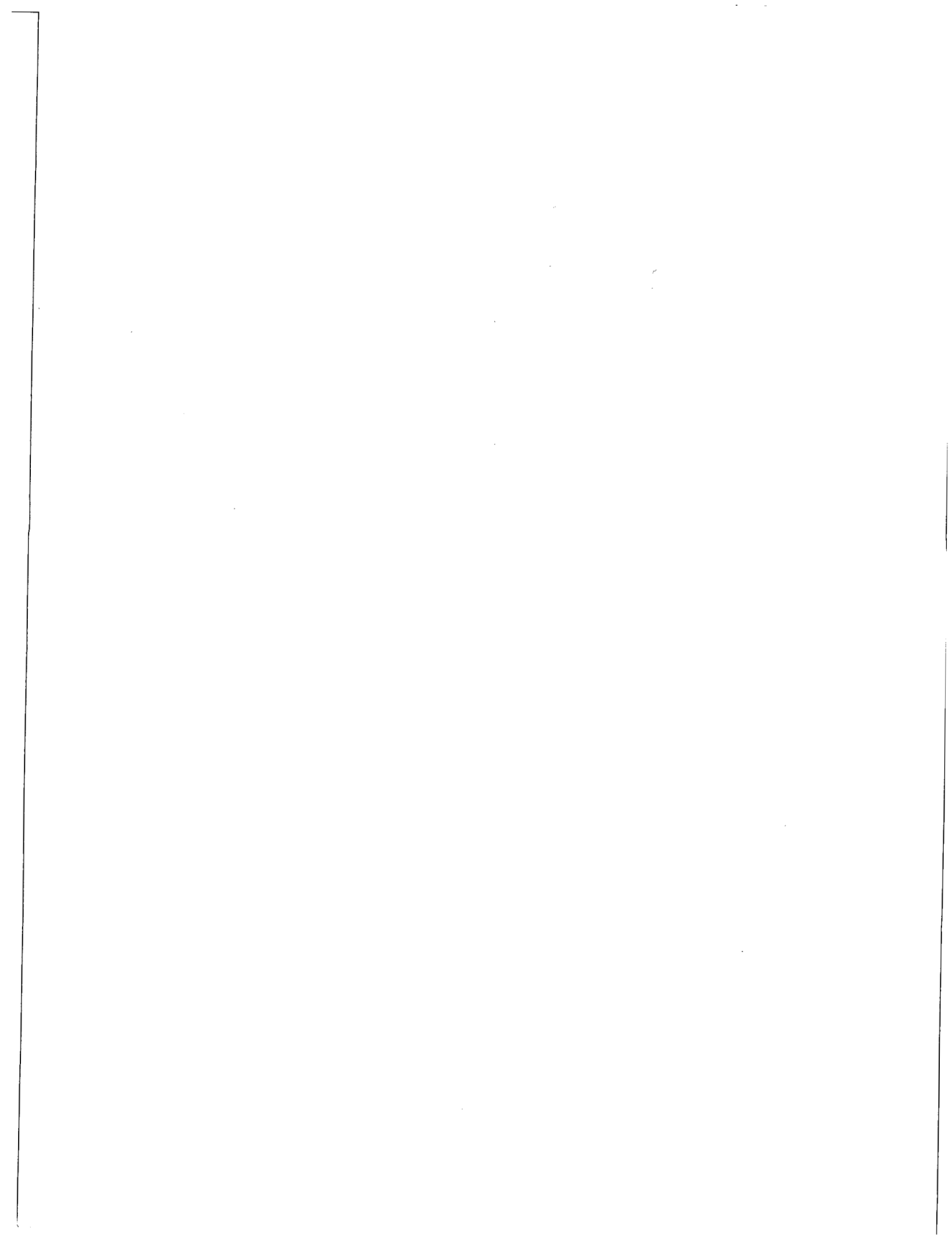


Figure 58 SSC Prediction for SAFR Pump Seizure: Reactivity Feedbacks



6. EVALUATION OF RACS/RVACS PERFORMANCE

Both PRISM and SAFR include a passive air cooling system for final decay heat removal under accident conditions. To be completely passive, these cooling systems are operative at all times, causing a minor parasitic energy loss during normal operation.

In these designs, as schematically shown in Figure 59, air is supplied to the bottom of the guard vessel, flowing upward along the guard vessel due to natural convection and being discharged through a stack providing sufficient draft to remove the decay heat under accident conditions.

In either concept, the heat rejection from the reactor vessel to the air cooling system is by radiation and convection across a gas gap between the reactor vessel and the guard vessel, and by radiation from the guard vessel to the opposite air cooling system surface (collector surface), and ultimately by convection from both surfaces to the rising air. Additionally, the SAFR concept includes fins on the collector surface as shown in Figure 60. For this concept the simultaneous effects of radiation and conduction on the collector surface are considered.

The evaluation of the passive air cooling system was performed using the PASCOL code, which was originally developed for analyzing a similar passive air cooling system in the modular high temperature gas cooled reactor program. This code can either be applied as a free standing program, given a spatial reactor vessel temperature distribution, or coupled to the relevant code for accident analysis. It solves simultaneously the quasi-steady momentum and energy equations for the air, coupled with simultaneous radiation, conduction and convection from the reactor vessel via the guard vessel and the other air cooling system surfaces to the coolant.

The performance evaluation reported here considers the operation under accident conditions. For the PRISM reactor, the heat transfer surfaces are not finned. As the vendor specified data did not include sufficient details to compute the inlet and exit ducting pressure drops, the system was evaluated parametrically with inlet and exit loss coefficients being varied between 1 and 10. The results, shown in Figure 61, indicate that the vendor's claimed performance can readily be obtained, if ducting is such that inlet and exit losses each amount to about four velocity heads. The vendor assumed solid surface emissivities of only 0.7, while values of 0.85 are readily achievable. Our evaluations showed that an increase in the heat removal rate of 16% is possible with such an increase in emissivity, as shown in Table 2.

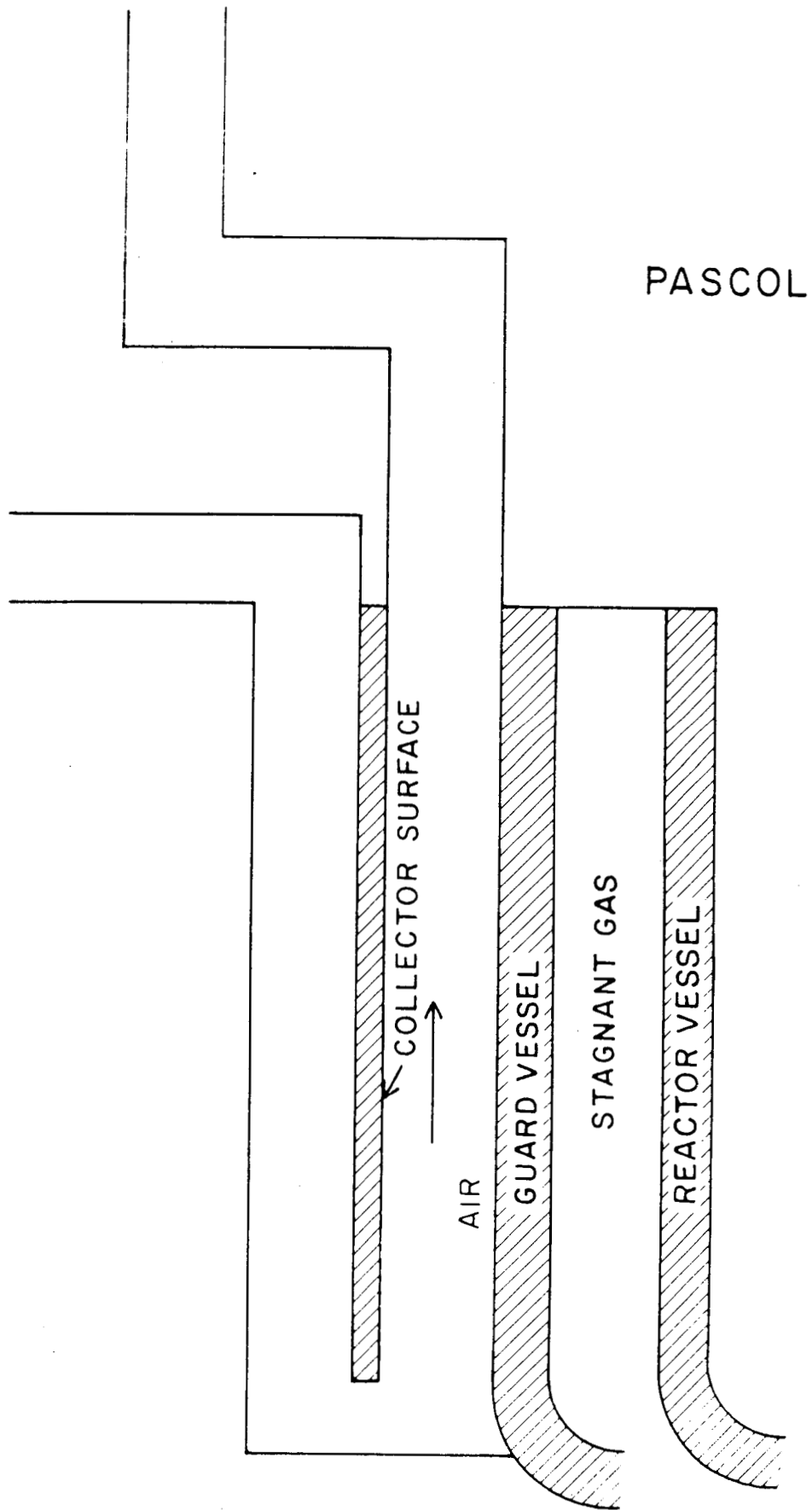


Figure 59 Schematic of Passive Air Cooling System for Advanced LMRs

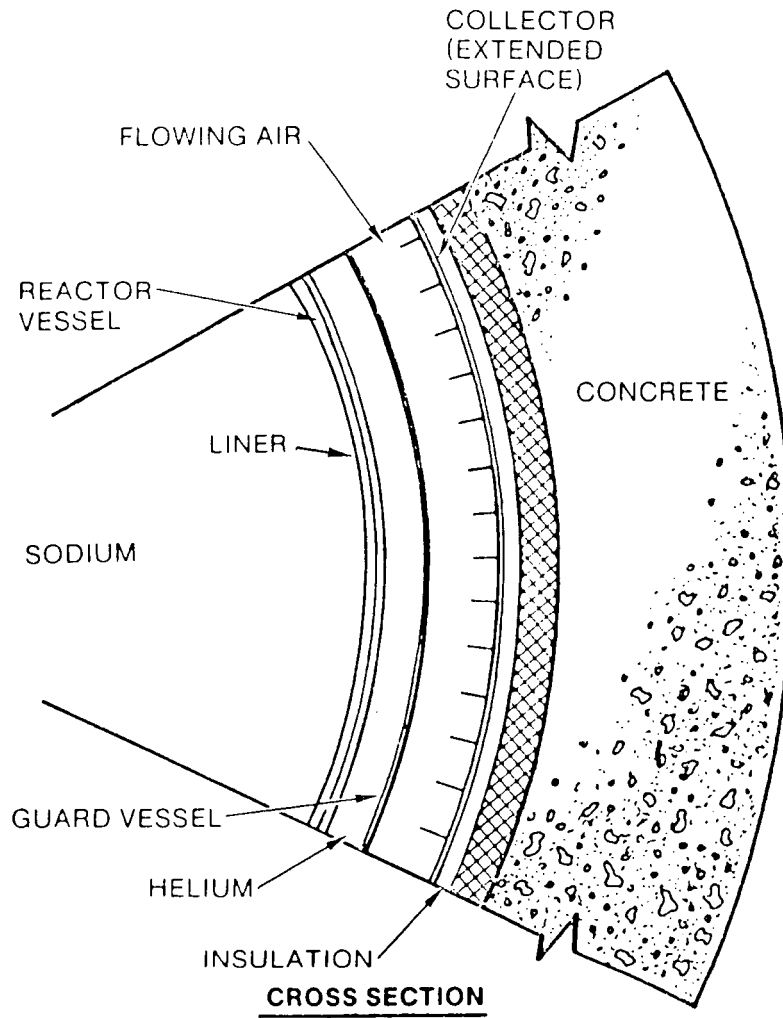


Figure 60 Top View, Section of SAFR Vessels and RACS (Note Fins)

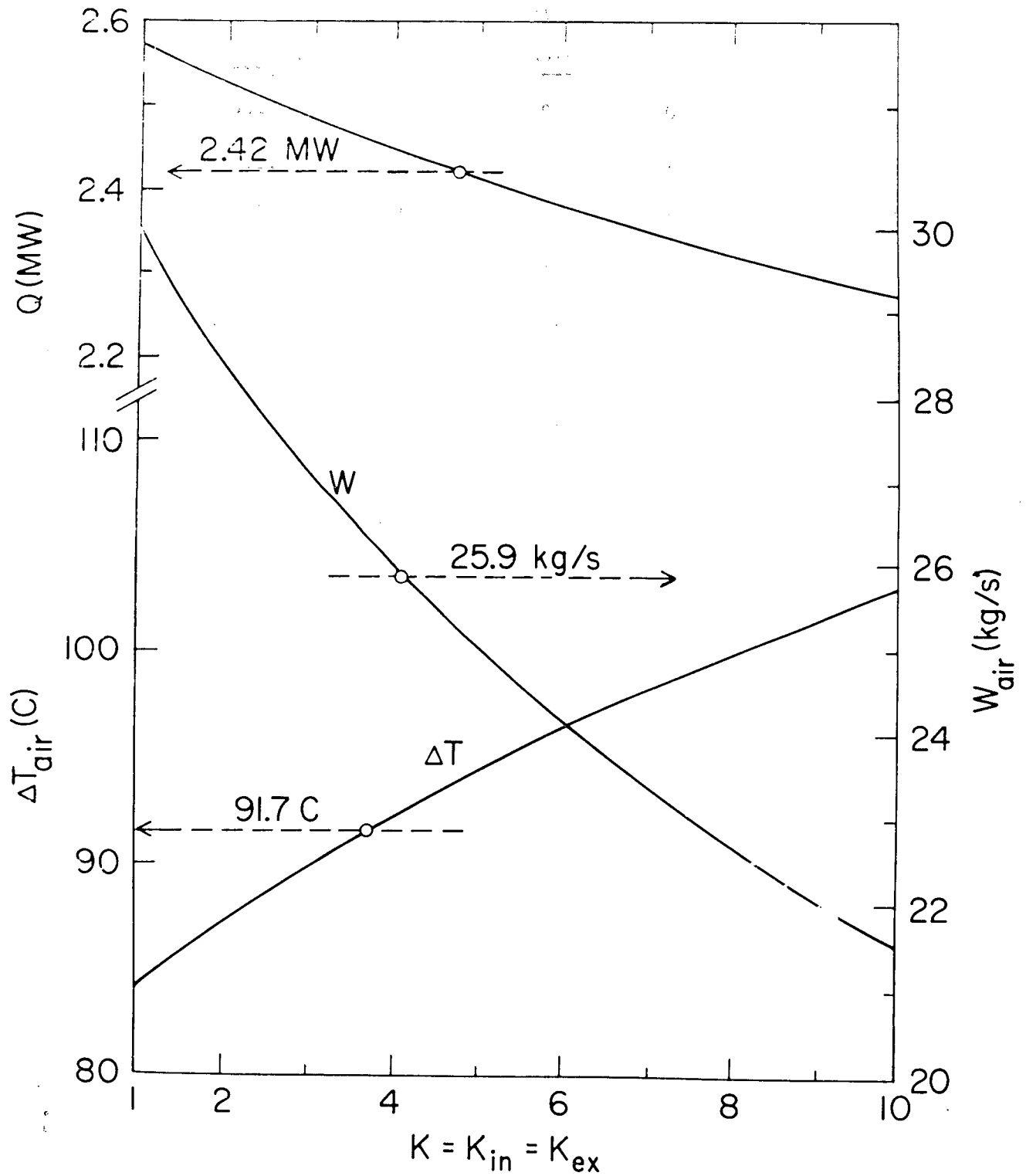


Figure 61 PRISM Passive Air Cooling System Performance During Decay Heat Removal as Function of Inlet and Outlet Ducting Flow Resistances

Table 2
 PRISM RVACS Performance During Decay Heat Removal Operation
 As Function of Steel Emmissivities
 ($K_{in} = K_{ex} = 4.0$)

<u>SOURCE</u>	<u>PASCOL</u>	<u>PASCOL</u>	<u>PASCOL</u>	<u>PASCOL</u>	<u>GE</u>
Emmissivity	0.5	0.7	0.85	0.999	0.7
Q (MW)	1.86	2.45	2.86	3.21	2.42
W (KG/S)	24.2	26.0	27.0	27.8	25.9
$T_{out} - T_{in}$ (C)	75.1	92.2	103.2	113.4	91.7

For the SAFR air cooling system an evaluation of the simultaneous conduction and radiation in the collector surface had to be made. Defining a performance factor:

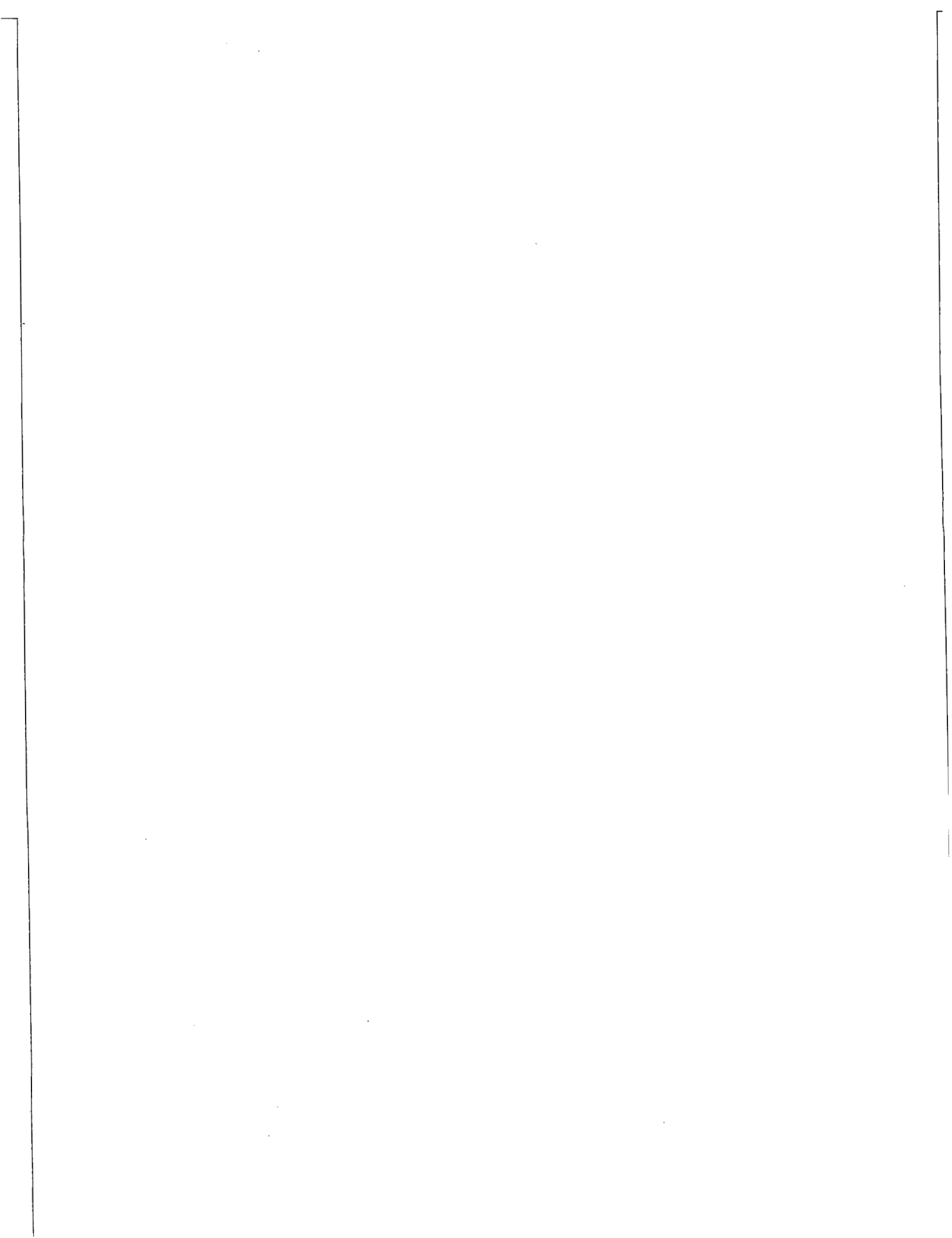
$$\phi = \frac{\text{total convective heat transfer to air}}{\text{convective heat transfer to air from guard vessel}}$$

it was found that a value of $\phi \approx 1.8$ to 2.5 can be expected under accident conditions. The vendor's claimed performance can be reached down to a value of $\phi = 1.5$. Increasing the emmissivity from the vendor's value of 0.65 to 0.85 resulted in 18% higher performance.

Table 3
 SAFR SHRS Thermal Performance With RACS Only as Function of
 Collector Heat Transfer Effectiveness

<u>SOURCE</u>	<u>PASCOL</u>	<u>PASCOL</u>	<u>PASCOL</u>	<u>PASCOL</u>	<u>RI/ANL</u>
Collector Area Effectiveness	1.5	2.0	4.0	1.5	?
Q (MW)	3.90	4.13	4.50	4.61	3.96
W (KG/S)	37.2	37.7	38.5	38.7	39
$T_{out} - T_{in}$ (c)	102.5	107.2	114.6	116.6	99.4
Emmissivity	0.65	0.65	0.65	0.85	0.65

As can be seen, both systems can readily achieve the required decay heat removal rate. Further increases in performance could readily be achieved. However, such performance increases may not be desirable, since they would raise the parasitic heat losses under normal operating conditions.



7. PROTECTED LOHS EVENTS - SIMPLE MODELS

While detailed thermal hydraulic computer code calculations are needed in order to predict peak temperatures under transient conditions, one can learn a great deal using simple models based on decay heat, heat capacity, and heat removal (e.g., RACS or RVACS performance). This is especially true for PRISM and SAFR, as the high thermal conductivities in the fuel, coolant, and structure tend to even out any transient temperature distributions.

7.1 Conservation of Energy Equation

If we assume that the reactor vessel is intact (i.e., no sodium entering or exiting) and that the intermediate loop is shut down, conservation of energy dictates that:

$$M c_p \frac{\partial T}{\partial t} = \int_v Q''' - \sum Q'_{bc} \quad (38)$$

where

- M = Mass of vessel and contents
- C_p = Average heat capacity of vessel and contents
- T = Average temperature of vessel and contents
- Q''' = Heat generation per unit volume
- Q'_{bc} = Heat entering or leaving

To be more precise, $\int_v Q'''$ is the decay heat of the reactor, Q_d , and the left hand side of Eq. (38) is really a sum of all the materials within the vessel. Further, we can define Q_{bc} as the sum of all gains and losses across the vessel boundary.

$$\sum_j M_j C_{pj} \frac{\partial T_j}{\partial t} = Q_d - Q_{bc}, \quad (39)$$

where there are j material regions within the vessel.

We can integrate Eq. (39) in time to project changes in temperatures during the transient period:

$$\sum_j M_j C_{pj} [T_j(t) - T_j(t=0)] = \int_0^t Q_d - \int_0^t Q_{bc} \quad (40)$$

which is equivalent to:

$$\sum_j M_j C_{pj} T_j(t) = \sum_j M_j C_{pj} T_j(t=0) + \int_0^t Q_d - \int_0^t Q_{bc} \quad (41)$$

During a long, slow heat up transient, the temperatures within the vessel will tend to even out. Thus, we make a simplifying assumption that at some

time t into the transient:

$$T_j(t) \approx \langle T \rangle_t, \text{ for all } j \quad (42)$$

Substitution of Eq. (42) into Eq. (41) leads to:

$$\langle T \rangle_t \approx \frac{\sum M_j C_{p_j} T_j(t=0) + \int_0^t Q_d - \int_0^t Q_{bc}}{\sum M_j C_{p_j}} \quad (43)$$

The approximate value of the summation terms in Eq. (43) are given in the table below:

	$\sum M_j C_{p_j}$	$\sum M_j C_{p_j} T_j(t=0)$
PRISM, Neglecting Containment Vessel	6.54E8 kg	4.29E11 kgK
PRISM, Including Containment Vessel	6.94E8 kg	4.54E11 kgK
SAFR, Neglecting Containment Vessel	1.93E9 kg	1.352E12 kgK

Decay heat curves were provided in the PRISM and SAFR documentation in tabular form. This information was used to generate integral decay heat curves ($\int_0^t Q_d$) for PRISM and SAFR, as shown in Figure 62.

While performance of RACS and RVACS were confirmed using PASCOL, the time dependent heat removal through these systems was available only through GE and RI/ANL calculations. Therefore, the RVACS heat rejection curve shown on Figure 63, as provided by GE, was integrated to get the curve on Figure 64 labelled "PRISM RVACS". Similarly, the curve on RI/ANL Figure 65 labelled "QRACS" was integrated to get the curve labelled "SAFR RACS" on Figure 64.

7.2 LOHS With RACS/RVACS Working

When Eq. (43) is used in conjunction with the integrated curves on Figures 62 and 64 to analyze the SAFR RACS only event, the average temperatures marked "X" on Figure 65 results. The trend over this 50 hour transient is very similar to the RI/ANL plots of hot and cold pool temperatures.

The equivalent analysis was done for PRISM, both with and without the containment vessel mass. The average temperatures are indicated on Figures 66 and 67. Further, an additional 100°F is added to each point to represent the approximate core outlet temperature, which compares directly to the values plotted by GE.

While the simple model results are not identical to those computed by GE

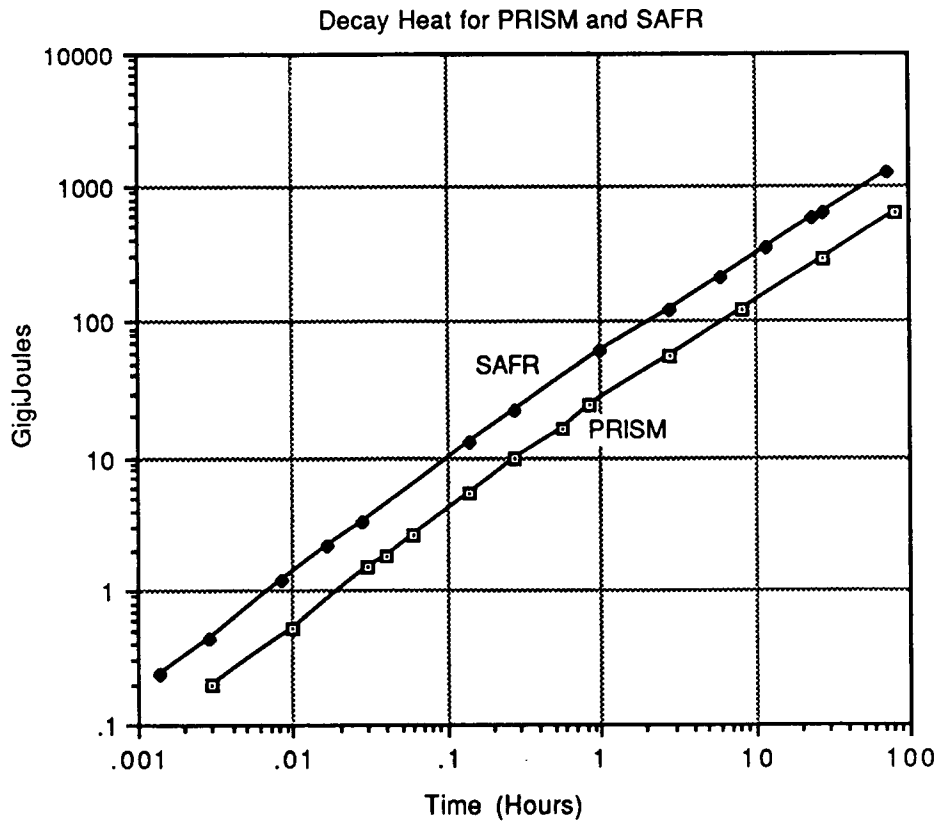


Figure 62 Integral Decay Heat vs. Time After Scram for PRISM and SAFR

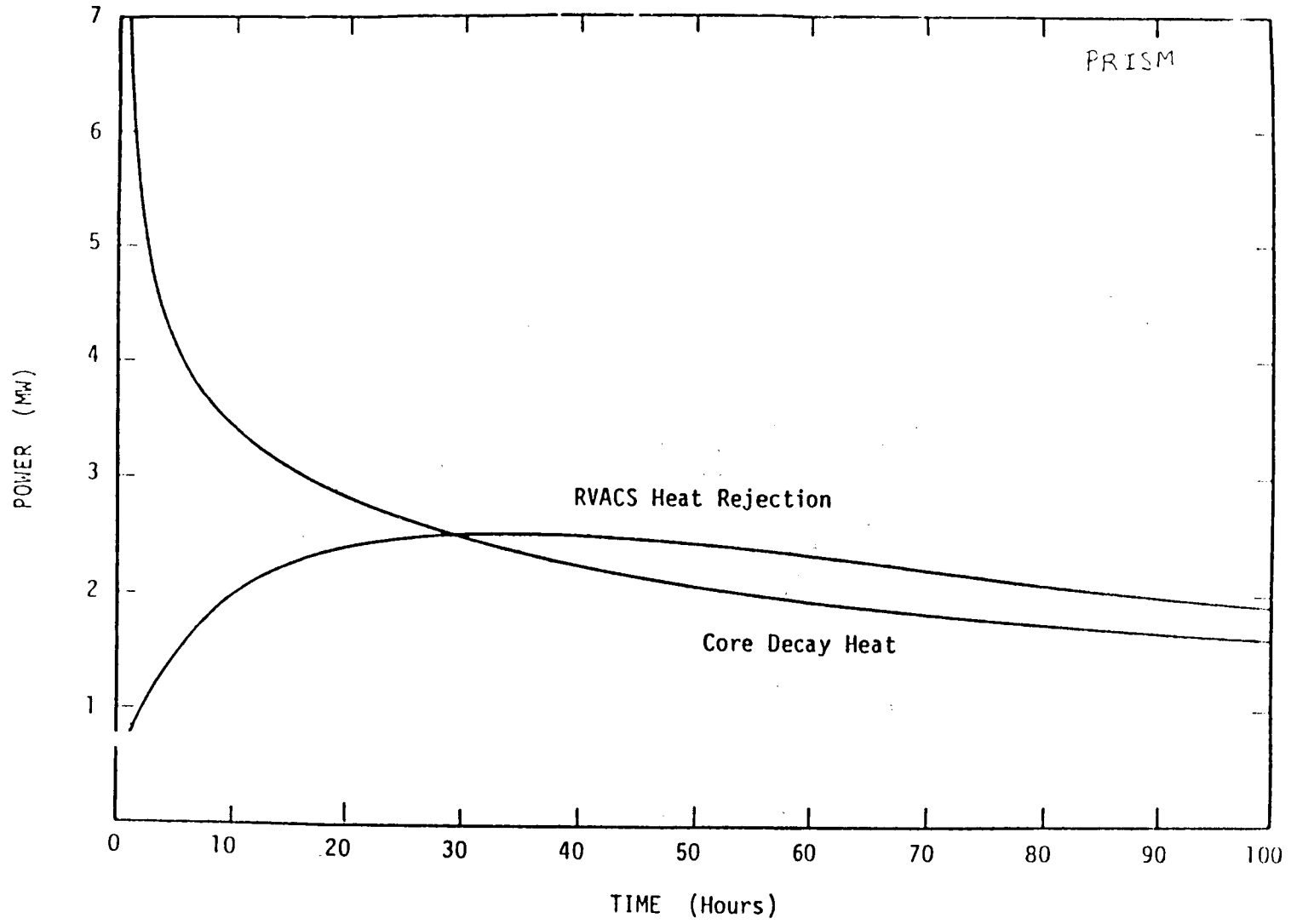


Figure 63 PRISM Decay Heat and RVACS Heat Rejection During LOHS

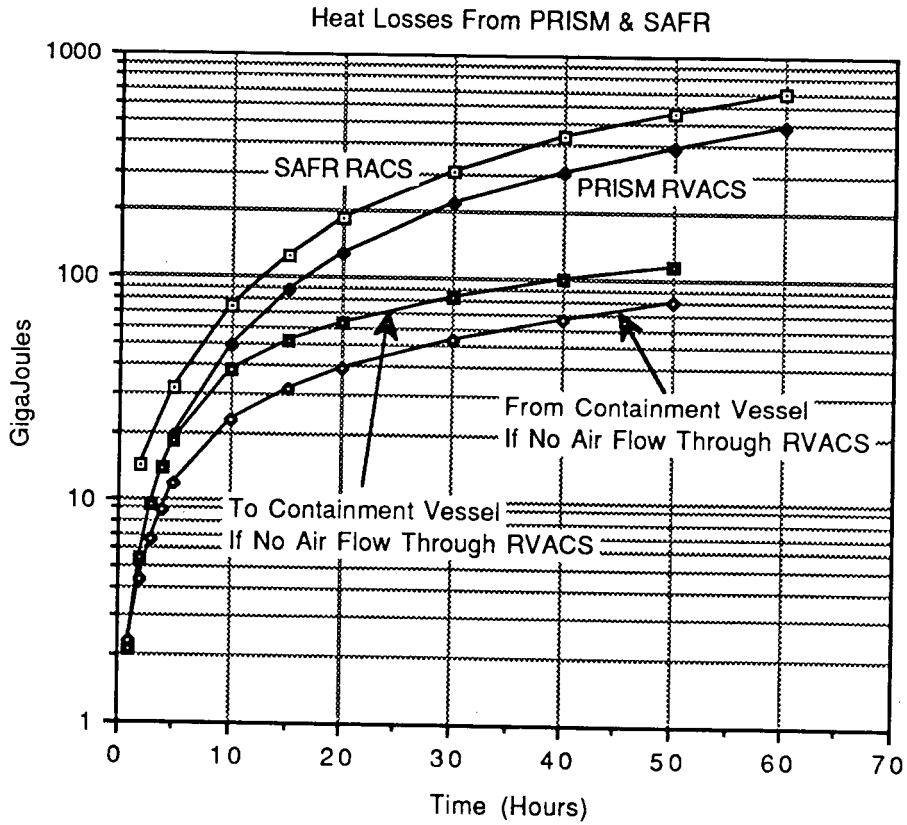


Figure 64 Integral Heat Removal vs. Hours After Scram for PRISM and SAFR

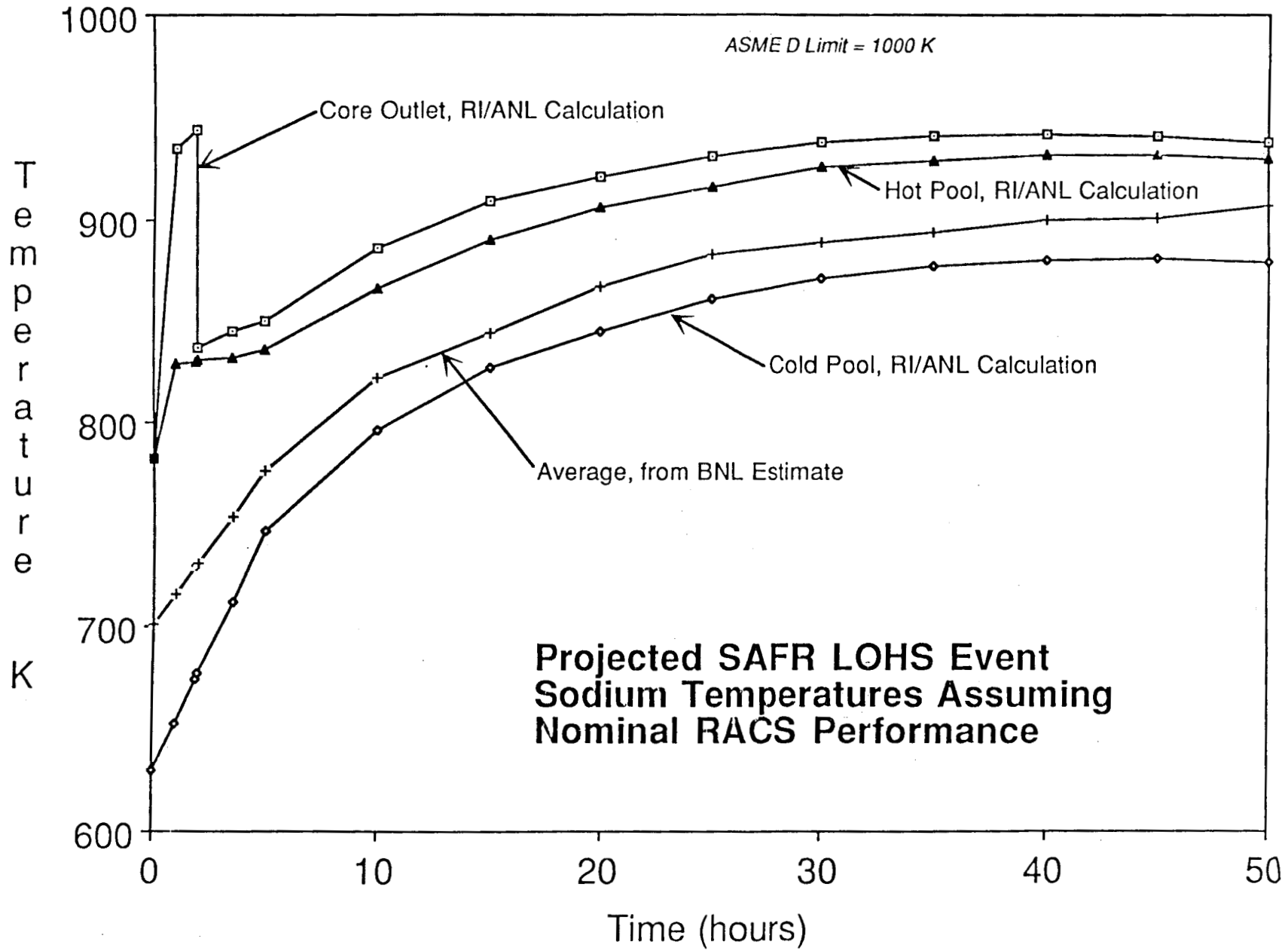


Figure 65 SAFR LOHS Temperatures and Heat Loads and Losses, includes BNL's Calculated Temperatures

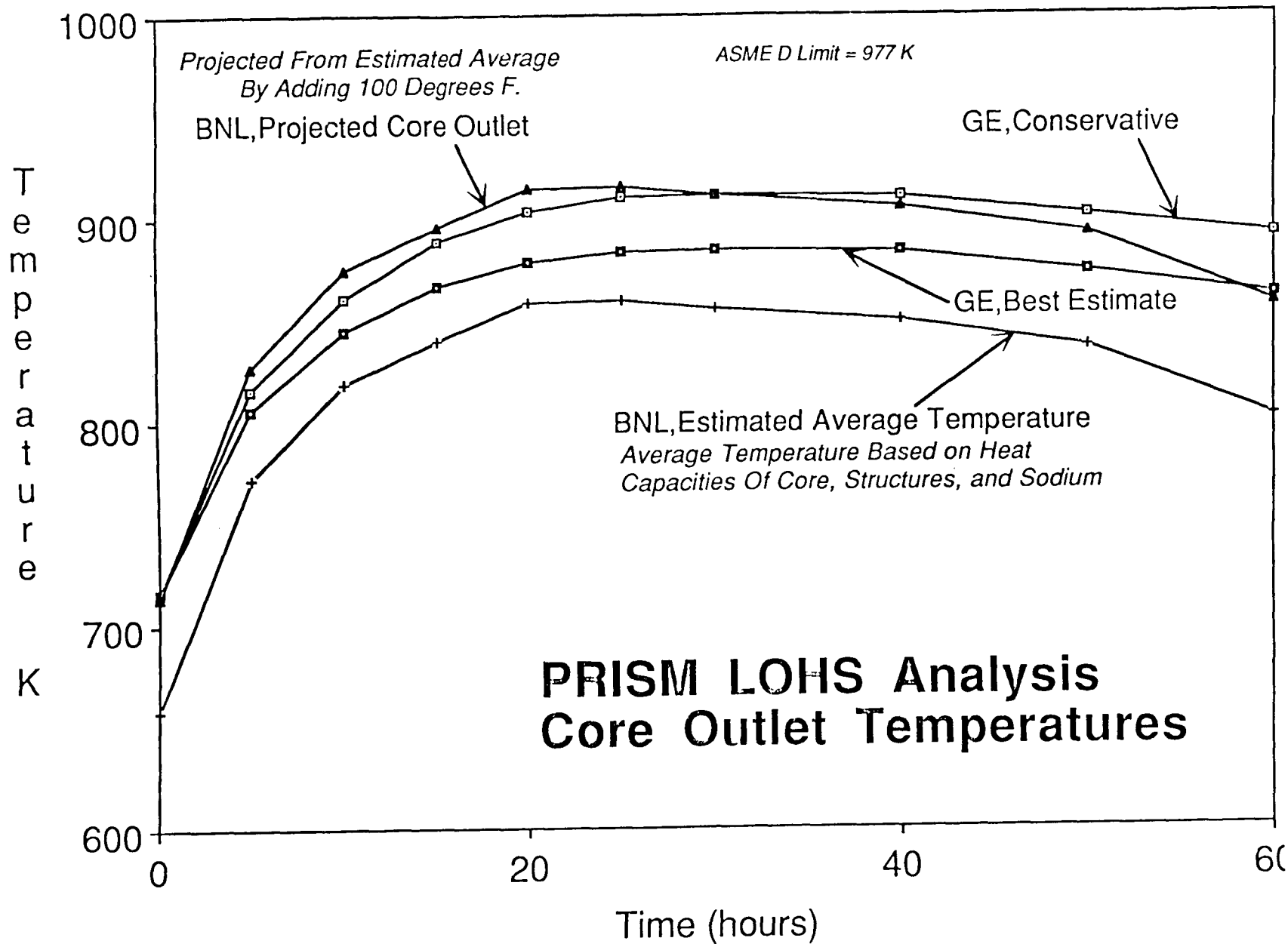


Figure 66 PRISM Core Outlet Temperature vs. Hours into LOHS, includes BNL's Calculated Temperatures, Neglecting Containment Vessel Mass

-100-

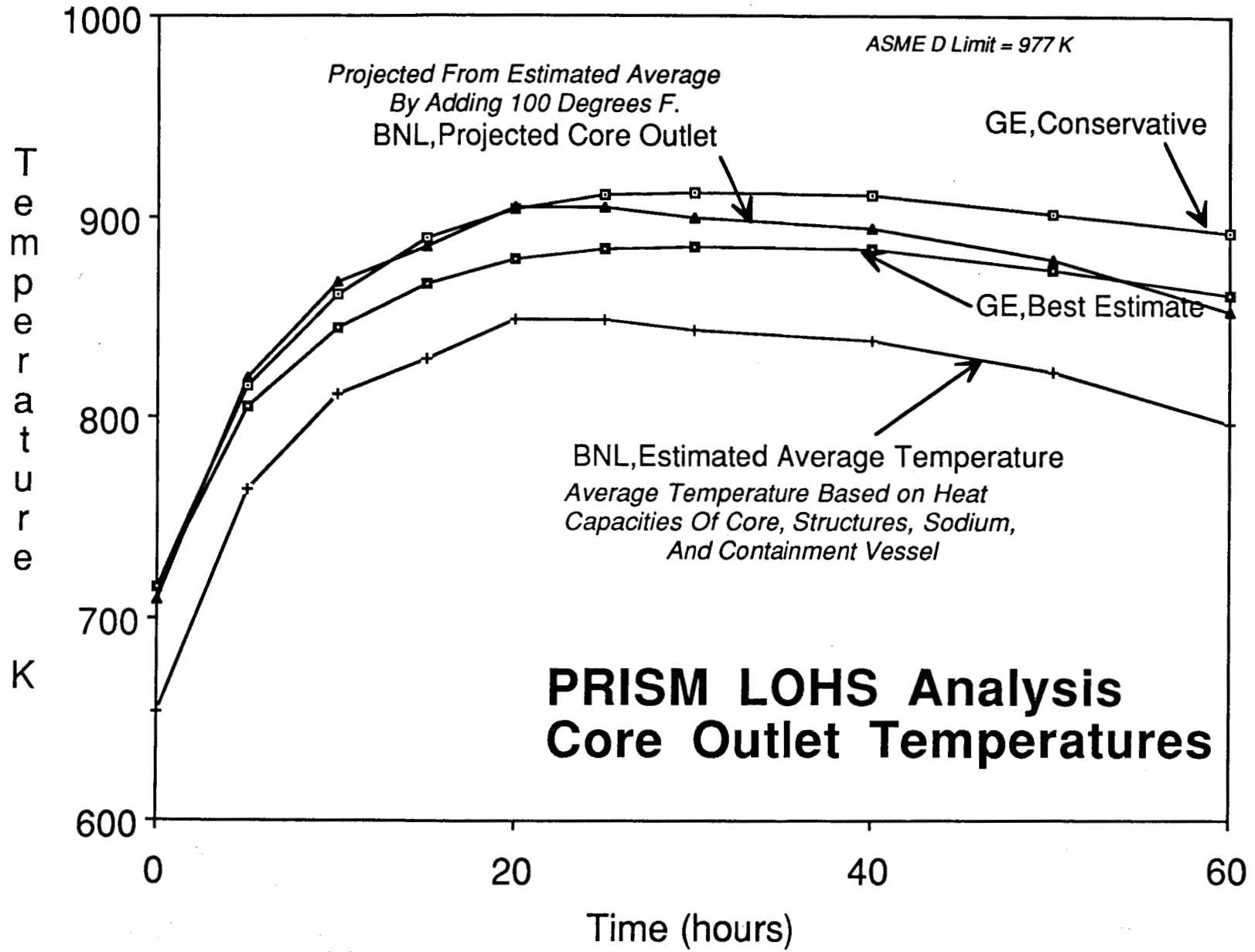


Figure 67 PRISM Core Outlet Temperatures vs. Hours into LOHS, includes BNL Calculated Temperatures including Containment Vessel Mass

and RI/ANL, the trends are clearly similar. Thus, we conclude that the results are at least approximately correct.

7.3 Adiabatic Heat-Up Cases

Having "benchmarked" our simple models for the RACS-only and RVACS-only cases, we went on to examine adiabatic heat-up cases. For SAFR, we are estimating eutectic penetrations in the 3/4 of one day range (some cladding ruptures in high burn-up fuel could come a little earlier) and sodium boiling in the 1 1/2 day range, as shown in Figures 68 through 70 (RI/ANL results included on 70). While these estimates are far from precise, the timing is not far from our expectations. However, for PRISM it appears that eutectic penetrations will develop as early as 1/2 day (again with some cladding ruptures earlier), and sodium boiling could come around 1 day into the transient as indicated in Figures 71 and 72. This trend in PRISM is developing more quickly than we anticipated, and appears to trace to a lower mass-to-power ratio in the PRISM reactor system. PRISM has about 1/3 the mass of SAFR, but generates a little less than 1/2 of the SAFR reactor power. However, we must note again that judging by our "benchmark" case of RVACS-only, that our estimates of the PRISM mass is probably low.

7.4 PRISM "Earth Heat-Up" Event

Because PRISM is sited in a silo, there is a potentially significant means of giving off decay heat in the event RVACS air flow is cut off (in addition to the loss of normal cooling and ACS). This involves radiating heat to the concrete/insulation of the silo, with some of the heat then conducted to the surrounding earth. This is comparable to an event considered for the MHTGR, although the geometry is somewhat different. An expanded view of the PRISM silo is shown in Figure 73.

These calculations were performed using a combination of our simple "back-of-the-envelope" model based on heat capacities and the PASCOL code, which models the RVACS. We began the calculation with estimates of the reactor vessel as a function of time (around 60 hours of transient), and used PASCOL to estimate the heat transfer rates outward from the reactor vessel. Then, using the estimated heat removal rate (from the reactor vessel wall) we calculated the corresponding reactor system temperature as a function of time. This temperature (including the reactor vessel) history was compared to the one assumed, as shown in Figure 74, and the process could have been repeated iteratively, if necessary. As we knew GE's prediction of the reactor vessel temperature vs. time for this transient, our initial "guess" turned out to be excellent and iterative improvements were unnecessary. Further, other temperatures cited in the GE write-up were entirely consistent with those calculated by BNL, as shown in Figure 75. (Note: the results with reference decay heat are shown in Figure 76.) Thus, both calculations indicate substantial fuel damage near the end of the first day (with some cladding ruptures developing a few hours earlier), and sodium boiling (and likely vessel failure) at about 36 hours. It therefore appears that large releases are unlikely before one day and may come closer to the 1 1/2 day period.

SAFR Adiabatic Heat-Up w/ Reference Decay Heat

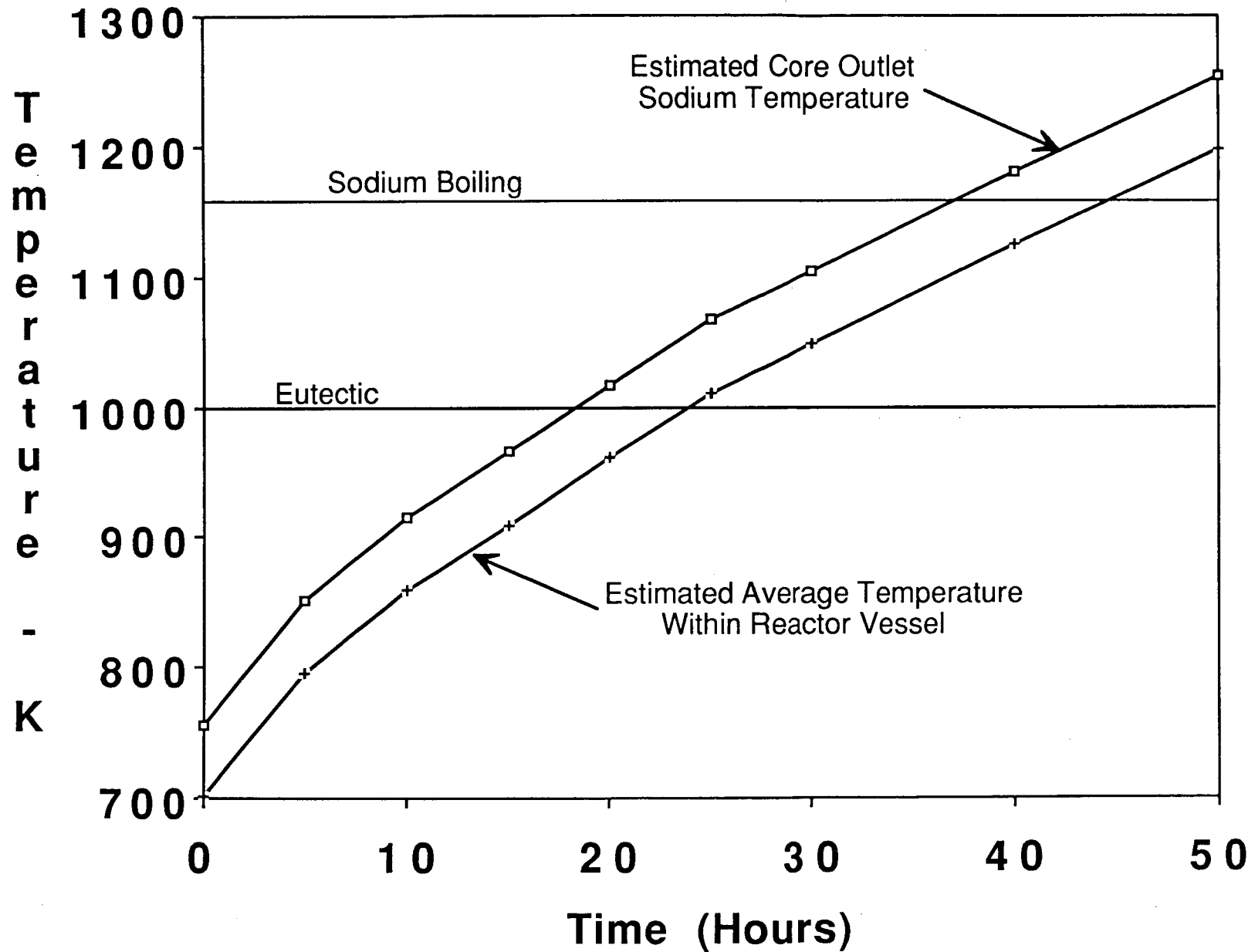


Figure 68 Projected SAFR Adiabatic Heatup Temperatures Using Reference Decay Heat

SAFR Adiabatic Heat-Up w/ 15% Extra Decay Heat

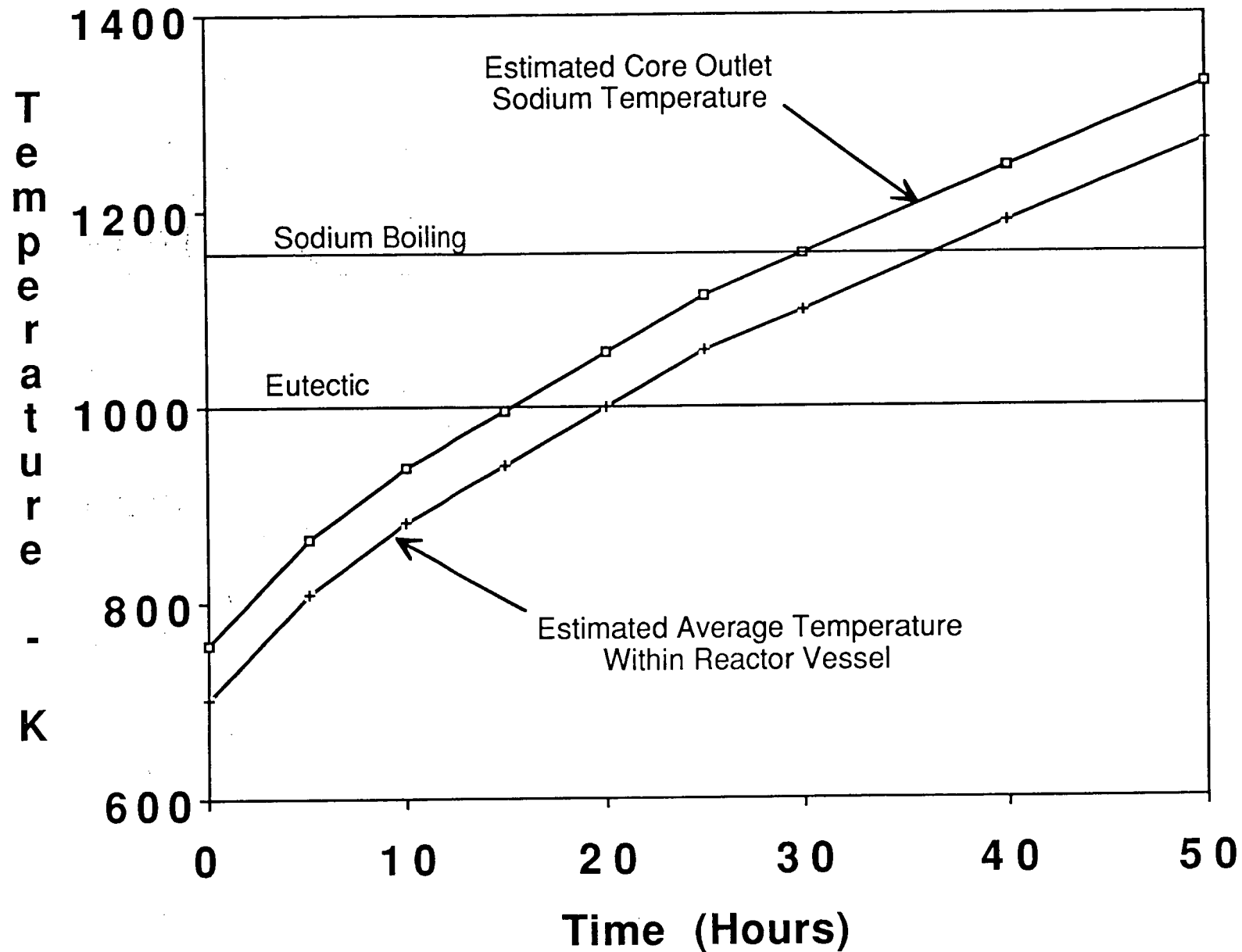


Figure 69 Projected SAFR Adiabatic Heatup Temperatures, 15% Extra Decay Heat

SAFR Adiabatic Heat-Up Core Outlet Sodium Temperatures

"Deterministic Event No. 3"

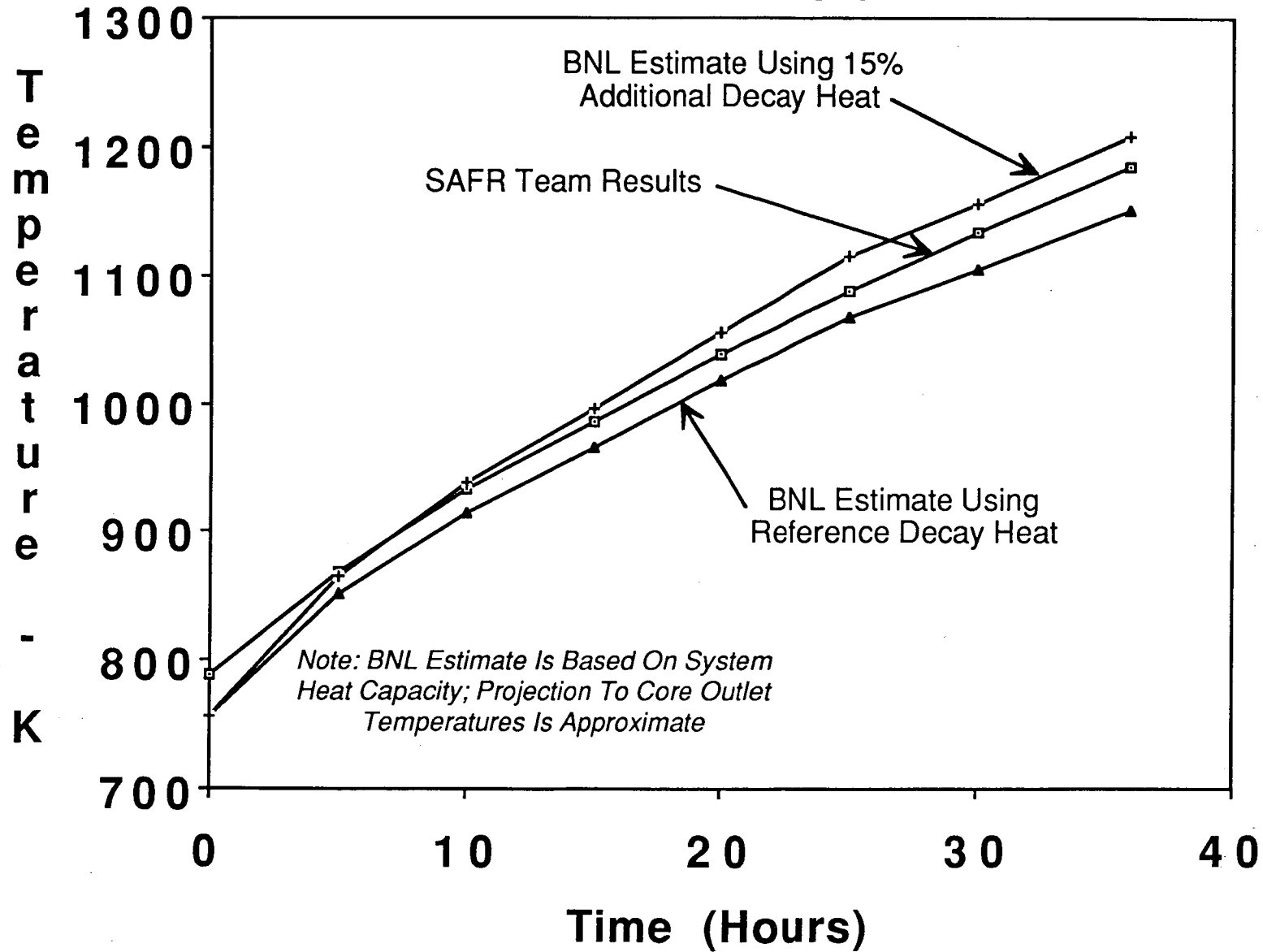


Figure 70 Projected SAFR Adiabatic Heatup Temperatures vs. RI/ANL Estimations

PRISM Adiabatic Heat-Up w/ Reference Decay Heat

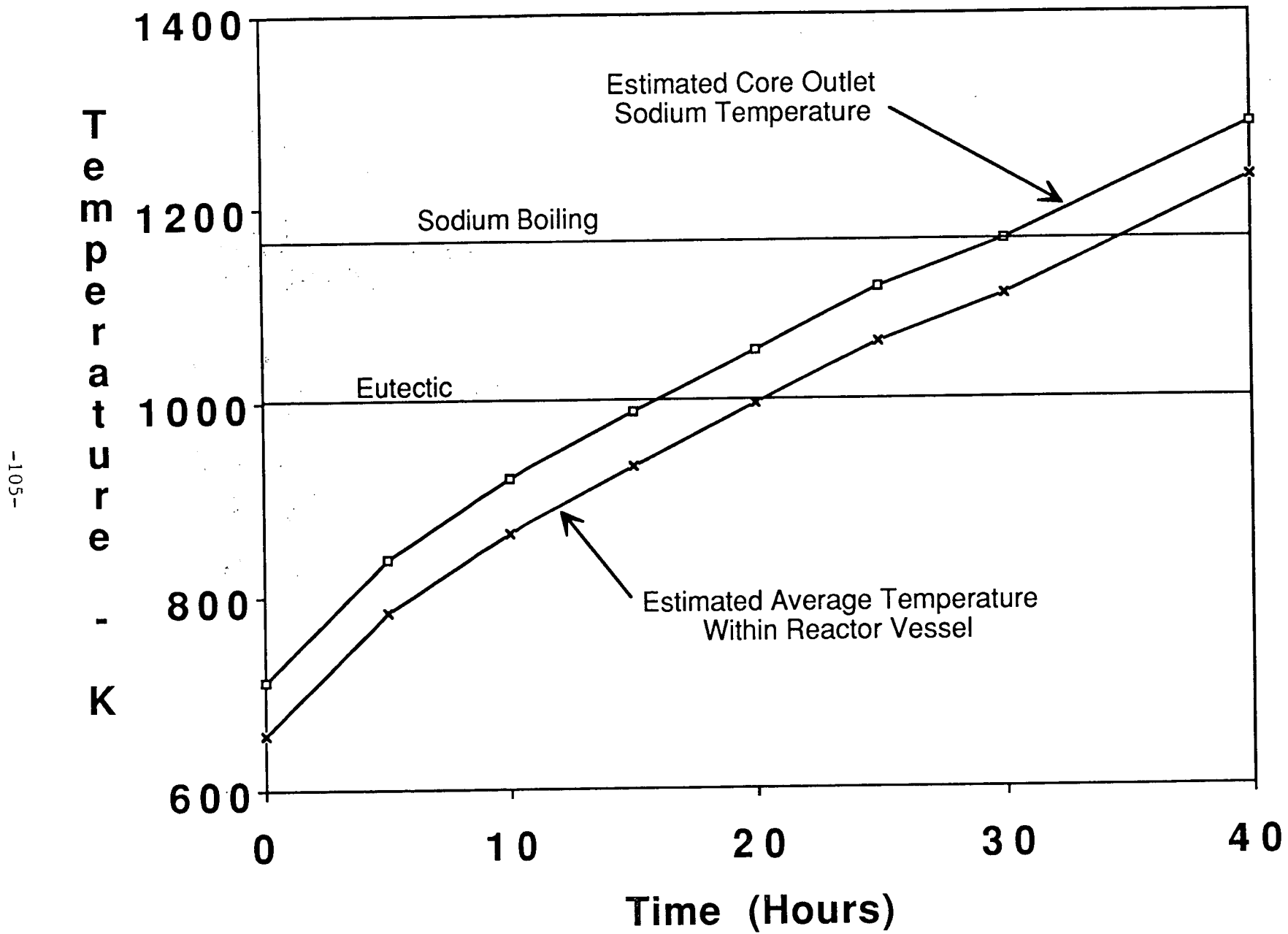


Figure 71 Projected PRISM Adiabatic Heatup Temperatures Using Reference Decay Heat

PRISM Adiabatic Heat-Up w/ 15% Extra Decay Heat

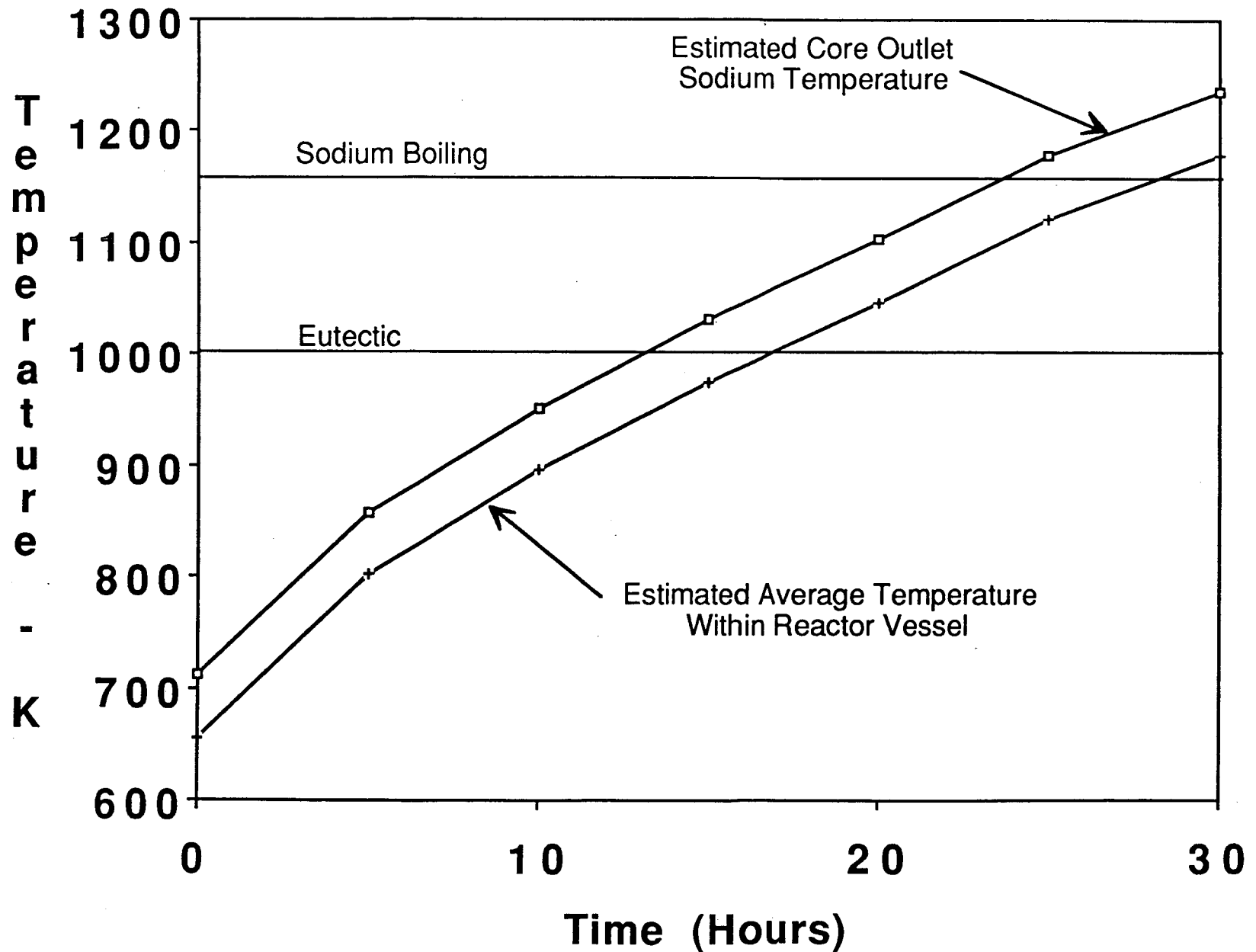


Figure 72 Projected PRISM Adiabatic Heatup Temperatures, 15% Extra Decay Heat

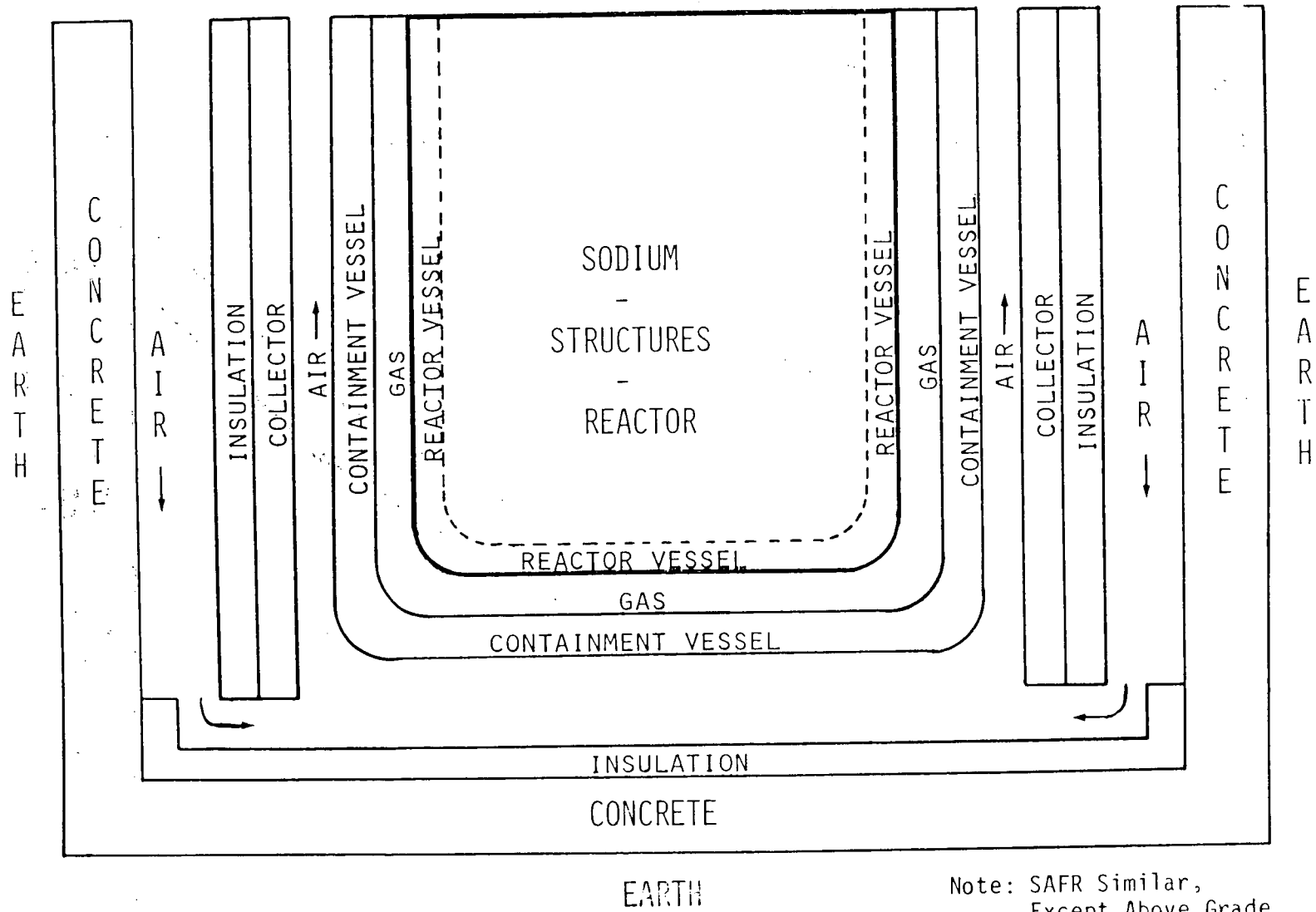


Figure 73 Schematic Drawing of PRISM Below-Grade Components

PRISM Temperatures During 36 Hour Earth Heat-Up

Deterministic Event No. 3

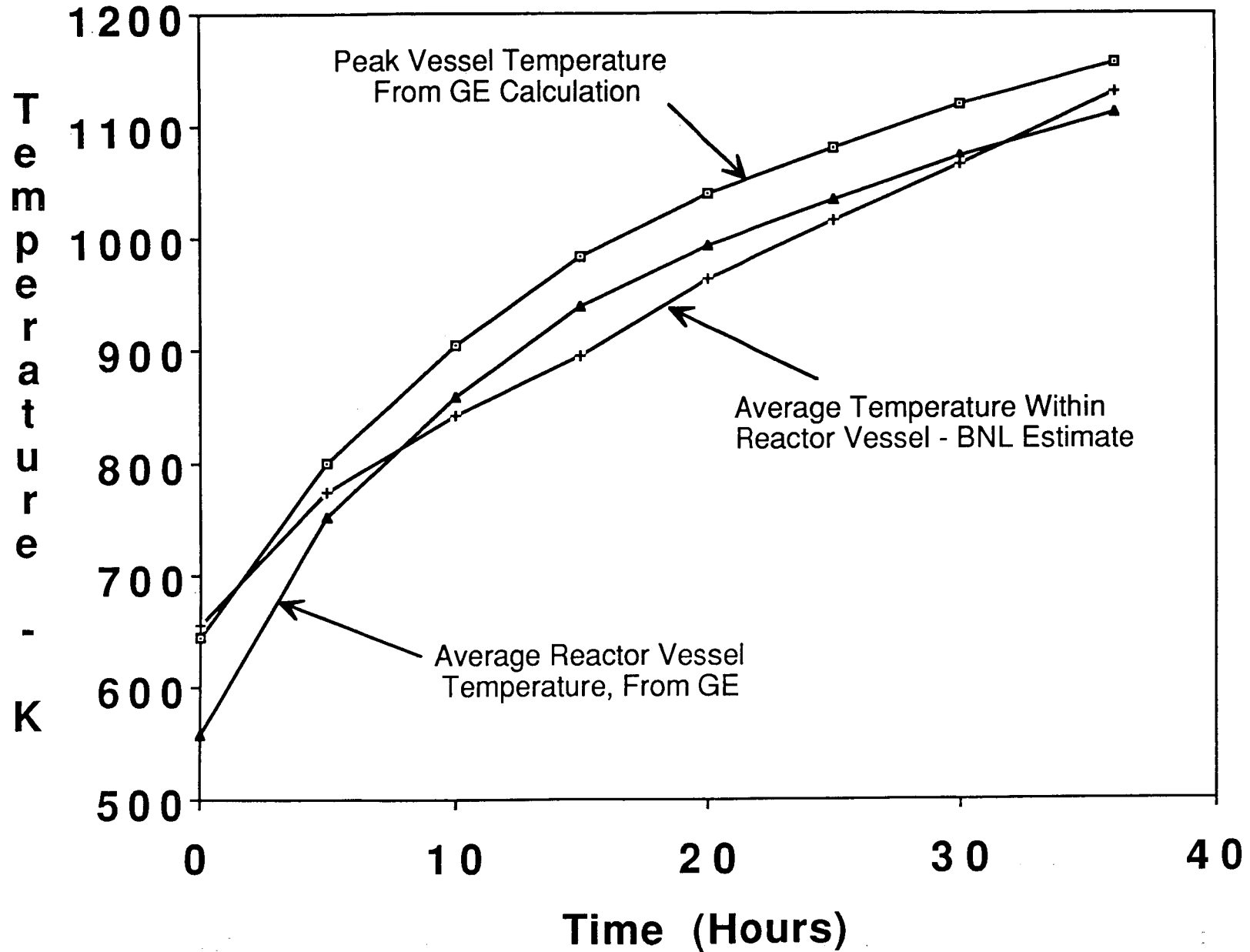


Figure 74 Projected Vessel Temperatures from PRISM Earth Heatup Event

PRISM Earth Heat-Up w/ 15% Extra Decay Heat

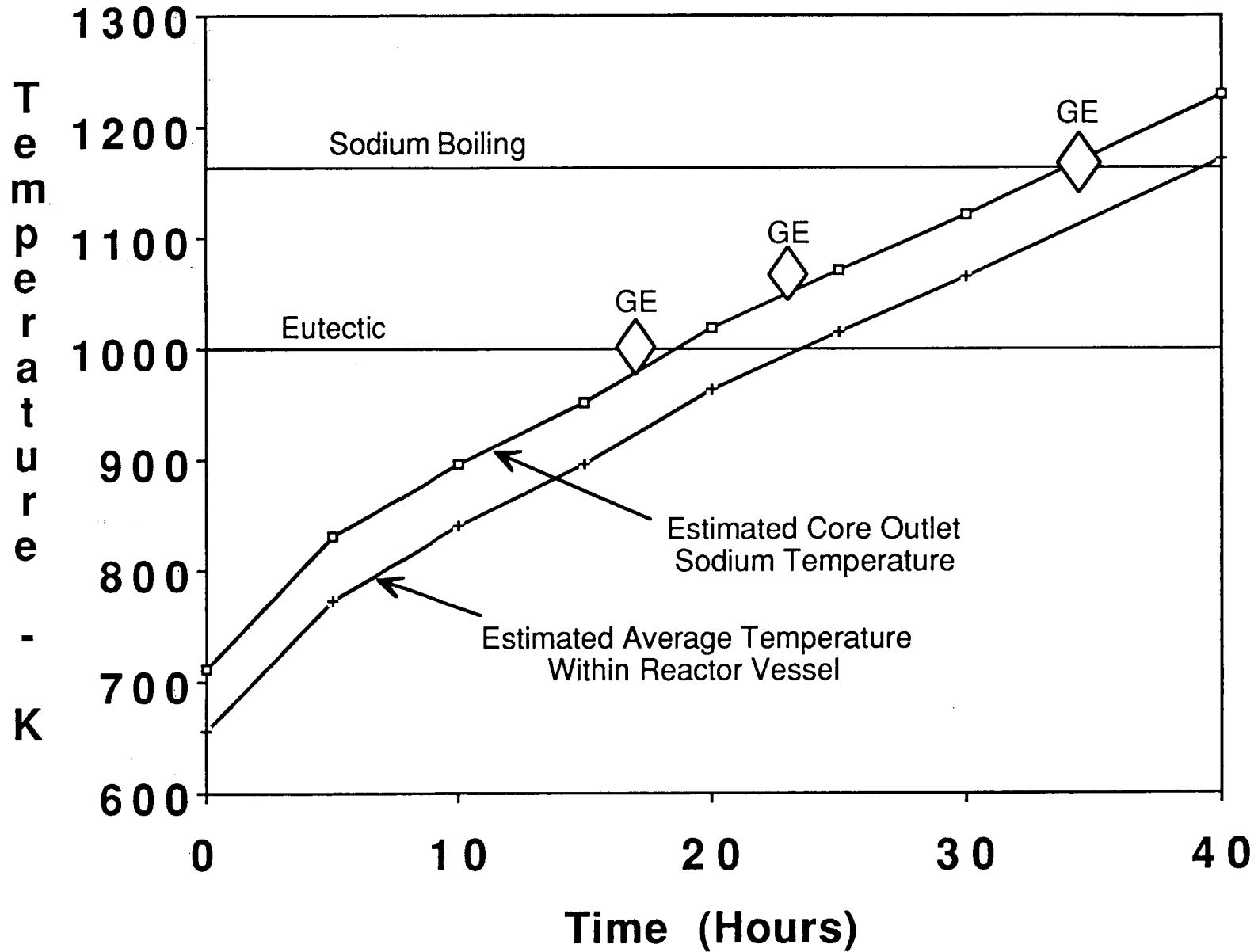


Figure 75 Projected PRISM Earth Heatup Temperatures Using 15% Extra Decay Heat

PRISM Earth Heat-Up w/ Reference Decay Heat

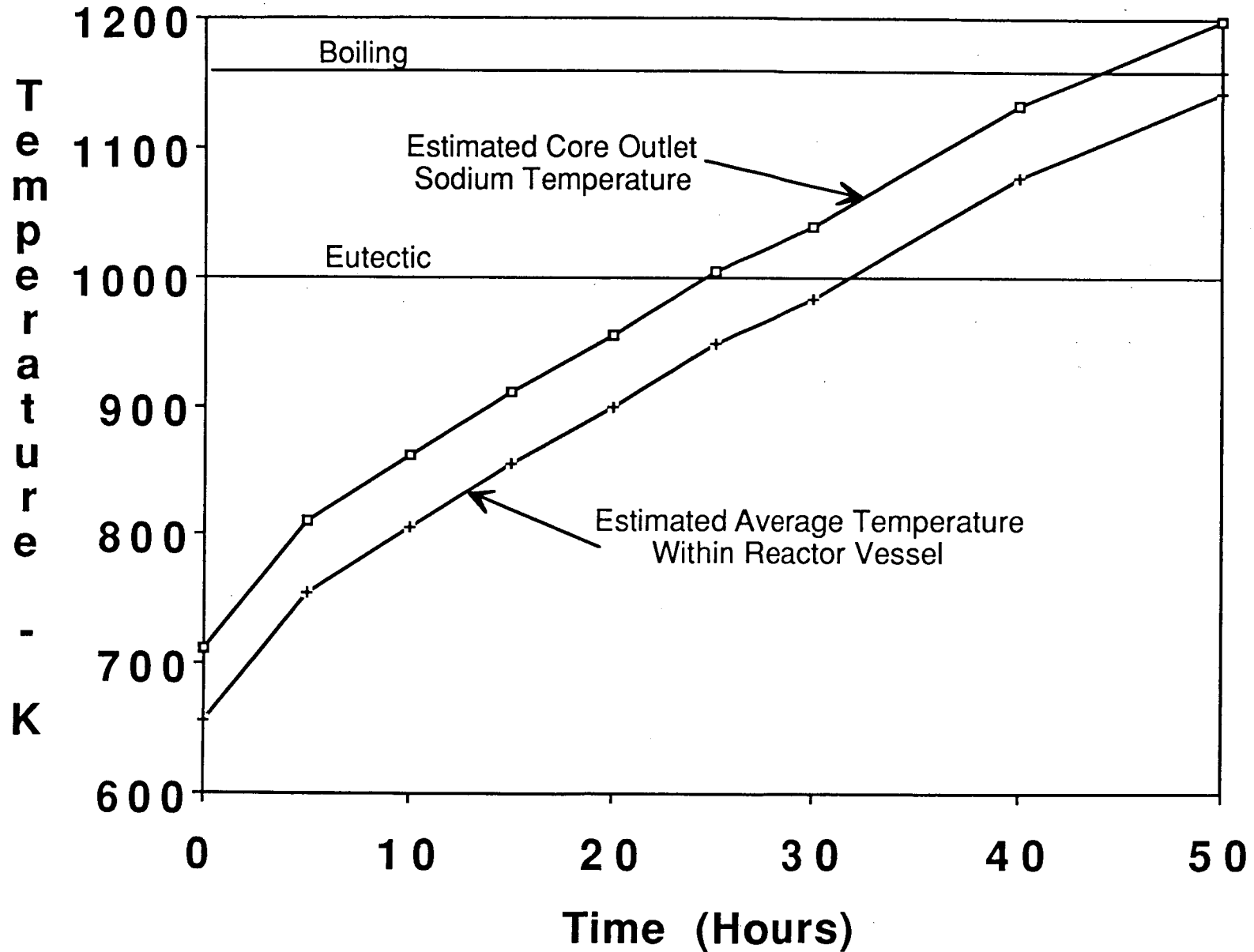


Figure 76 Projected PRISM Adiabatic Heatup Temperatures Using Reference Decay Heat

8. MINET SIMULATION OF PRISM LOHS-RVACS EVENT

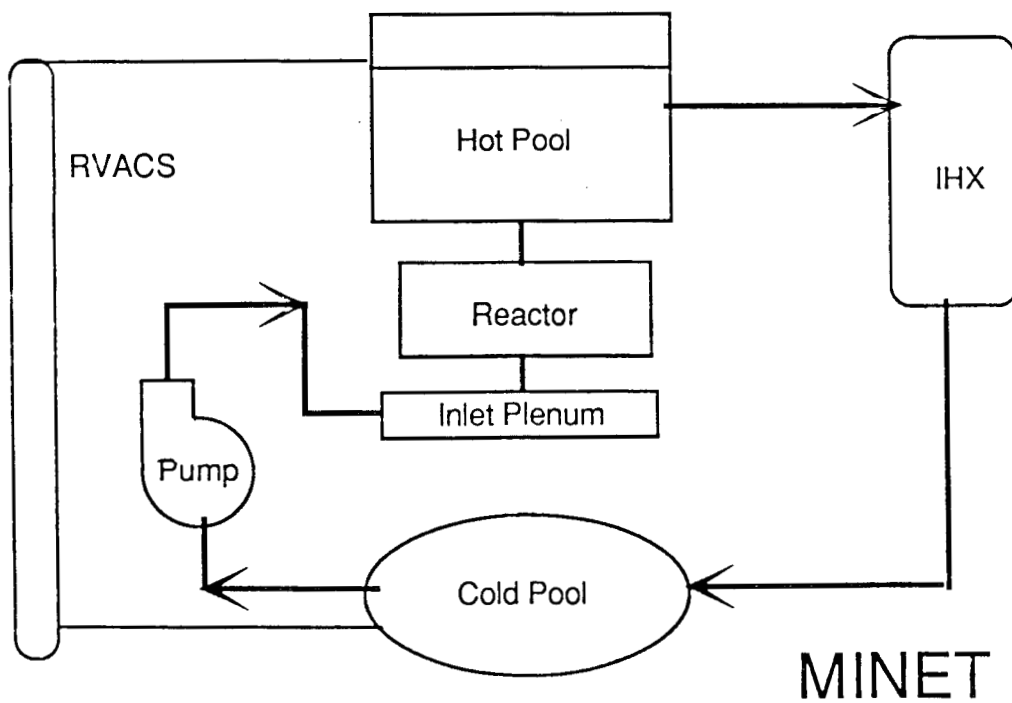
In addition to the simplified analysis discussed in the previous section, we analyzed the PRISM LOHS event using the MINET Code [Van Tuyle, 1984]. The representation utilized is indicated schematically in Figure 77. The reactor was assumed scrammed very early, and a GE decay heat curve (with 15% additional heating compared against best estimate) was specified as a boundary condition. It was assumed that heat removal through the IHX dropped to zero quickly, and that the RVACS heat removal was as shown in Figure 63. MINET tracked the thermal expansion of the sodium, and determined that the RVACS spill-over began about 5 1/2 hours into the event. From that time onward, a substantial amount of sodium flowed directly from the hot pool along the inside wall of the reactor vessel and into the cold pool.

The reactor outlet sodium temperatures calculated by MINET are plotted in Figure 78, along with the corresponding values from the GE calculations and from the simple model discussed in the previous section. For the first 6 hours, the two computer calculations are in excellent agreement, and both predict RVACS spill over around 5.5 hours (although this is not apparent in Figure 78). During that early period, the hand calculations are off primarily due to the crude assumption that the sodium outlet temperatures are 100°F above the estimated vessel average temperature. Between 6 and 22 hours, all three calculations are in good agreement. After 22, the RVACS heat removal and the decay heat approach each other closely (see Figure 63), so that small errors in either parameter are exaggerated when the difference is taken, and this is further increased when the difference is integrated over several thousands of seconds. Therefore, the discrepancy apparent in the 22 to 48 hour period is easy to understand. Furthermore, only the GE calculation includes a model of RVACS performance as a function of temperatures within the vessel. If the MINET calculation contained an equivalent model, the RVACS performance would be increased by several percent during this time period, which would decrease the sodium temperatures so that they are closer to the GE values. Similarly, if the hand calculation included this RVACS temperature dependence, the RVACS performance would drop significantly after 30 hours, leading to higher temperatures.

It should be noted that ASME Service Condition C and D (structural damage) temperatures are about 922 K and 977 K, respectively, for the PRISM design. Therefore, even if the most conservative analysis is correct, the outcome of this very unlikely event is probably acceptable.

A MINET simulation of the SAFR LOHS event was not performed, due to DOE's early decision to commit to the GE team (PRISM) for further development. Had we performed such a calculation, it is likely that the results would have been quite similar to the PRISM case.

Advanced Liquid Metal Reactor



bnl
aui

Figure 77 . Representation of PRISM Used for Long LOHS Simulation

PRISM LOHS

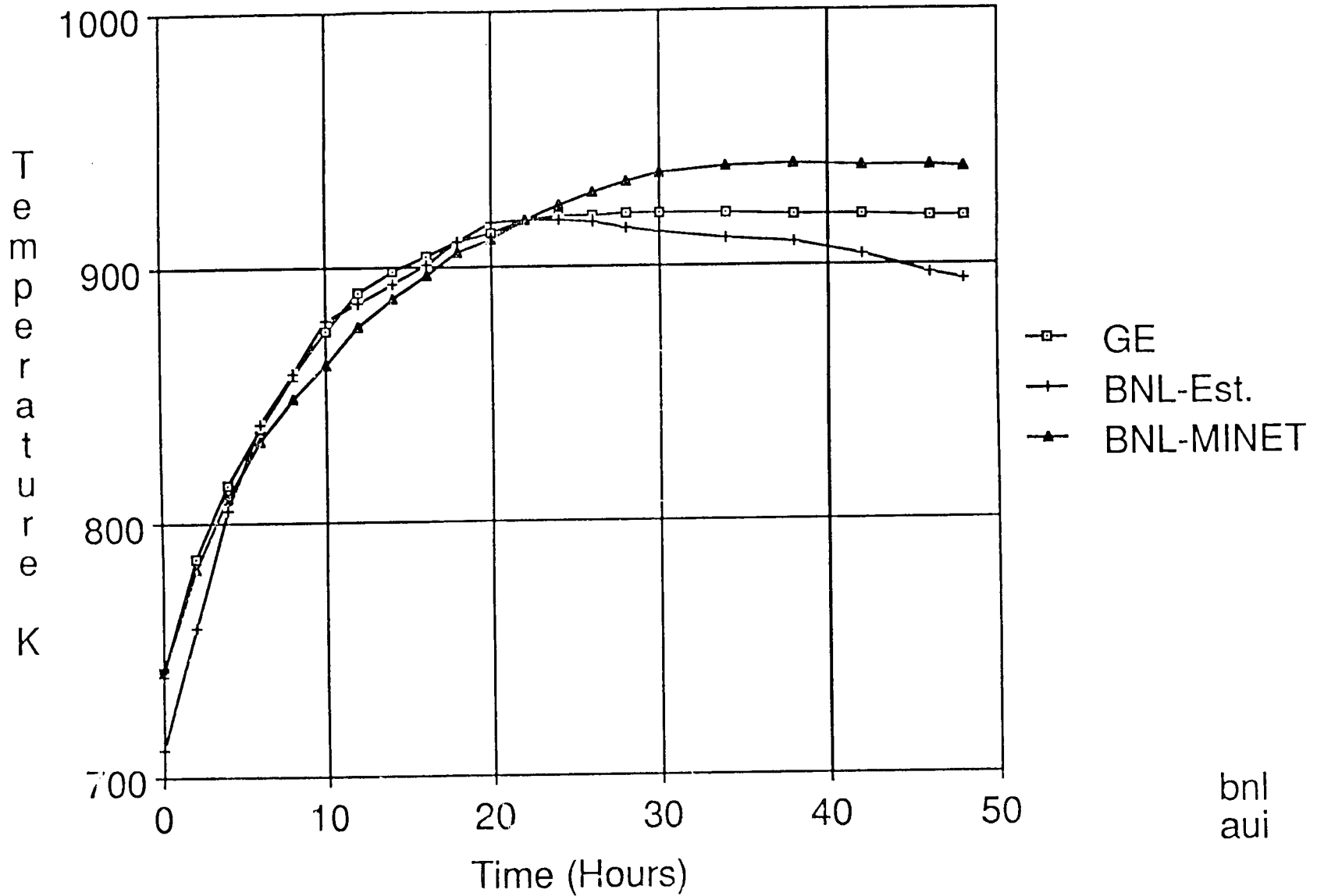
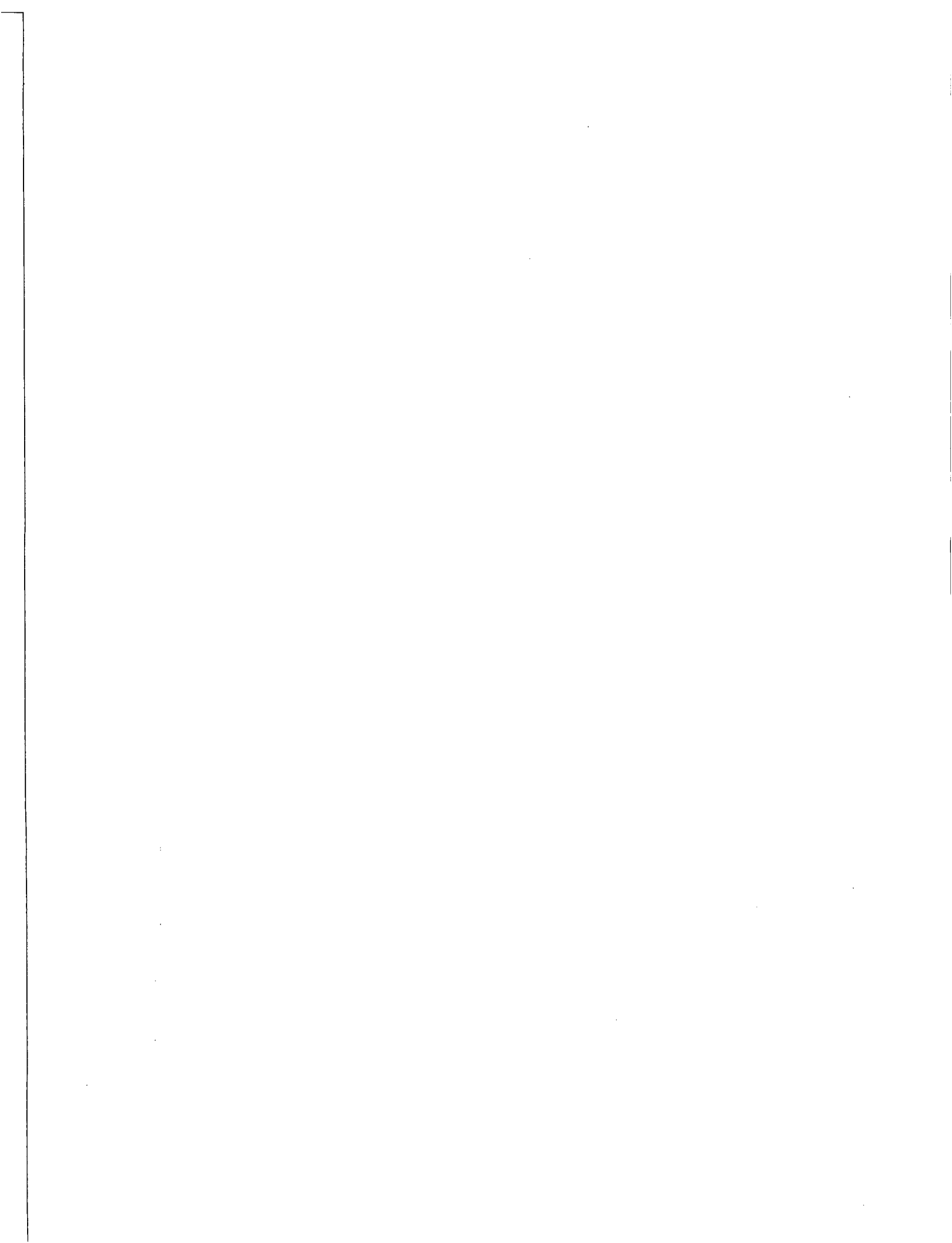


Figure 78 Calculated Reactor Outlet Sodium Temperatures

-113-114

bnl
aui



9. SUMMARY

There are several examples in both PRISM and SAFR where inherent or passive systems provide for a safe response to off-normal conditions. This is in contrast to the engineered safety systems utilized on current U. S. Light Water Reactor (LWR) designs.

One important design inherency in the LMRs is the "inherent shutdown", which refers to the tendency of the reactor to transition to a much lower power level whenever temperatures rise significantly. This type of behavior was demonstrated in a series of unscrammed tests at EBR-II [N.E.D., 1986]. The second key design feature is the passive air cooling of the vessel to remove decay heat. These systems, designated RVACS in PRISM and RACS in SAFR, always operate, and are believed to be able to prevent core damage in the event that no other means of heat removal is available.

Our effort was focused mainly to confirm the inherent reactor shutdown and the passive shutdown heat removal for two major reasons. First, these are the new design features that set these designs apart from more conventional liquid metal cooled reactors, such as Phenix, SNR-300, CRBR, MONJU, and the Soviet breeder reactors. Second, if both the inherent shutdown and the passive shutdown heat removal were absolutely reliable, and therefore infallible, then one would conclude that these are very safe reactors. (As a further note, when a reactor appears to have these characteristics, one is driven to consider major changes in the geometry as possibly threatening, and this usually leads one to consider seismic challenges and sabotage as major threats.)

We have concluded that the ANL estimates of the reactivity feedback parameters for PRISM and SAFR are probably reasonably accurate. However, we are cautious about the uncertainties in these feedbacks and believe that the margins for the inherent shutdown must be large at this time in order to compensate for these uncertainties.

Our SSC calculations for the three major unscrammed events in PRISM, including loss-of-heat sink (LOHS), loss of flow (LOF), and transient over power (TOP), were very similar to those submitted by GE. Safety margins appear to be significant for all three events, with the unscrammed LOF having the smallest margins. Three related unscrammed events were also analyzed, including a pipe break, a TOP/LOF combination, and an LOF missing one (of four) pump coastdown. The pipe break, which results in a flow short-circuit rather than a loss of sodium inventory, is slightly worse than an instantaneous stoppage of one of the pumps and results in a rapid power reduction (the inherent shutdown) and appears to be largely benign. The combined TOP/LOF is less likely than either a TOP or an LOF, and has smaller safety margins than either. Clearly, GE should design to minimize the likelihood of this event. The margin for the unscrammed LOF missing one pump coastdown is nearly zero. As the chance of losing one of the coastdowns, which are provided for the electromagnetic (EM) pumps by the synchronous machines, has to be significant, it would be prudent for GE to design to better accommodate this event, i.e., to ride out an unscrammed LOF on three pump coastdowns.

For the three basic unscrammed events in SAFR, i.e., the LOHS, LOF, and TOP events, our SSC calculational results were similar to those provided by ANL for RI/SAFR. The only problem here was that the ANL calculations show control rod drive line expansion that is very quick, and this helps their calculated safety margins. While the SSC results were similar to those submitted by ANL, as long as the enhanced control rod drive line expansion was utilized, these calculations consistently showed somewhat smaller safety margins for SAFR than for PRISM. This traces directly to RI's desire to run SAFR significantly hotter than PRISM in order to use a superheated steam cycle and achieve higher thermal efficiency (40% versus 32%).

In addition to the three basic unscrammed events in SAFR, we looked at two variations - a 20 cent TOP combined with an LOF and a pump seizure (one of two centrifugal pumps). The safety margins for the 20¢ TOP/LOF were not large for SAFR, and would be smaller for a 35¢ TOP/LOF. For the pump seizure event, it was determined that the rapid reduction in reactor flow rate could be accommodately inherent as long as the other pump continued to function. However, the other pump should see a surge in flow (25 to 30%), and cavitation may be anticipated. A related concern is that pump seizures are actually more likely during a coastdown, so RI may have had to design to survive the ULOF with only one coastdown.

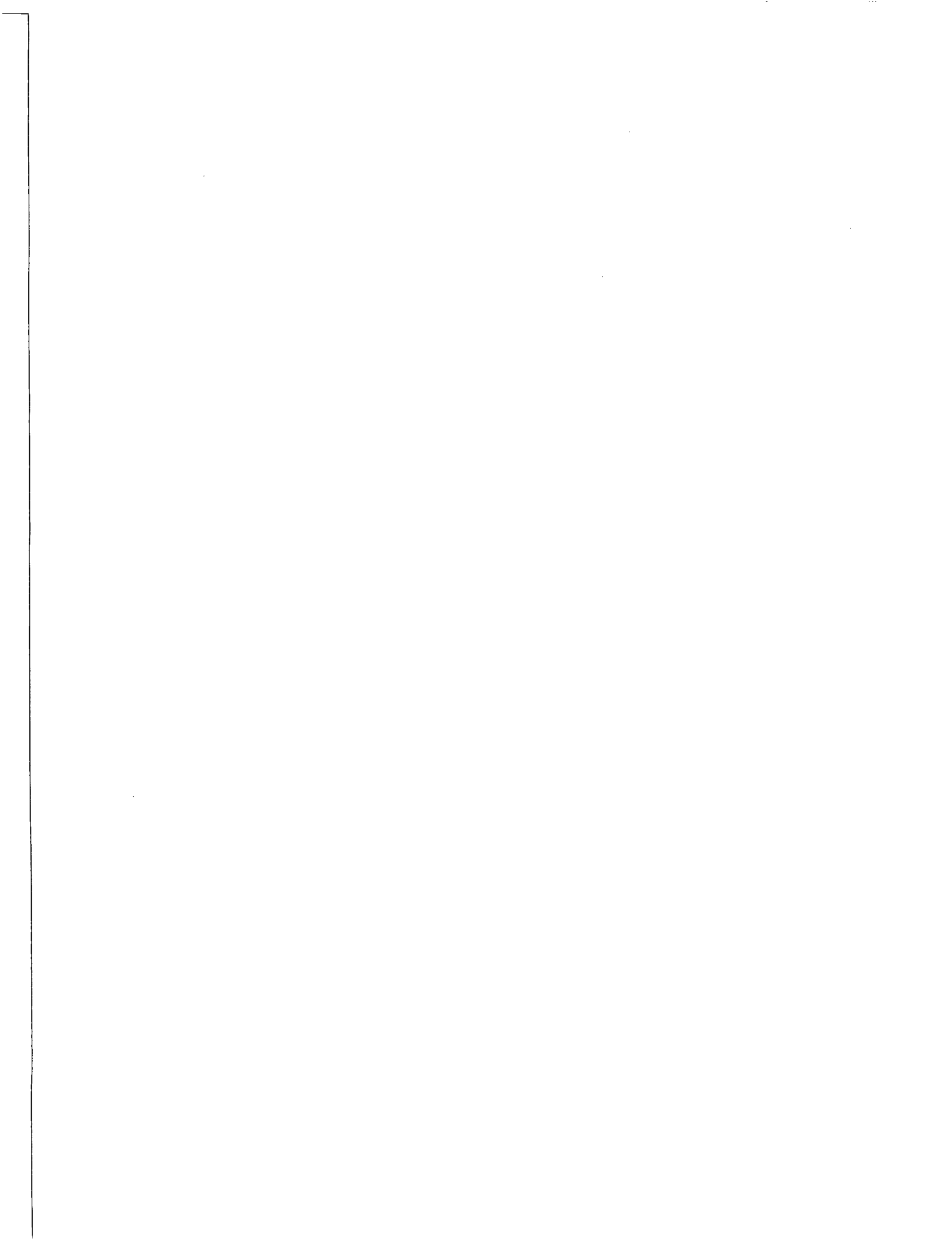
In order to assess the passive cooling system, we adapted the PASCOL code, which we developed to model the comparable system in the Modular High Temperature Gas Reactor (MHTGR), which is designated the RCCS. We specified the reactor vessel temperature and calculated the natural draft air flow, and the various heat transfer processes. Using conservative parameters, we were able to match the performance predictions made by both GE and RI/ANL. Parametric cases showed excellent fault tolerance, particularly with regard to partial blockages of the air flow passages. In short, performance of the PRISM RVACS and SAFR RACS should be at least as good as projected, and the problems associated with partial blockages appear to be minimal.

One advantage of pool type LMRs, particularly if metal fuel is used, is that the high heat capacity, high thermal conductivity system can survive a fairly lengthy heat up event, i.e., a total loss of heat removal. This was demonstrated using simple hand calculations, which gave results that were quite similar to those provided by GE and RI/ANL for cases with and without functioning air-cooled vessel systems. If the air flow is totally blocked, many hours are available to unblock the air flow pathways, or conceivably to arrange for an ad-hoc evacuation.

A computer code calculation of a postulated LOHS, with RVACS cooling only, was performed using MINET. Results were very similar to those provided by GE, particularly during the first day of transient time. Both code calculations indicated that the sodium spillover that increases RVACS performance occurs about 5 1/2 hours into the event.

In summary, most of the key calculations submitted by the SAFR and PRISM design teams were independently verified and/or replicated. While the inherent "shutdown" appears to work for key postulated events, some variant cases were identified as posing significant safety concerns - in that the

inherent shutdown safety margins would be too small. The passive means of shutdown cooling, using RACS or RVACS, appears to be an excellent approach, as the performance is projected to be good and the reliability should be very high.



REFERENCES

E. B. Baumeister, et al., "Inherent Safety Features and Licensing Plan of the SAFR Plant," Proceedings of the International Conference on Fast Breeder Systems, 1, p. 3.4-1, September 13-17, 1987.

R. C. Berglund, et al., "Design of PRISM, An Inherently Safe, Economic, and Testable Liquid Metal Fast Breeder Reactor Plant," Proceedings of the ANS/ENS International Conference on Fast Breeder Systems, Volume 2, Pasco, WA, September 13-17, 1987.

N. W. Brown, et al., "Inherent Safety and Design Certification of PRISM," Proceedings of the International Conference on Fast Breeder Systems, 1, p. 3.5-1, September 13-17, 1987.

H. S. Cheng and G. J. Van Tuyle, "A Simple Model for Radial Expansion Reactivity in LMRs," Safety of Next Generation Power Reactors, Seattle, WA, May 1988.

H. S. Cheng, "PTKINS - A Point Kinetics Program," Brookhaven National Laboratory, April 26, 1976.

J. J. Duderstadt and L. J. Hamilton, Nuclear Reactor Analysis, John Wiley & Sons, New York, 1976.

"The Experimental Breeder Reactor II Inherent Safety Demonstration," Nuclear Engineering and Design, 101, April 1986.

E. E. Feldman and D. Mohr, "Unprotected Loss-of-Heat Sink Simulation in the EBR-II Plant," ASME Paper 84-WA/HT-7.

E. L. Gluekler, N. W. Brown, C. L. Cowan, A. Hudsbedt, and R. A. Meyer, "Safety Characteristics of a Small Modular Reactor," Proceedings of the Int. Topical Meeting on Fast Reactor Safety, 1, pp. 69-74, 1985.

J. G. Guppy, et al., "Super System Code (SSC, Rev. 2) An Advanced Thermohydraulic Simulation Code for Transients in LMFBRs," Brookhaven National Laboratory Report, NUREG/CR-3169, BNL-NUREG-51650, April 1983.

G. L. Hofman, et al., "Metallic Fuels Handbook," Argonne National Laboratory Report, ANL-IFR-29, November 1985.

International Atomic Energy Agency (IAEA), Status of Liquid Metal Cooled Fast Breeder Reactors, IAEA Technical Report Series No. 246, Vienna, Austria, 1985.

R. A. Knief, "Nuclear Energy Technology," Hemisphere Publishing Corp., McGraw Hill Brook Co., 1981.

P. G. Kroeger and G. J. Van Tuyle, "Evaluation of Advanced Liquid Metal Reactor Passive Air Cooling Systems," Transactions of the American Nuclear Society, Los Angeles Winter Meeting, November 1987, also BNL-NUREG-39957.

W. Kwant, et al., "PRISM Reactor Design and Development," Proceedings of the International Conference on Fast Breeder Systems, 2, p. 8.6-1, Sept. 13-17, 1987.

J. R. Lamarsh, Introduction to Nuclear Reactor Theory, Addison-Wesley Publishing Co., Reading, MA, 1966.

R. T. Lancet and J. F. Marchaterre, "Inherent Safety of the SAFR Plant," Proceedings of the Int. Topical Meeting on Fast Reactor Safety, 1, pp. 43-50, 1985.

R. D. Oldenkamp, E. Guenther, and S. Golan, "The Sodium Advanced Fast Reactor," Proceedings of the ANS/ENS International Conference on Fast Breeder Systems, Volume 2, Pasco, WA, September 13-17, 1987.

A. Padilla, Jr. and D. J. Hill, "Comparison of Reactivity Feedback Models for the FFTF Passive Safety Tests," Proceedings of the Safety of Next Generation Power Reactors Conference, Seattle, WA, May 1988.

W. R. Robinson, et al., "First Treat Overpower Tests on U-Pu-Zr Fuel: M5 and M6," Transactions of the American Nuclear Society, 55, Los Angeles, CA, November 1987.

G. C. Slovik and G. J. Van Tuyle, "Analysis of Postulated Unscrammed Loss-of-Flow in SAFR Using SSC," Transactions of the American Nuclear Society, Vol. 57, Washington, DC, November 1988.

G. C. Slovik, G. J. Van Tuyle, B. C. Chan, R. J. Kennett, and A. Aronson, "Evaluating Advanced LMR Reactivity Feedbacks Using SSC," Proceedings of the 1988 ANS Topical Meeting on Safety of Next Generation Power Reactors, May 1-5, 1988, Seattle, WA.

G. J. Van Tuyle, "A Momentum Integral Network Method for Thermal-Hydraulic Systems Analysis," Nuclear Engineering and Design, 91, pp. 17-28, 1986.

G. J. Van Tuyle, P. G. Kroeger, G. C. Slovik, M. Karasulu (NYPA), and G. Grochowski (NYPA), "Comparing the Inherent Safety of the Modular LMRs and HTGRs and the PIUS Concept," Proceedings of the 1988 ANS Topical Meeting on Safety of Next Generation Power Reactors, May 1-5, 1988, Seattle, WA.

G. J. Van Tuyle, B. C. Chan, and G. C. Slovik, "Initial Pipe Break Analyses for Advanced LMR Concepts Using MINET," Transactions of the American Nuclear Society, Los Angeles Winter Meeting, November 1987, also BNL-NUREG-39956.

G. J. Van Tuyle, T. C. Nepsee, and J. G. Guppy, "MINET Code Documentation," Brookhaven National Laboratory Report, BNL-NUREG-51742, February 1984.

K. Wirtz, "Lectures on Fast Reactors," American Nuclear Society, La Grange Park, IL, 1978.

NRC FORM 335 (8-87) NRCM 1102, 3201, 3202		U.S. NUCLEAR REGULATORY COMMISSION		1. REPORT NUMBER (Assigned by PPMB: DPS, add Vol. No., if any)	
BIBLIOGRAPHIC DATA SHEET		SEE INSTRUCTIONS ON THE REVERSE		NUREG/CR-5364	
				BNL-NUREG-52197	
2. TITLE AND SUBTITLE		3. LEAVE BLANK		4. DATE REPORT COMPLETED	
Summary of Advanced LMR Evaluations - PRISM and SAFR				MONTH	YEAR
				February	1989
5. AUTHOR(S)		6. DATE REPORT ISSUED			
G. J. Van Tuyle, G. C. Slovik, B. C. Chan, R. J. Kennett, H. S. Cheng, P. G. Kroeger				MONTH	YEAR
				October	1989
7. PERFORMING ORGANIZATION NAME AND MAILING ADDRESS (Include Zip Code)		8. PROJECT/TASK/WORK UNIT NUMBER		9. FIN OR GRANT NUMBER	
Brookhaven National Laboratory Upton, New York 11973				A3827	
10. SPONSORING ORGANIZATION NAME AND MAILING ADDRESS (Include Zip Code)		11a. TYPE OF REPORT		b. PERIOD COVERED (Inclusive dates)	
Division of Regulatory Applications Office of Nuclear Regulatory Research U.S. Nuclear Regulatory Commission Washington, DC 20555		Formal			
12. SUPPLEMENTARY NOTES					
13. ABSTRACT (200 words or less)					
<p>Independent Safety Analyses of the DOE sponsored Advanced Liquid Metal Reactor (LMR) Concepts: PRISM and SAFR, performed at BNL between 1986 and 1988, are reported. In most cases, BNL calculational results were very similar to those provided by General Electric (GE) for PRISM and the Rockwell International (RI)/Argonne National Laboratory (ANL) team for SAFR. Two key features of these designs are the inherent reactor "shutdown" (transition to low power in response to high temperatures) and passive shutdown heat removal (natural draft air cooling of the reactor vessel).</p> <p>There are two key factors in the inherent shutdown, the reactivity feedback parameters and the projected reactor response during postulated unscrammed transients. Reactivity feedback parameters provided by the GE and RI/ANL teams were utilized in the BNL calculations, after some comparative studies and simplified calculations confirmed that the supplied parameters were at least approximately correct. Independent computer analyses of the unscrammed response to various challenges yielded results that were very similar to those submitted for both designs, and indicated that the inherent shutdown should work for many postulated events. However, for the loss-of-flow (LOF) events, there are some very low probability events where the safety margins are minimal, given that the positive sodium void worth makes sodium boiling highly undesirable.</p>					
14. DOCUMENT ANALYSIS - a. KEYWORDS/DESCRIPTORS				15. AVAILABILITY STATEMENT	
PRISM, SAFR, Liquid Metal Reactors				Unlimited	
				16. SECURITY CLASSIFICATION	
b. IDENTIFIERS/OPEN-ENDED TERMS				(This page)	
				Unclassified	
				(This report)	
				Unclassified	
				17. NUMBER OF PAGES	
				18. PRICE	